CHEMICAL REVIEWS

Review

pubs.acs.org/CR

Single-Molecule Fluorescence Spectroscopy of Photosynthetic Systems

Toru Kondo, Wei Jia Chen, and Gabriela S. Schlau-Cohen*

Department of Chemistry, Massachusetts Institute of Technology, 77 Massachusetts Avenue, Cambridge Massachusetts 02139, United States

ABSTRACT: Photosynthesis begins when a network of pigment−protein complexes captures solar energy and transports it to the reaction center, where charge separation occurs. When necessary (under low light conditions), photosynthetic organisms perform this energy transport and charge separation with near unity quantum efficiency. Remarkably, this high efficiency is maintained under physiological conditions, which include thermal fluctuations of the pigment−protein complexes and changing local environments. These conditions introduce multiple types of heterogeneity in the pigment−protein complexes, including structural heterogeneity, energetic heterogeneity, and functional heterogeneity. Understanding how photosynthetic light-harvesting functions in the face of these fluctuations requires understanding this heterogeneity, which, in turn, requires characterization of individual pigment−protein complexes. Single-molecule spectroscopy has the power to probe individual complexes. In this review, we present an overview of the common techniques for single-molecule fluorescence spectroscopy applied to photosynthetic systems and describe selected experiments on these systems. We discuss how these experiments provide a new understanding of the impact of heterogeneity on light harvesting and thus how these systems are optimized to capture sunlight under physiological conditions.

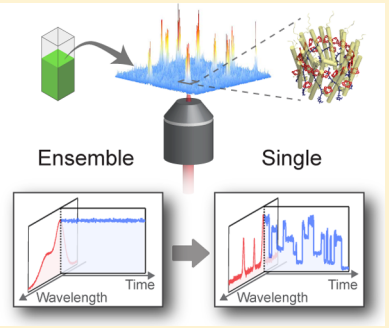

CONTENTS

Special Issue: Light Harvesting

Received: March 24, 2016

DOI: 10.1021/acs.chemrev.6b00195
Chem. Rev. XXXX, XXX, XXX−XXX

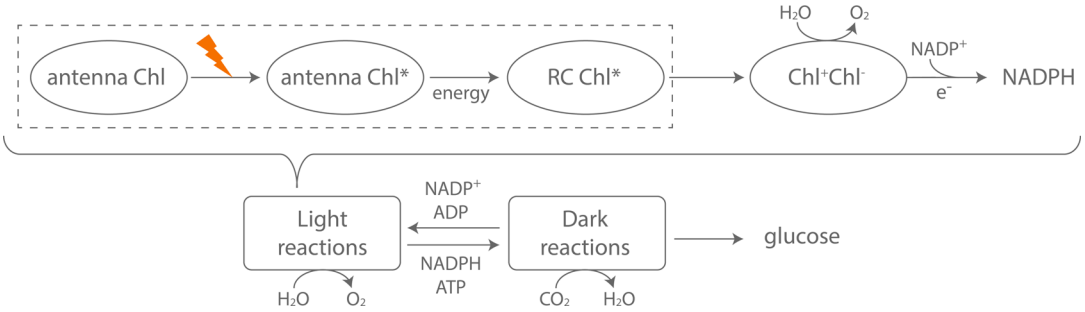

Figure 1. Overview of photosynthesis in plants and algae. Energy is absorbed in the antenna chlorophyll and migrates to the reaction center, where charge separation occurs. The charge-separated state produces an electrochemical gradient across the membrane, which drives downstream biochemical reactions to generate biomass. Here, we focus on photosynthetic light harvesting, which is the initial absorption and energy migration processes indicated by the dashed box.

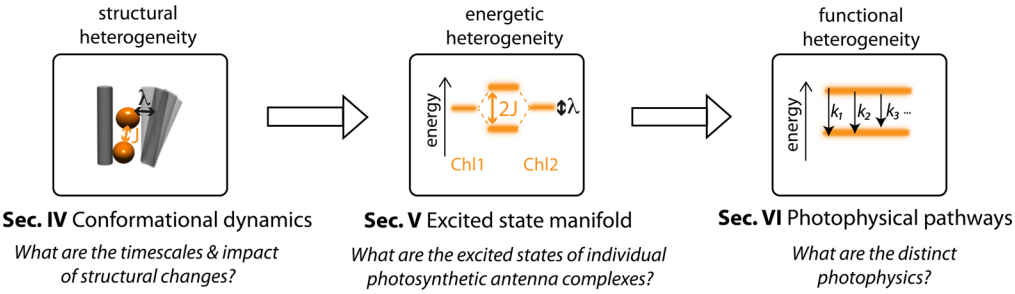

Figure 2. Photosynthetic pigment–protein complexes exhibit heterogeneity in structure, energy, and function. Thermal fluctuations of the protein structure change the magnitude of the electrodynamic couplings between the molecules, which changes the excited state manifold and the function. In sections 4, 5, and 6, we describe single-molecule experiments that explore each type of heterogeneity.

1. INTRODUCTION

Photosynthesis converts sunlight to biomass, providing energy for most life on Earth, as illustrated in Figure 1.[1] Photosynthesis begins with light harvesting, in which absorption of solar energy and subsequent transport of the absorbed energy occur within sophisticated networks of pigment–protein complexes. Absorbed energy migrates through these networks to reach a dedicated complex, known as the reaction center, where charge separation occurs. Remarkably, photosynthetic organisms exhibit near unity quantum efficiency under low light conditions, meaning nearly all absorbed photons can drive a charge separation event.[1] This achievement is particularly striking under physiological conditions because, at room temperature, thermal fluctuations introduce dynamics into the nuclear degrees of freedom. These are stochastic dynamics that result in heterogeneity of molecular structure. As discussed in section 2, this structural heterogeneity causes heterogeneity in the energetic landscape and, in turn, function (Figure 2).[2−4] While all of these characteristics are highly related, they provide a framework to explore how heterogeneity manifests in photosynthetic systems. In particular, it is not fully understood how photosynthetic systems overcome the barriers or traps introduced by heterogeneity that lower the efficiency of energy transport. Here, we describe the ways in which single-molecule spectroscopy has explored the heterogeneity that exists alongside highly efficient energy transport.

The first step toward reconciling these two features is understanding the extent of structural, energetic, and functional heterogeneity. Thermal fluctuations, a major source of structural heterogeneity, are asynchronous, and thus their impact on energy and function averages out in ensemble measurements. In contrast, single-molecule experiments enable characterization of individual pigment–protein complexes to build up the distribution of behaviors. By probing single copies, we recover information that is lost in the process of ensemble averaging.

Because of the questions described above, photosynthetic systems have been a long-standing target for single-molecule spectroscopy. Less than a decade after the first single-molecule experiments,[5,7,8] single light-harvesting complexes were observed for the first time.[9] These observations launched a large body of fruitful research to understand the role of heterogeneity in photosynthetic solar energy conversion. These efforts have focused on the light-harvesting complexes, responsible for initial absorption and energy transport, from a diverse set of photosynthetic systems, including purple bacteria,[10−13] green sulfur bacteria,[14] cyanobacteria,[12,15,16] and higher plants.[17,18] The first single-molecule experiments on photosynthetic systems explored structural heterogeneity within light-harvesting complex 2 (LH2) from purple bacteria.[19] In the intervening years, a series of experiments have characterized the molecular basis of this heterogeneity, how it impacts the excited state manifold, and the conformational dynamics exhibited by LH2.[2] These tools have been extended to other photosynthetic

DOI: 10.1021/acs.chemrev.6b00195
Chem. Rev. XXXX, XXX, XXX−XXX

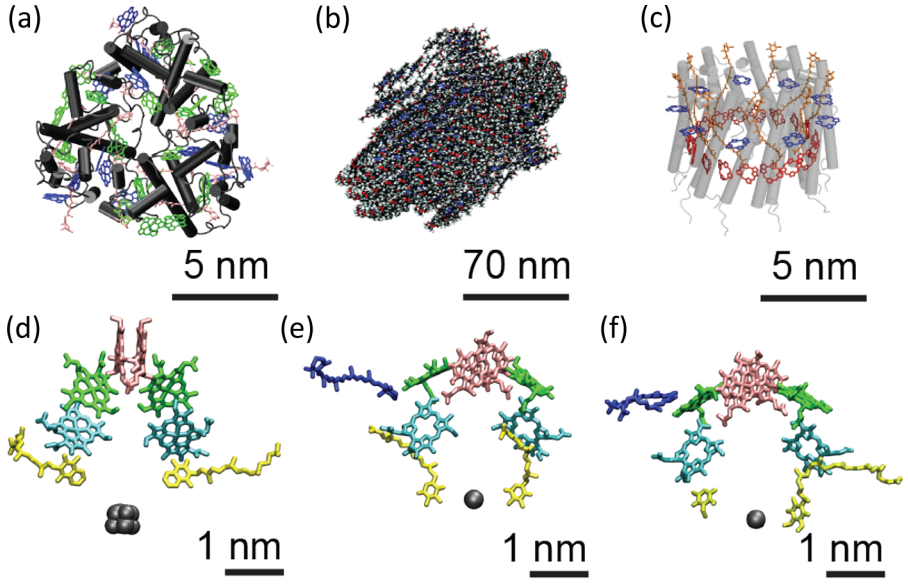

Figure 3. Comparison of structures of the antenna (top row) and reaction centers (bottom row). The light-harvesting complexes are: (a) LHCII from higher plants is a pigment−protein complex where the protein matrix (gray) surrounds the embedded pigments (Chl *a* in green, Chl *b* in blue, and carotenoids in pink);[26] (b) the chlorosome from green sulfur bacteria is a molecular aggregate formed from BChl;[27] and (c) LH2 from purple bacteria is a pigment−protein complex where the protein matrix (gray) surrounds the embedded pigments (BChl *a* in red and blue and carotenoids in orange).[28] The reaction centers, with only cofactors shown, are (d) the photosystem I reaction center with the so-called "special pair", the Chl *a* that serves as the site of charge separation (pink), the Chl *a* (green, and cyan), the quinones (yellow),[29] and the iron−sulfur cluster (gray); (e) the photosystem II reaction center with the Chl *a* (pink and green), the pheophytin (cyan), the quinones (yellow), and the nonheme iron (gray);[30] and (f) the type-II bacterial reaction center with the BChl (pink and green), the bacteriopheophytin (cyan), and the quinones (yellow), and the nonheme iron (gray).[31] While the antenna complexes exhibit a variety of architectural motifs, the basic structure of the reaction center is much more highly conserved.

complexes, including light-harvesting complex II (LHCII) from green plants.[20] In these experiments, the multiple functional roles of LHCII were explored, in particular how LHCII responds to conditions that mimic different solar intensities.[17,18] LH2 and LHCII have been the most widely studied photosynthetic systems at the single-molecule level. However, part of the power of single-molecule techniques is that they have been broadly applicable to photosynthetic systems. For these systems, applying these techniques has revealed new insight into the potential energy landscape of photosynthetic proteins, which, even more generally, provides insight into protein structural dynamics.

Here, we present insights from single-molecule experiments on not only LH2 and LHCII but also on other photosynthetic systems. While the field of single-molecule fluorescence spectroscopy on photosynthetic systems is too large to describe all results in a single review, we highlight experiments on several different photosynthetic systems performed at both cryogenic and physiological temperatures to illustrate the breadth of the field.

Single-molecule studies of photosynthetic systems have been primarily performed with fluorescence-based techniques.[21] Thus, here we introduce the single-molecule fluorescence microscopes commonly used for photosynthetic systems. Because of the sensitivity required for a single-molecule fluorescence observation, the detector is a major consideration in the design of an experiment. While there have been many improvements in fluorescence experimental tools, the development of high sensitivity and low noise detectors (avalanche photodiodes, CCD cameras, and CMOS cameras) has in particular driven progress in single-molecule investigation.[22,23]

In this paper, we review single-molecule fluorescence experimental tools in the context of research progress on photosynthetic systems. In section 2, we begin by providing a brief background on photosynthetic light harvesting and solar energy conversion. In section 3, we present the technical aspects of single-molecule fluorescence spectroscopy by summarizing the experimental considerations and techniques used to achieve single-molecule sensitivity. In sections 4, 5, and 6, we then describe ways in which these single-molecule experiments explore the static and dynamic heterogeneity exhibited by photosynthetic systems. In particular, we present examples of physical insights gained in the following key areas: (1) observation of conformational dynamics (structural heterogeneity); (2) characterization of the excited states (energetic heterogeneity); and (3) exploration of photophysical processes, such as energy transfer (functional heterogeneity). Through these experiments, single-molecule spectroscopy reveals the heterogeneity within light-harvesting systems, which is an important step in understanding how they flourish in complex and dynamic natural environments. While here we focus on natural systems, single-molecule experiments can also be used to explore and characterize the heterogeneity in artificial light-harvesting systems.[24,25] The energetic heterogeneity revealed through these experiments provides a critical parameter in identifying how well we reproduce natural function. In future directions, comparing this parameter for natural and artificial systems can aid the optimization of artificial light-harvesting devices.

DOI: 10.1021/acs.chemrev.6b00195
Chem. Rev. XXXX, XXX, XXX−XXX

2. PHOTOSYNTHETIC LIGHT HARVESTING AND SOLAR ENERGY CONVERSION

The early events in photosynthesis occur within a protein network that can be divided, roughly, into two parts: (1) the antenna, and (2) the reaction center. The antenna, which consists of light-harvesting complexes, is responsible for the initial absorption and energy migration. As illustrated in Figure 3, top, the light-harvesting complexes exhibit a large variety in size, shape, and architectural motif as well as pigment and protein composition and cellular location. These complexes range from a ∼10 nm protein structure with embedded pigments to a ∼100 nm pigment-only molecular aggregate. Despite these striking differences, single-molecule spectroscopy has served as an incisive tool to explore each of these complexes, including their structures, conformational dynamics, and excited state manifolds. In sections 4−6, we will present examples of how single-molecule spectroscopy has provided insight into these light-harvesting complexes.

The reaction centers are responsible for the final energy transport steps, charge separation, and charge transport. As illustrated in Figure 3, bottom, reaction centers across multiple organisms exhibit a more conserved architectural motif. Furthermore, the primary (charge transfer) pigments within reaction centers are always circular tetrapyrroles, e.g., chlorophyll (Chl) and bacteriochlorophyll (BChl). Observing fluorescence from the reaction center is challenging because the cations that result from the electron transport chain quench the excited states. However, observing fluorescence from the antenna complexes has been relatively straightforward. While not all antenna complexes are single-molecule visible, single-molecule cryogenic and room temperature experiments have successfully characterized the heterogeneity in excited states and explored the conformational dynamics of the protein structure, as discussed in sections 4 and 5 below. However, cryogenic experiments have also overcome the limitations of observing RC fluorescence to successfully probe the trap (red-shifted) states, as discussed in section 6 below for photosystem I (PS I) from higher plants.

In this section, we give an overview of the components of pigment−protein complexes and their dynamics. We also introduce two well-studied photosynthetic systems, the light-harvesting complexes from purple bacteria and from higher plants.

2.1. Pigment−Protein Complexes

Photosynthetic pigment−protein complexes are specialized proteins with the position and orientation of the embedded pigments finely tuned to produce efficient and directional energy and electron flow. Because the sun is a low density energy source (∼1 kW/m^2), the pigments are packed within a protein matrix at a high concentration to maximize solar absorption. For example, the pigments within the major light-harvesting complex of photosystem II (LHCII) are found at ∼0.3 M.[26] This concentration is 2 orders of magnitude above the advent of concentration quenching for these pigments in solution.[32] Within the protein matrix, the pigments are positioned with intermolecular distances and relative orientations that minimize quenching processes and optimize for energy transport.

The high concentration of these pigments, or dense packing, means that there are only a few angstroms between pigments and between the pigments and the surrounding protein. These short distances lead to significant pigment−pigment (J) and pigment−protein (λ) electrodynamic couplings, as illustrated in Figure 2, left.[6] The balance of these couplings determines the excited state energies and drives the energy transport dynamics.[33−35] Notably, these couplings are the same order of magnitude as k_BT at room temperature (200 cm^{-1}).[6] k_BT determines which of the conformational substates are thermally accessible. Structural differences among the conformational substates introduce heterogeneity in intermolecular interactions. This includes heterogeneity in the transition energies of the pigments (diagonal disorder) induced by changing pigment−protein distances and orientations and heterogeneity in the pigment−pigment coupling (off-diagonal disorder) induced by changing pigment−pigment distances and orientations. Notably, the diagonal disorder is the same order of magnitude as the intermolecular couplings themselves and, as a result, the balance of the pigment−pigment and pigment−protein couplings changes.[6] This changing balance, in turn, introduces heterogeneity in the excited state manifold and the dynamics of energy transport (Figure 2). Single-molecule spectroscopy has shown that absorption, energy transport, and dissipation properties vary from complex to complex and within a single complex over time, features which are lost in ensemble measurements because the variation in these properties is averaged over a huge number of molecules.

To describe these complexes and their dynamics, we construct a Hamiltonian for the total pigment−protein complexes following ref 36. The Hamiltonian can be constructed from the diabatic Hamiltonian for the individual pigments in their protein environment. For an individual pigment, j, this is given by

$$\hat{H}_j(x_j) = \hat{H}_{j,g}(x_j)|\varphi_{j,g}\rangle\langle\varphi_{j,g}| + \hat{H}_{j,e}(x_j)|\varphi_{j,e}\rangle\langle\varphi_{j,e}| \quad (1)$$

where the two terms represent the Hamiltonian for the ground and excited states, respectively, modulated by all the environmental (e.g., protein) and nuclear degrees of freedom (x_j). As discussed above, in a photosynthetic complex, the individual pigments are closely spaced within their surrounding environment. As a result, they couple to each other with the pigment−pigment couplings (J_{ij}). Thus, the Hamiltonian for a pigment−protein complex ($\hat{H}_{PPC}$) containing N pigments is given by

$$\hat{H}_{PPC} = \sum_{j=1}^{N} [\hat{H}_{j,g}(x_j)|\varphi_{j,g}\rangle\langle\varphi_{j,g}| + \hat{H}_{j,e}(x_j)|\varphi_{j,e}\rangle\langle\varphi_{j,e}|] + \sum_{i<j}^{N} \hbar J_{ij}[|\varphi_{j,e}\rangle\langle\varphi_{j,g}| \otimes |\varphi_{i,g}\rangle\langle\varphi_{i,e}| + |\varphi_{i,e}\rangle\langle\varphi_{i,g}| \otimes |\varphi_{j,g}\rangle\langle\varphi_{j,e}|] \quad (2)$$

Although the pigment−pigment couplings (J_{ij}) can, in principle, be modulated by the environmental and nuclear degrees of freedom (x_j), we assume the nuclear dependence of these parameters is small. The neglect of these modulations has been justified by numerical calculations that show the modulation of the electronic transitions is the dominant effect in these types of linear aggregates.[37]

With this Hamiltonian, the Franck−Condon transition energy ($\hbar\Omega_j$) of the jth pigment is given by

$$\hbar\Omega_j = \hat{H}_{j,e}(x_j) - \hat{H}_{j,g}(x_j) \quad (3)$$

For an ensemble, the transition energy for the pigment is a Boltzmann-weighted average of the transition energies from all

DOI: 10.1021/acs.chemrev.6b00195
Chem. Rev. XXXX, XXX, XXX−XXX

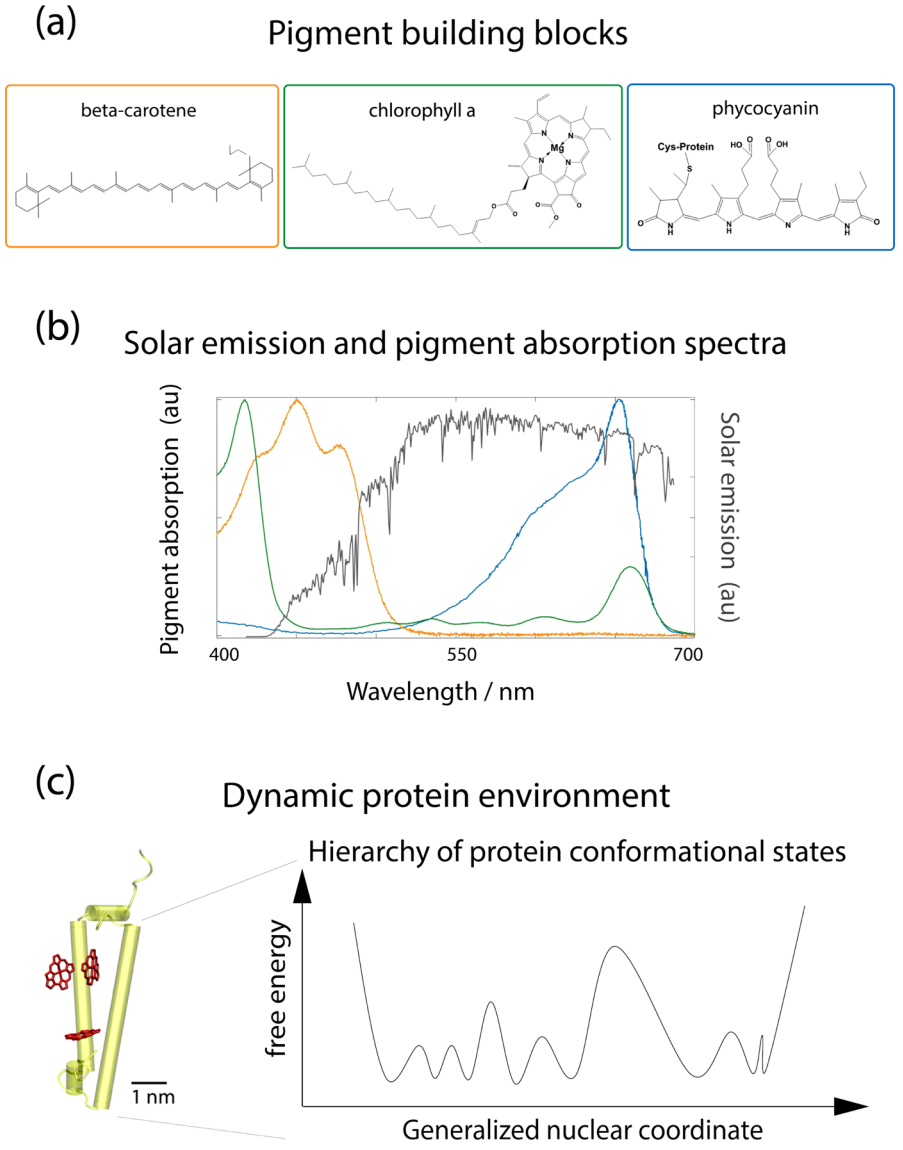

Figure 4. Pigment−protein complexes are optimized by pigment selection, protein environment, and protein dynamics. (a) Common pigments in photosynthetic light harvesting are shown. The carotenoid beta-carotene (left, orange box) is abundant in plants, fruits, and vegetables. Carotenoid variants have a photoprotective role in many photosynthetic organisms. Chl *a* (center, green box) is found in higher plants, green algae, and some bacteria. Chls are circular tetrapyrroles, and Chl variants are the major light-harvesting pigment in these organisms. Phycocyanobilin (right, blue box) is a phycobilin pigment. Phycobilins are open tetrapyrroles that covalently bind to the protein structure. Phycobilin variants are the light-harvesting pigments in cyanobacteria, red algae, and cryptophytes. (b) Photosynthetic systems achieve broad solar coverage (gray line) through this set of pigments (orange, green, and blue lines indicate absorption spectra of carotenoid, Chl *a*, and phycocyanin, respectively), with further spectral tuning by different substituent groups to generate other pigment variants and by electrochromic shifts induced by the protein-binding pocket. (c) A simplified model of the protein energy landscape is shown (right). The multiple levels of barrier heights as a function of a generalized nuclear coordinate gives rise to the so-called hierarchy of conformational substates, as well as conformational switching between these substates. This rugged, dynamic protein energy landscape combines with pigments to produce photosynthetic pigment−protein complexes (left). In these complexes, pigments are embedded within a surrounding protein scaffold, with just a few angstroms between the neighboring pigments and between the pigments and the surrounding protein. As a result, the conformational dynamics of the protein introduces dynamics into the electronic structure.

possible nuclear configurations. Within a pigment−protein complex, the transition energy varies from pigment to pigment due to electrochromic shifts induced by different protein environments.[38] The size of these variations depends on the system, but they are approximately k_BT at room temperature.[6] For a single pigment−protein complex, the transition energy of the diabatic state of each pigment experiences fluctuations due to the dynamics of the nuclear and environmental degrees of freedom (in particular, the surrounding protein environment). The fluctuations are described by the collective energy gap coordinate

$$\hat{u}_j = \hat{H}_{j,e}(x_j) - \hat{H}_{j,g}(x_j) - \hbar\langle\Omega_j\rangle \tag{4}$$

Importantly, the collective energy gap coordinate describes information about fluctuations in both the ground and excited state due to the surrounding degrees of freedom. This term for the fluctuating collective energy gap is used in models to describe the excited state dynamics after photoexcitation.[33,36,39] As described above, the modulations of the electronic transition

DOI: 10.1021/acs.chemrev.6b00195
Chem. Rev. XXXX, XXX, XXX−XXX

are known as diagonal disorder and the modulations of the pigment−pigment couplings (J) are known as off-diagonal disorder because these are the diagonal and off-diagonal elements, respectively, of the electronic Hamiltonian.

From this framework, we extract several features that are explored through single-molecule experiments, as described in sections 4, 5, and 6. The first is that the excited states interrogated spectroscopically are the delocalized eigenstates of the pigment−protein Hamiltonian. Because of the pigment−pigment couplings, J_{ij}, the eigenstates are no longer the diabatic states of the individual pigments. Instead, they are delocalized states consisting of linear combinations of the excited states of the uncoupled pigments. As described in section 5, single-molecule spectroscopy provides insight into this delocalization. Furthermore, the nuclear and environmental degrees of freedom modulate the electronic transition energies. Thus, these degrees of freedom impact the excited state energies, and the dynamics of these degrees of freedom produce changing excited state energies and dynamics. Because protein dynamics occur on many time scales, fluctuations in the collective energy gap emerge on many time scales. Single-molecule spectroscopy directly or indirectly accesses several of those time scales.

The building blocks to construct the pigment−protein complexes are a few pigments and a surrounding protein matrix. In many photosynthetic organisms, including higher plants, green algae, and bacteria, the pigments are chlorophyll variants and carotenoids. These two pigments serve complementary purposes. (Bacterio)chlorophyll are porphyrins with a rigid, planar structure (Figure 4a, center). They serve as the primary light-harvesting molecule (Figure 4b), with a relatively long excited state lifetime (~ns) that allows for energy and charge transfer processes to occur. In contrast, carotenoids are polyenes with a long, floppy structure (Figure 4a, left). They serve as accessory light harvesters by rapidly transferring energy to the chlorophyll. In addition, triplet states are rapidly transferred to the carotenoids. They provide photoprotection by rapid dissipation of these chemically active triplet states.[40] Furthermore, they may also provide additional photoprotection through their short excited state lifetime (~ps) that allows for rapid dissipation of potentially damaging excess energy.[40] Thus, this combination of pigments enables photosynthetic systems to retain both light-harvesting and photoprotective functionalities.

2.2. Protein Dynamics and Spectral Diffusion

One major challenge in describing pigment−protein complexes is characterizing how the protein matrix impacts the pigments. That is, how do fluctuations in the protein matrix impact the electronic excited states (fast dynamics) and what are the conformational substates (slow dynamics). Changes in the excited state energies due to the dynamic protein environment are known as spectral diffusion. Single-molecule spectroscopy provides insight into these multitime scale dynamics.

Single-molecule spectroscopy is a powerful tool for identifying individual conformational substates and elucidating the dynamics that govern the transitions between substates. We use a reaction coordinate picture to describe the potential energy landscape as shown in Figure 4c.[41,42] A rugged landscape exhibits more complex (multitime scale) dynamics than crystalline systems[43,44] due to the variety of potential energy barrier heights between different conformational substates, which create an effective hierarchy of substates, illustrated in Figure 4c.[44−46] Conformational variation results in changes to the fluorescent emission, mediated by perturbation of the interaction between the environmental degrees of freedom and the pigment.[47,48] High energetic barriers between substates (and thus slow dynamics) result in discrete peak positions, known as inhomogeneous broadening. Low energetic barriers (and thus fast dynamics) result in a broadened line shape in absorption and fluorescence spectra, known as homogeneous broadening. The spectral peak of a lone molecule in a protein is significantly broadened (several 100 cm^{-1}) by these faster fluctuations. Although proteins often have a continuum of barrier heights and thus time scales of protein fluctuations, inhomogeneous and homogeneous broadening are divided by protein dynamics longer than and shorter than the time scale of the experiment, respectively.[6,46,49]

In single-molecule experiments, the fluorescence emission exhibits temporal dynamics as the protein switches between conformational substates. Changes in fluorescence emission on the second time scale report on conformational substates with a high potential energy barrier.[11,12,18,50,51] For example, in the bacterial photosynthetic antenna protein complex, LH2, the room temperature fluorescence spectrum showed a temporal change in peak position of a few 100 cm^{-1} on a time scale of seconds.[50,51] Thus, at room temperature, single-molecule observations provide information on slow dynamics, which give rise to the inhomogeneous line width.

On the other hand, fast dynamics, which give rise to the homogeneous line width, is averaged out during the measurement, as indicated by broadened spectral peaks such as those observed for single LH2 complexes.[11,50,51] Indeed, spectral diffusion can occur on a nanosecond scale in a biological system at room temperature, even if the system is at equilibrium.[52] As a result, conformational substates with a low energy barrier in the energy landscape are obscured, even at the single-molecule level.

Cryogenic conditions provide a powerful tool to increase the resolution of protein dynamics and conformational substates. At low temperature, especially liquid-helium temperature, the fast dynamics are slowed down or almost completely frozen[44,52,53] and the lower tier of the energy landscape becomes resolvable.[46,44,52,53] Spectral hole burning verified that spectral dynamics took place on time scales longer than about 100−1000 ms at cryogenic temperature.[53] Thus, cryogenic single-molecule spectroscopy provides access to substates in the lower energy landscape. Cryogenic conditions narrow the spectral line width by freezing out the fast dynamics.[54] By combining cryogenic conditions with single-molecule spectroscopy, we can thus obtain the intrinsic line shapes of single molecules, which reveal the photophysical properties of the embedded pigments.

2.3. Bacterial Photosynthesis

Light-harvesting complexes from purple bacteria are the most widely studied photosynthetic systems at the single-molecule level because of their exceptional photostability. In purple bacteria, photosynthetic light harvesting occurs in membrane structures, known as chromatophores. The chromatophore membrane contains transmembrane pigment−protein complexes, including the peripheral light-harvesting complexes (LH2) and light-harvesting complex 1 (LH1), which surrounds the reaction center (RC).[55] The peripheral light-harvesting complexes perform the initial absorption and energy transport steps. Excitation energy is transferred from the LH2 network to LH1 and then to the RC. The RC sits in the center of the LH1.

DOI: 10.1021/acs.chemrev.6b00195
Chem. Rev. XXXX, XXX, XXX−XXX

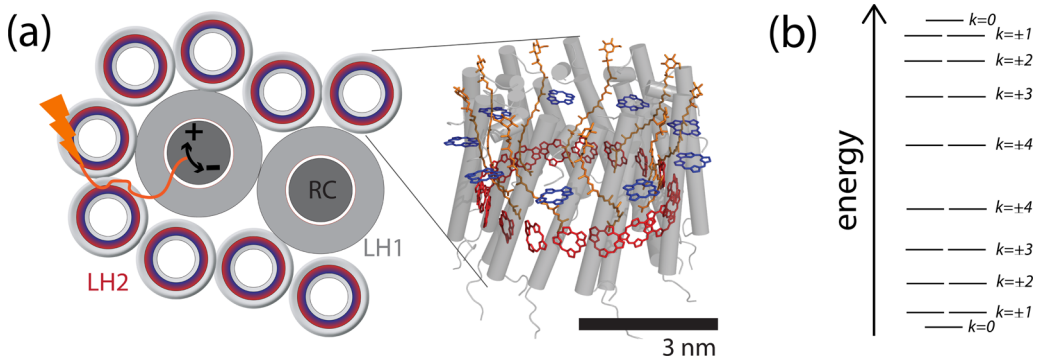

Figure 5. Light harvesting in purple bacteria. (a) The light-harvesting apparatus in purple bacteria consists of antenna complexes (primarily LH2) that surround LH1, which contains a reaction center. Energy migrates from the antenna to the reaction center, where charge separation occurs. LH2 has a cylindrical structure with 8−10 subunits (depending on the species), each of which contains three BChl (red, blue) and one carotenoid (orange). The BChl are organized into two concentric rings, the B800 (blue) and B850 (red) rings.[28,56] (b) Electronic structure of the B850 ring without inhomogeneity. The equivalency of the BChl binding pockets and the strong coupling between the BChl produces a band-like structure in which the excited states are completely delocalized over the 18 BChls that form the B850 ring.[2] In reality, thermally induced inhomogeneity between the subunits is thought to partially localize the excited states.

In this transport process, excitations generally move downhill in energy but must overcome an energetic barrier to reach the RC.[2]

The structures of the peripheral light-harvesting complexes, as well as the organization within the membrane, vary by species and growth conditions. The peripheral light-harvesting complex, usually known as LH2, has a cylindrical structure.[2] This structure for *Rhodopseudomonas (Rps.) acidophila* strain 10050 is shown in Figure 5a. The cylindrical structure emerges from the association of eight, nine, or ten protein subunits depending on growth conditions and species.[56] For example, two well-studied species, *Rps. acidophila* and *Rhodobacter (Rb.) sphaeroides* are nonameric, whereas *Rhodospirillum (Rsp.) mobilizchianum* is an octamer. Furthermore, for certain species, such as *Rhodopseudomonas palustris*, the number of subunits has been shown to change with light conditions.[57] The functional implication of the variation in number of subunits remains an open question.

The cylindrical structure of the LH2 protein gives rise to a ring organization of the BChls. In many species, including the well-studied *Rps. acidophila* and *Rb. sphaeroides*, this produces two concentric BChl rings known as the B800 and B850 rings, named by the wavelengths of their absorption maxima.[28] This LH2 variant is also referred to as B800-850. Depending on the species and growth conditions, the protein structure, and thus the absorption maxima, vary. For example, *Rps. acidophila* strain 7050 grown under low light produces a light-harvesting complex with absorption peaks at 800 and 820 nm, or B800-820 (also known as LH3).[2] For the B800-850 variant of LH2, each subunit contains one carotenoid and three BChls, with one in the B800 ring and two in the B850 ring. In the B800 ring, the BChls are weakly coupled to their neighbors. In contrast, in the B850 ring, the BChls are strongly coupled to their neighbors, which gives rise to excited states delocalized across several pigments.[2,58]

Because of the cylindrical motif, the electronic structure of the B850 ring is often modeled as a circular aggregate. In the absence of disorder, that is, identical transition energies on all pigments, the excited states become delocalized over the entire ring. This delocalization gives rise to a series of doubly degenerate states in addition to two nondegenerate states as illustrated in Figure 5b.[2] The lowest energy state ($k = 0$) is a dark state. The oscillator strength is in the two degenerate states $k = \pm 1$, which are perpendicular to each other across the B850 ring. While the circular aggregate model provides a useful framework, in reality thermal fluctuations destroy the degeneracy of the subunits, which can confine the excited states. Estimates of the resulting delocalization lengths vary from two BChl to near-complete delocalization over the ring. These estimates are discussed in detail in ref 2 and 58.

While LH2 has a relatively low fluorescence quantum yield (~4%), it is more photostable than many other pigment−protein complexes, such as those from higher plants.[59] This, together with the fact that inhomogeneity in the excited state energies of the LH2 is an order of magnitude greater than that of most other photosynthetic complexes,[6] make it an ideal target for single-molecule investigations.

2.4. Plant Photosynthesis

In light harvesting, the general structural organization and mechanisms of higher plants share many similarities with purple bacteria. As in purple bacteria, energy migrates through local networks of light-harvesting complexes to reach a dedicated location, the reaction center (RC), where charge separation occurs. There are two types of photosystems, photosystems I (PS I) and II (PS II), each containing one of two types of reaction centers (Figure 6a−d). In higher plants, light harvesting occurs within membrane stacks, known as the thylakoid, and PS I and PS II are spatially separated within the thylakoid. PS II is found in the stacked region of the membrane known as the grana, while PS I is found in the peripheral membrane area known as the stroma lamellae.[63] Single-molecule studies of PS I have revealed hidden details of the electronic structure, as discussed in section 6. Light-harvesting complexes associate with both PS I and PS II.[6,64] The primary light-harvesting complex of PS II (LHCII) is found in plants and green algae, and single-molecule experiments of LHCII have been particularly insightful.

As shown in Figure 6d, the architectural motif of light-harvesting complexes from higher plants differs from the analogous light-harvesting complexes from purple bacteria. LHCII is a trimeric complex. Within each constituent monomer, the pigments are bound into nonequivalent binding sites. Each monomer contains eight Chl *a*'s, six Chl *b*'s, and four carotenoids.[26] Energy rapidly transfers on a femto- and picosecond time scale from the carotenoids and Chl *b* to Chl

DOI: 10.1021/acs.chemrev.6b00195
Chem. Rev. XXXX, XXX, XXX−XXX

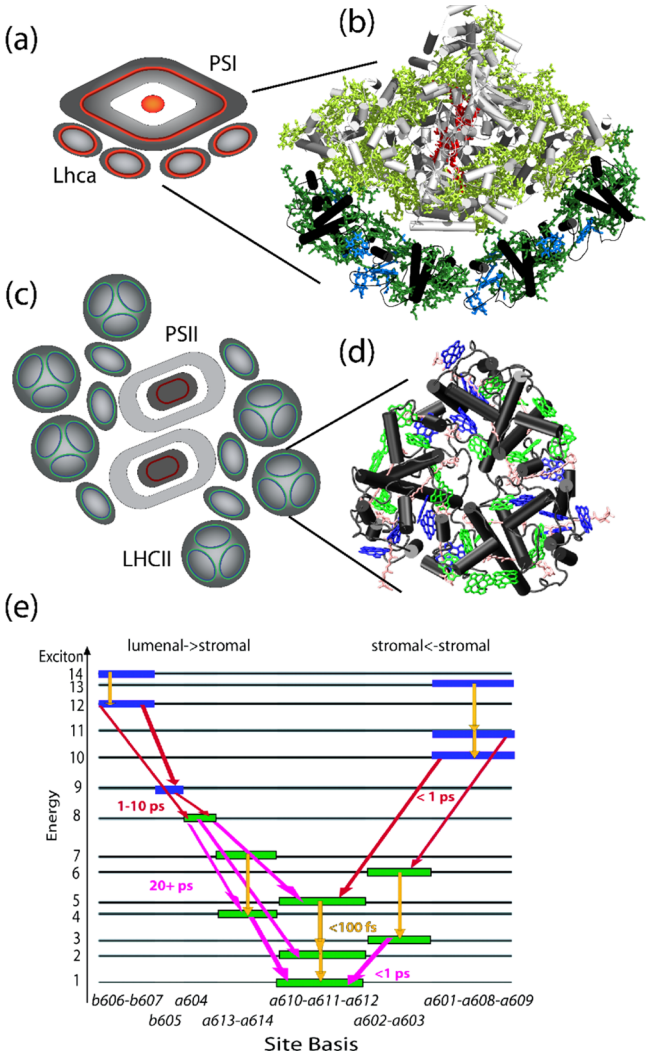

Figure 6. Light harvesting in higher plants. (a) Model of the PS I supercomplex from higher plants. (b) The structural model of the PS I and peripheral antenna Lhca,[60,61] containing 92 Chl *a* (light green) in the core and 45 Chl *a* (green) and 12 Chl *b* (blue) in Lhca (PDB: 4XK8).[60] Electron transfer cofactors are shown in red. (c) Model of the PS II supercomplex from higher plants. The core complexes including the PS II reaction center is surrounded by the primary antenna complex, LHCII. (d) The structural model of a trimeric LHCII, where each monomer contains eight Chl *a* (green) and six Chl *b* (blue) (PDB: 1RWT).[26] (e) Schematic of the pathways of energy flow in LHCII. Energy rapidly relaxes from the Chl *b* (blue bar) to the Chl *a* band (green bar) on a femto- to picosecond time scale. The excited state (exciton) levels are shown with their composition of chlorophyll in the nomenclature of ref 26. Adapted from ref 62. Copyright 2016 American Chemical Society.

a,[62,65] and fluorescence occurs out of the Chl *a* band. Through single-molecule experiments, the intrinsic heterogeneity of this important complex can be explored. Although LHCII has a higher quantum yield (22%) than LH2 (~4%), at the single-molecule level the emission rate is lower due to the photophysics of the triplet state.[59] Despite this limitation, there have been extensive single-molecule investigations, including characterization of the conformational dynamics of LHCII that may play a role in the photoprotective process known as nonphotochemical quenching (NPQ).

Whereas purple bacteria perform anoxygenic photosynthesis, plants, algae, and cyanobacteria perform oxygenic photosynthesis. The advent of oxygenic photosynthesis introduced the four-electron process of water splitting.[1] As a result, the light-harvesting machinery must produce four electrons in quick succession to prevent the formation of reactive intermediates. To achieve this even under low light conditions (e.g., cloudy days), higher plants have an excess of light-harvesting complexes that regulate the energy transport chain so that the amount of excitation energy does not exceed the capacity of the reaction center. This regulation is part of NPQ. NPQ protects the reaction center by preventing absorbed energy buildup, which can form deleterious photoproducts.[66−69]

The short-time component of NPQ is the dissipation of excess energy in the light-harvesting complexes during periods of intense sunlight. While the light-harvesting complexes are known to be the site of dissipation, the molecular mechanism of the dissipation process remains under debate, although several models have been proposed that include conformational changes to produce energy-transfer, charge-transfer, or Chl-carotenoid excited states.[70,71] Single-molecule studies of these light-harvesting complexes have explored the mechanisms, via the conformational dynamics, that may play a role in NPQ.

3. SINGLE-MOLECULE FLUORESCENCE SPECTROSCOPY

Fluorescence spectroscopy is a powerful and ubiquitous tool for two key reasons: (1) the observed fluorescence depends on the population in the excited state, which in turn depends on all processes occurring off the excited state. Thus, multiple processes can be explored via the observed fluorescence; and (2) fluorescence is detected free from the background of the incident laser by spectral and spatial filtering, and thus the signal from single objects is relatively easy to detect. In this section, we discuss experimental considerations, both for the sample and for the apparatus, for a variety of single-molecule fluorescence experiments.

Single-molecule fluorescent detection requires optimization of the signal-to-noise (SNR) ratio. In conventional optical measurements, we detect a signal from a bulk sample containing approximately 10^5 or more molecules. Decreasing the sample size down to a single molecule decreases the signal level, driving the need to optimize the SNR for single-molecule observations. In this section, we describe the three key aspects for optimization, the sample (section 3.1), the optical setup (section 3.2), and the detectors (section 3.3). Specifically, these three aspects require the following: (A) the particle must be sufficiently emissive for single-molecule detection and isolated from other copies or contaminants to minimize background. Meeting this criterion requires a fluorescent signal strong enough to overcome the noise due to the thousands of molecules in the surrounding environment. (B) The optics must be designed to constrain the illuminated area to a small excitation volume to decrease the background and for high collection efficiency of the emission to maximize the SNR. (C) The detector must be highly sensitive with low noise.[72] Experimental design depends on the desired combination of parameters and the time resolution required for these parameters. In single-molecule studies of photosynthetic systems, these parameters are fluorescence intensity, lifetime, anisotropy, and spectrum. Here, we introduce different optical schemes used in single-molecule experiments[73] and current detector technology and trade-offs. We discuss how detection of these parameters is optimized by the sample (section 3.1), the optics (section 3.2), and the detectors (section 3.3), and

DOI: 10.1021/acs.chemrev.6b00195
Chem. Rev. XXXX, XXX, XXX−XXX

how improvements in all these areas have driven progress in single-molecule spectroscopy.

3.1. Sample Considerations

3.1.1. Principles of Fluorescence. Fluorescence is the radiative decay from the electronic excited state to the electronic ground state. As illustrated in Figure 7, upon absorption of a photon, a molecule is promoted to the excited state. After excitation, the molecule can undergo radiative (fluorescence) or nonradiative decay back to the ground state. Thus, fluorescence is only one of many pathways that can occur from the excited state surface. Fluorescence intensity and lifetime depend on the relative time scales of these processes.[74] The fluorescence intensity (I_F) is determined by the following parameters:

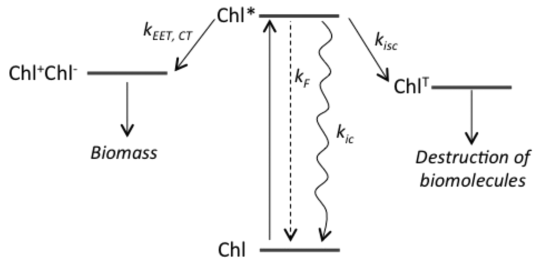

Figure 7. Simplified schematic of photophysical pathways in photosynthesis. Upon absorption of a photon (upward arrow), excited Chl (Chl*) can transfer an electron (Chl^+Chl^-), which drives downstream biochemistry. On a much slower time scale, the excited state can undergo fluorescence decay (k_F, dotted line) and intersystem crossing can produce triplet states (Chl^T), which generate deleterious photoproducts. To prevent photodegradation, photosynthetic systems activate internal conversion (k_{IC}, wiggly line) pathways that safely dissipate excess energy. In higher plants and algae, these processes are known as nonphotochemical quenching (NPQ).

$$\frac{I_F}{\text{Abs}} \propto \Phi_F = \frac{k_F}{k_F + k_{IC} + k_{ISC} + k_P} \quad (5)$$

where the fluorescence intensity (I_F) over absorbance (Abs) is proportional to the fluorescence quantum yield (Φ_F), which is given by the rate of radiative decay (k_F) over the sum of all rates (radiative decay, k_F, internal conversion, k_{IC}, intersystem crossing, k_{ISC}, and charge transfer photochemistry, k_P). The observed fluorescence lifetime (τ_{obs}) is determined by these same parameters, as follows:

$$\begin{aligned}\tau_{obs} &= (k_F + k_{IC} + k_{ISC} + k_p)^{-1} \\ &= (\tau_F^{-1} + \tau_{IC}^{-1} + \tau_{ISC}^{-1} + \tau_p^{-1})^{-1}\end{aligned} \quad (6)$$

where the time scales (τ) are the inverse of the rates (k). From these two equations, we can extract the following relationship,

$$I_F \propto k_F \tau_{obs} = \tau_{obs}/\tau_F \quad (7)$$

As shown by this equation, relative changes in fluorescence intensity and observed lifetime can indicate the parameter changing within the photosynthetic complex. Specifically, proportional changes in intensity and observed lifetime are caused by a change in k_{IC}, k_{ISC}, or k_P. In contrast, more complex scaling between intensity and observed lifetime is caused by a change in k_F or in multiple parameters. Thus, correlated measurements of these two variables allow the microscopic parameter to be determined. This provides insight into the physical mechanism behind changes in the photophysical pathways.[11,18]

Fluorescence spectra can report on the energetics of the excited states. As excited state energies shift, the peak of the fluorescence can undergo a corresponding shift as a signature of these dynamics.

3.1.2. Signal to Background in Single-Molecule Experiments. A single-molecule visible particle must undergo thousands of excitation and emission cycles to allow collection of a sufficient number of photons for analysis. The ability to undergo these cycles emerges from several specific photophysical characteristics, including absorption cross-section, fluorescence quantum yield, and photobleaching quantum yield. These characteristics vary widely depending on the photosynthetic system. This variation allows some systems, such as LH2, to be well studied at the single-molecule level, whereas others, such as the Fenna−Matthews−Olson complex from green sulfur bacteria, cannot be observed at the single-molecule level.[75] Here, we review these photophysical characteristics, which have driven the choice of photosynthetic systems.[72]

First, the particle must have a high absorption cross-section to allow sufficient excitation, which for a molecular dye is often a value comparable to the size (~1 Å^2).[21] Excitation properties are generally reported as the molar extinction coefficient at the maximum of their absorption peak.[76] For chlorophylls, the extinction coefficient is ~70000 cm^{-1} M^{-1} at the maximum of their Q_y absorption (660 nm for Chl *a*).[77]

Second, the particle must be a strong emitter, which comes from two parameters. The first is that the fluorescence quantum yield, Φ_F, as defined in eq 5 above, is high, with a value as close to unity as possible.[76] For photosynthetic antenna complexes, the values are generally 0.04 to 0.10 for chlorophyll-containing complexes and as high as 0.98 for phycobiliproteins.[11,58,78] The second parameter is that the photobleaching quantum yield, Φ_B, is low. The inverse of this parameter, $1/\Phi_B$, reports on the average number of excitation cycles before photobleaching.[21]

Photobleaching is a general term used in single-molecule spectroscopy to describe the photodegradation of a fluorescent particle. This process is hypothesized to occur via radical formation or via a photo-oxidative process, mediated by reactive intermediates generated from the triplet state.[79−81] In single-molecule experiments, photobleaching quantum yield is reduced by the addition of triplet scavengers and by oxygen removal, either through scavengers or deoxygenation with argon or nitrogen.[82,83] At room temperature, most molecular dyes photobleach after the emission of ~10^6 photons.[21] The average number of photons that a specific fluorescent particle will emit before photobleaching is given by Φ_F/Φ_B.[21] While ideally both of these parameters are optimal, for chlorophyll-containing complexes the low photobleaching quantum yield enables single-molecule studies despite the relatively low fluorescence quantum yield. That is, although the signal level is lower than other single-molecule visible systems, extended observation times enable studies of these systems.

In photosynthetic complexes, the pigments are chlorophyll, carotenoids, and phycobilins. The more rigid structure of the tetrapyrroles (chlorophyll and phycobilins) gives rise to a longer excited state lifetime (~ns), because the rigidity decreases the number of vibrationally mediated nonradiative decay channels. The longer lifetime provides a window for solar energy conversion. In many organisms, including higher plants and purple bacteria, chlorophylls are found neighboring

DOI: 10.1021/acs.chemrev.6b00195
Chem. Rev. XXXX, XXX, XXX−XXX

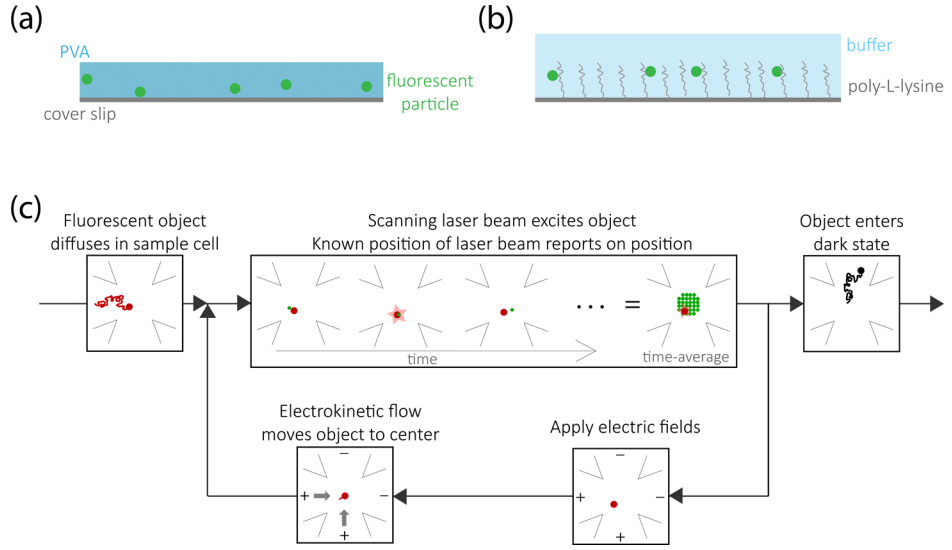

Figure 8. Sample immobilization for single-molecule spectroscopy. (a) Photosynthetic systems can be immobilized by spin-coating at low concentration in a polymer matrix, such as poly(vinyl) alcohol (PVA). (b) In another approach, photosynthetic systems can be immobilized by electrostatic interactions with a poly-L-lysine coated coverslip. (c) The ABEL trap enables extended solution-phase observation of single fluorescent objects. The ABEL trap merges microscopy and microfluidics to implement a closed-loop feedback system. A diffusing fluorescent object enters into an observation region defined by a scanning laser beam. When the laser beam overlaps with a particle, it emits a photon. Because the position of the laser beam is known, upon detection of a fluorescent photon, the position of the particle is known. Electric fields are applied in x and y (the horizontal and vertical axes on the diagram) to induce electrokinetic flow to move the object to the center of the observation region. By repeating this cycle faster than diffusion, the object is maintained in the field of view until it enters a dark state, at which point it diffuses away.

carotenoids and the triplet states have a high efficiency (near 100%) of transfer from the chlorophyll to the carotenoid. This prevents triplet-state-mediated photobleaching and decreases the photobleaching quantum yield. This pathway is thought to play an important photoprotective role under natural conditions as well.[84]

3.1.3. Sample Preparation. To ensure the detected signal arises from only one particle at a time, single-molecule experiments require a dilute sample at ~pM level in which the particles are separated either spectroscopically or spatially. For spatial separation, a distance greater than the size of the point spread function separates target particles. The point spread function is the 3D diffraction pattern of light emitted from an infinitesimal point source, which is transmitted to the image plane via an objective. The plane wave of light produces an Airy disk pattern on the focal plane. The disk size, the diameter of the first dark ring of the diffraction pattern, is given by 1.22 λ/NA, where NA is the numerical aperture of the objective and λ is the wavelength of light. Therefore, the spatial resolution of the fluorescence image in a traditional imaging system is restricted to the wavelength scale of the laser source.[85] In recent years, a suite of imaging techniques have emerged with high spatial resolution beyond diffraction limit.[85,86] However, these approaches are not required for single-molecule spectroscopy on photosynthetic complexes, which is strongly focused on revealing physical and photochemical properties of individual complexes rather than imaging their spatial distributions in vivo. Therefore, the most straightforward approach is dilute samples.

Traditionally, dilute samples have been prepared by immobilizing single proteins at picomolar concentrations through two approaches: (1) encasing the sample in a polymer matrix, such as poly(vinyl) alcohol (PVA), by spin-coating a thin film of sample mixed with polymer onto a coverslip (Figure 8a); and (2) attaching the sample to a functionalized charged surface, such as poly-L-lysine coated coverslip, via nonspecific electrostatic interactions (Figure 8b).

For cryogenic experiments, a dilute sample is spin-coated on a coverslip or placed in a cavity between two coverslips and rapidly frozen to preserve its native state.[87] A cryostat or an insulated Dewar flask is used to maintain temperature.[88,89] The superfluid state of liquid helium under negative pressure is used to achieve temperatures down to 1.5 K.

Upon immobilization, both a polymer environment and electrostatic interactions can introduce perturbations to the true protein structure. Even localized interactions may cause significant structural changes in proteins through allosteric effects.[90,91] The excited state manifold and dynamics of photosynthetic pigment−protein complexes are highly sensitive to angstrom-scale structural changes. As a result, these two immobilization approaches have at times produced conflicting results, which may be due to the effects of the immobilization method. For example, results differ on whether disorder in LH2 emerges from elliptical or localized distortions.[10]

To minimize potential perturbations from immobilization, Cohen and Moerner developed a novel single-molecule technique, the anti-Brownian electrokinetic (ABEL) trap, which merges microfluidics and microscopy to enable extended observation of single particles in solution. The ABEL trap is implemented in a modified confocal microscope, in which the laser beam scans an observation area and the sample is held in a microfluidic cell (Figure 8c).[3,92,93]

The ABEL trap functions via a closed-loop feedback system. The first step is position determination of the single particle under observation. Position determination is achieved by scanning the laser beam. When the laser beam overlaps with the particle, the particle emits a photon. Upon detection of the photon, the particle position is inferred based on the known laser position. The microfluidic cell contains integrated electrodes. Application of a voltage induces an electrokinetic

DOI: 10.1021/acs.chemrev.6b00195
Chem. Rev. XXXX, XXX, XXX−XXX

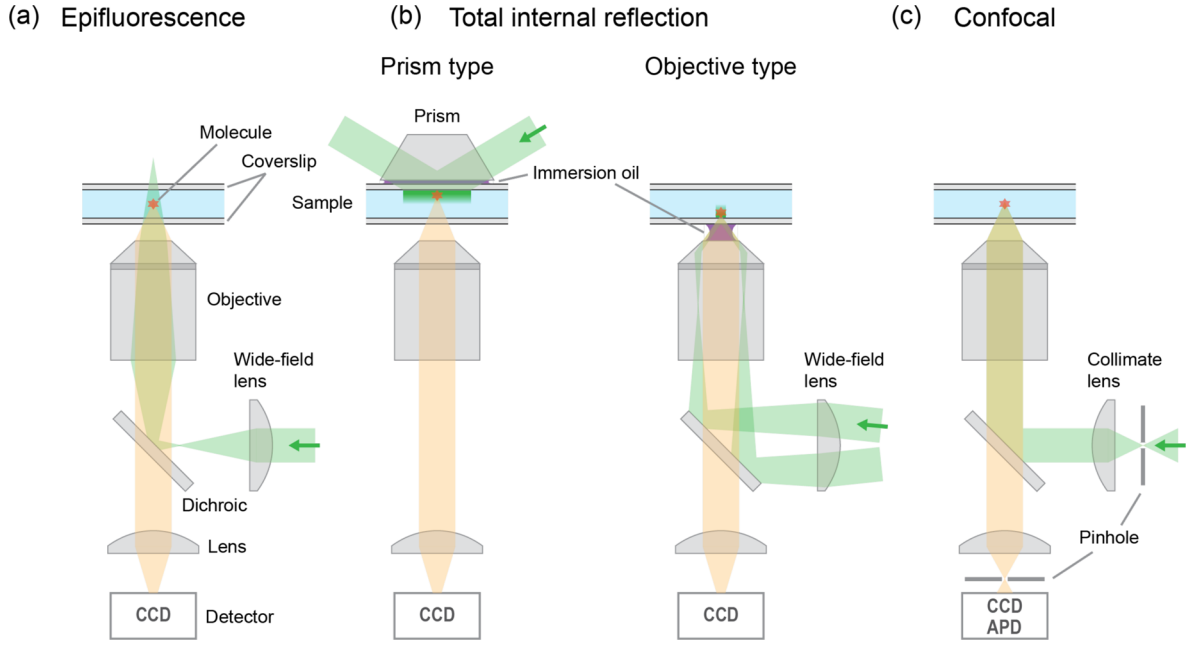

Figure 9. Schematic of the fluorescence microscopes generally used for single-molecule experiments. (a) Epifluorescence or wide-field microscopy. (b) Total internal reflection fluorescence microscopy employing prism (left) and objective (right) to induce an evanescent light field close to the coverslip surface, where index-matching immersion oil is necessary. (c) Confocal microscopy where a CCD detector is used to measure fluorescence spectrum of single molecule. The excitation and fluorescence light are shown in green and orange, respectively. CCD detector in confocal microscopy is used to measure fluorescence spectrum of single molecule. In these microscopies, a liquid immersion (oil, water, or silicon) objective is often utilized for high resolution observation with a high NA of more than 1.

flow that returns the particle to the center of the observation region. Repeating this cycle on a microsecond time scale counters the millisecond process of diffusion. In more recent incarnations of the ABEL trap, position estimation is refined using knowledge of particle diffusion and real-time estimates of diffusion parameters. Thus, the ABEL trap has been used to simultaneously measure both photophysical parameters (fluorescence emission intensity, lifetime, and spectrum)[11,12] and structural parameters (diffusion coefficient and mobility, reporting on size and charge, respectively).[93,94] The ABEL trap is not limited to report on excited state properties but also processes such as oligomerization or dissociation. While there are many approaches to study photosynthetic systems, the solution-phase environment in the ABEL trap is a new platform particularly well-suited to investigate heterogeneity and dynamics of soluble photosynthetic proteins.[11,12,15,18,95]

On the other hand, the ABEL trap has several drawbacks. First, it is much more difficult to construct than a traditional single-molecule confocal experiment, as it requires fabrication of the microfluidic sample cells and extensive coding to implement the closed loop feedback system. Second, the ABEL trap does not work well for dim emitters or to study blinking (entering of dark states). It relies on position determination via photon detection, which requires a certain photon detection rate to maintain trapping. Therefore, dim emitters do not provide sufficient photons and blinking events cause the object to diffuse out of the trapping region. Third, the trap requires an electric field to induce electrokinetic flow for trapping. An electric field can induce structural or energetic changes, such as by the Stark effect. However, for photosynthetic systems, the field strengths are 1 to 2 orders of magnitude below those used in Stark experiments.[96]

The final consideration for sample preparation is the solution surrounding the photosynthetic system. The components of the buffer are critically important for maintaining the native state of the protein. First, for membrane proteins, low detergent concentration causes aggregation or other structural changes, which can induce photophysical changes.[97] In some single-molecule experiments, these effects have been used to explore aggregation-induced photophysics. Second, glycerol is often added to prevent evaporation or as a cryoprotectant, yet glycerol has been shown to alter the photophysics.[98] This has been extensively characterized for PS I at the single-molecule level.[98,99] However, ensemble studies have also shown that glycerol impacts the photophysics in other photosynthetic systems, such as the Fenna–Matthews–Olson complex from green sulfur bacteria.[100] In combination, these studies suggest that glycerol should be added with caution, if at all, to the solution for studies of photosynthetic systems.

3.2. Fluorescence Microscopy Techniques for Single-Molecule Measurements

Several microscopy techniques have been used for photosynthetic systems. The choice of technique depends on the experiment, including the desired observables (intensity, lifetime, polarization, spectrum), time resolution, speed of data collection, and parallelization. Here, we review commonly used techniques.

3.2.1. Wide-Field Epifluorescence Microscopy. Wide-field epifluorescence microscopy has long been used to observe the cell tissues and subcellular structure of organisms. The introduction of fluorescent dye labeling techniques allowed further access to the cell interior and to proteins at the single-molecule level. These advances have extended the application of single-molecule microscopy to many fields of research.

Conventional epifluorescence microscopes were initially shown to enable single-molecule observations by suppressing background and stray light.[101] Figure 9a shows a schematic

DOI: 10.1021/acs.chemrev.6b00195
Chem. Rev. XXXX, XXX, XXX−XXX

representation for an epifluorescence microscope, in which noncollimated excitation light diffused by a lens is weakly focused onto the sample and illuminates an area of around 10 μm in diameter on the focal plane of the objective. Fluorescence from each molecule is collected by the same objective, isolated from the excitation light using a dichroic mirror and emission filters, and detected as a 2D image by a CCD detector. If the fluorescence intensity is higher than the background, including luminescence, scattering, and stray light from the substrate, solution and the optical system itself, then individual molecules can be observed as bright spots.

Obtaining a clear image with high spatial resolution requires efficient collection of the weak fluorescence from a single molecule. For efficient collection and high spatial resolution, the choice of objective numerical aperture (NA) is important. The NA is described by

$$\mathrm{NA} = n \times \sin\theta \tag{8}$$

where n is the refractive index of the medium between the target molecule and the objective, and θ is the half-opening angle of the objective. The minimized focal spot size is the diffraction-limited spot, and the diffraction-limited sizes along the focal plane of the objective (xy-plane) and along the perpendicular optical axis (z-axis) become smaller in proportion to NA and NA^2, respectively. As the spot size becomes smaller, the spatial resolution of the image improves and background light decreases. Therefore, the NA should be as high as possible. Typically, single-molecule observations utilize liquid (oil, water, or silicon) immersion objectives. An oil (n = 1.52) immersion objective exhibiting a high NA of >1.4 is useful for observing a single molecule close to the coverslip surface, as is the case in spin-coated samples, because the refractive index of oil matches well with that of the coverslip, thus eliminating any optical aberrations. If the target molecule is in aqueous solution or inside a cell, water (n = 1.33, NA = ~1.2) and silicon (n = 1.40, NA = ~1.3), respectively, are better choices for the immersion objective. Although these media provide lower NAs, spherical aberration due to mismatched n is suppressed.[102−104]

3.2.2. Total Internal Reflection Fluorescence (TIRF) Microscopy. Although epifluorescence microscopy can be used to simultaneously observe an entire wide-field image containing many individual particles, it suffers from background luminescence from the illumination of out-of-focus fluorophores. One method for background luminescence suppression in wide-field measurements is to restrict the volume of illumination, which can be achieved using total internal reflection fluorescence (TIRF).[105,106]

In TIRF microscopy, the evanescent light field induced by total internal reflection is used for illumination. This evanescent light field occurs on the interface between two dielectric media with different refractive indices and decays exponentially as a function of distance from the interface.[105,107,108] For example, the penetration depth of the evanescent field of a 532 nm light source is estimated to be 100−200 nm, depending on the incident angle.[107−109] Therefore, the area to be illuminated is confined to the immediate vicinity of the interface, thereby suppressing background luminescence.[73]

TIR is usually created using a prism or an objective. Figure 9b, left, shows a schematic of the prism-type TIRF microscope, in which the evanescent field is induced on the boundary between the sample and the coverslip on the side opposite to the objective.[110] The prism can induce a broad evanescent field[111] and is thus used to widen the optical field-of-view. However, because the objective gathers fluorescence radiated from the other side, its working distance must be long and the sample medium should be made as thin as possible. These requirements are removed in the objective-type TIRF microscope,[112] in which excitation light is focused on the back focal plane at the edge of the objective with a high NA so that the evanescent field occurs on the objective side instead (Figure 9b, right). Nonetheless, the optical field-of-view in the objective-type TIRF is restricted, and the SNR is deteriorated by an increase in light scattering within objective.

TIRF microscopy was used to investigate heterogeneity in the transition dipole moments and fluorescence spectra of single chlorosomes, the light-harvesting antenna from green sulfur bacteria.[14,113] The highly polarized evanescent field,[107] which leads to variations in the excitation efficiency of the molecule depending on the orientation of the molecular transition dipole moments, allowed structural dynamics and nanoscale geometry to be monitored at the single-molecule level[114,116]

3.2.3. Confocal Microscopy. TIRF microscopy is often used to produce a 2D image of the surface of the specimen with low background luminescence and permits simultaneous observation of multiple single molecules. On the other hand, confocal microscopy is used to probe the interior of biological specimen as well as molecules in solution. Notably, in confocal microscopy, we can achieve rapid and multiparameter detection, including fluorescence intensity, lifetime, polarization, and spectra. Figure 9c shows the schematic setup for confocal microscopy.

The essential difference between a confocal microscope and the wide-field microscopes described in the first section is the use of pinholes. In a confocal microscope, excitation light is passed through a pinhole and focused onto the focal plane of the objective at the diffraction limit to illuminate a restricted elliptical volume of <1 μm^3 = 1 femto L. Out-of-focus background light is cut off by the pinhole on the detector side so that only fluorescence from the focal spot is detected with a high signal-to-background ratio.[73] An APD detector with high sensitivity and low dark noise allows for detection of weak single-molecule fluorescence. A 3D fluorescence image can also be obtained by scanning the position of the specimen and/or laser spot. In one approach, the sample position is scanned with a piezoelectric stage. In a second, $x-y$ (2D) laser scanning is achieved by changing the incident angle of the excitation light with a tilting mirror[117−120] or a moving stage.[121,122] z-Axis (3D) laser scanning can also be performed by changing the divergence of the incident beam.[122]

In solution or a cellular matrix, fluorescence from a single target molecule is often obscured by other light sources, including autofluorescence. The major advantage is that confocal microscopes can be used to make point observations when a single molecule is located on the focal spot so that it is the dominant source of fluorescence for that restricted area. Because of this advantage, confocal microscopy is the most common technique for single-molecule spectroscopy on photosynthetic systems.

The detection system can be designed to observe the desired combination of fluorescence brightness (intensity), polarization, lifetime, and spectrum. By combining confocal microscopy with time-correlated single photon counting (TCSPC) that enables time-tagged photon detection, fluorescence lifetimes on the scale of nanoseconds can be measured

DOI: 10.1021/acs.chemrev.6b00195
Chem. Rev. XXXX, XXX, XXX−XXX

for individual molecules.[123] A commonly used version of confocal microscopy for single-molecule studies of photosynthetic systems detects the fluorescence spectrum by using a CCD spectrometer instead of an APD detector. A line-scanning spectromicroscope allows for rapid measurement of the fluorescence emission spectrum at any position in 3D space with diffraction-limited resolution. This technique has, for example, permitted spatial mapping of the stoichiometric ratios between photosynthetic components in cyanobacterial cell.[124] Scanning the excitation wavelength while monitoring fluorescence intensity provides the fluorescence excitation spectrum, which is related to the absorptive properties of single molecules. Both excitation and emission spectra were also measured in a single molecule to investigate the correlation between the spectral properties of the ground and excited states.[125] By incorporating a wave plate in the laser or detection path and rotating polarization angle of the excitation and emission lights, we can also estimate the angle of the transition dipole moment of single molecule. The polarization analysis has revealed dynamics in the excitonic structure of light-harvesting complex[9,126] and been utilized to identify spectrally overlapped emitters in a large pigment−protein complex.[127]

3.2.4. Cryogenic Microscopy. As described above, the objective lens must be positioned as close to the sample as possible in order to maximize the collection solid angle for detection of single-molecule emission. For experiments at room temperature, high NA aberration-corrected compound objectives, composed of multiple lenses, can be easily obtained. In cryogenic experiments, however, samples are often located in the cooling space, or immersed in a liquid refrigerant as shown in Figure 10a, i. This prevents delicate high-quality objectives from being used because the refrigerant may distort or even damage the optics. As such, cryogenic microscopy requires special objectives and setups as shown in Figure 10b. This is an especially important consideration for reaction center-containing photosynthetic systems. Even at low temperatures, count rates for these systems are as low as tens of counts per second. Many important single-molecule experiments on photosynthetic systems have been performed at cryogenic temperatures and have required highly efficient objectives compatible with cryostats. Thus, a major experimental challenge is the development of objectives, which motivates the discussion here.

First, the objective may be positioned inside or outside of the cryostat (Figure 10a, i and ii, respectively), the former being preferred in early cryogenic spectroscopy of single molecules embedded in a crystalline matrix.[128] Single molecules were illuminated by a diffraction-limited light beam produced by lens,[129−131] concave parabolic mirror,[132] pinhole,[133] or optical fiber[8] placed near the sample within the cryostat (Figure 10b, i−iv, respectively). The first cryogenic single-molecule spectrum of the biological complex, LH2, was observed with an aspheric singlet with NA = 0.55 incorporated into a confocal microscope.[117,134] Gradient index optics with a NA of 1.08 increased the collection efficiency in cryogenic experiments (Figure 10b, v).[118] While an improvement, singlet lenses cannot correct chromatic aberration.

To compensate for aberration, alternative objectives have been developed, including: (1) A compound objective with NA = 0.85 at liquid helium temperatures (Figure 10b, vi);[119,135] (2) a solid immersion reflective object with NA = 0.72 that corrects chromatic aberration and was developed especially for cryogenic microscopy (Figure 10b, vii);[136] and (3) a new Schwarzschild-type reflective object (NA = 0.6) that consists of

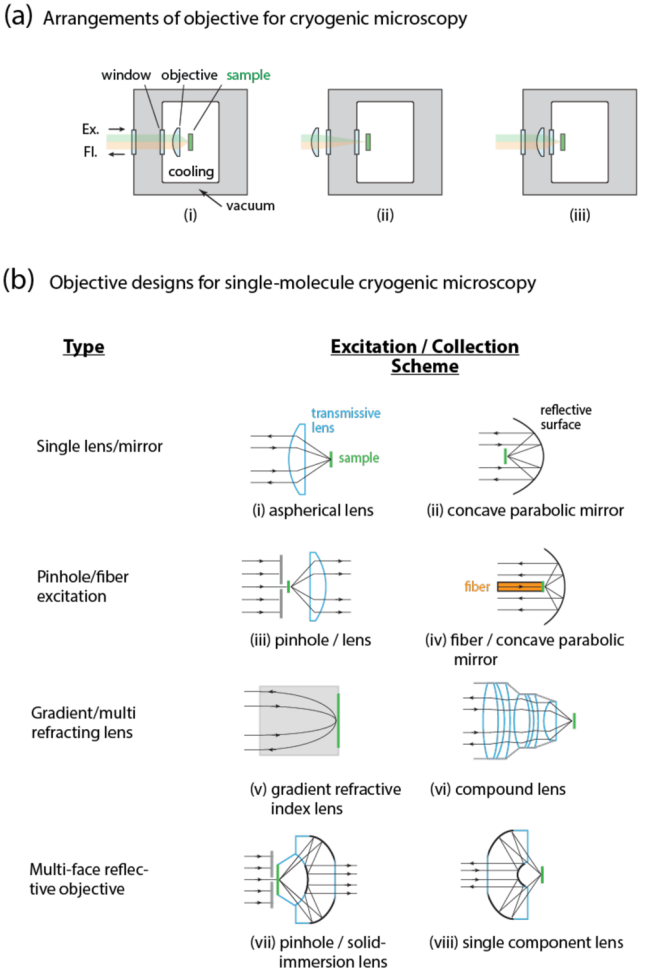

Figure 10. (a) Arrangement of the objective within a cryogenic microscope. The objective is positioned close to a sample inside (i) and outside (ii) the cryostat or in the vacuum space (iii). (b) Schematic of various objectives designed for high collection efficiency while maintaining the sample at cryogenic temperatures. Excitation of the sample and collection of fluorescence were achieved by (i) aspherical lens, (ii) concave parabolic mirror, (iii) pinhole/lens, (iv) optical fiber/concave parabolic mirror, (v) gradient refractive index lens, (vi) compound lens, (vii) solid immersion reflecting objective, and (viii) single component reflecting objective. Transmissive objectives and reflective surfaces are shown by bold lines in light blue and black, respectively. The green bold line represents a sample plane.

a single fused silica piece with two spherical mirrors coated on two opposite surfaces (Figure 10b, viii),[137] which reduces optical aberrations and is robust against the cold. Further improvements decreased the spherical aberration[138] and expanded the use of cryogenic microscopy into the IR region,[139] enabling broad wavelength regimes[121,139] and two-photon excitation experiments.[140] The latest model, in which one of the coupled mirrors has an aspherical curve, has achieved an NA of almost unity (0.99).[141,142] Meanwhile, immersion objectives were also used at low temperature[143,144] and enabled high NA (1.25) observation,[145] although they can work only at temperatures higher than the melting point of the immersion fluid (liquid propane, iso-pentane, or propanol).

Another method for resolving optical aberrations in single-molecule spectroscopy involves placing the high-quality compound objective outside the cryostat (Figure 10a, ii).

DOI: 10.1021/acs.chemrev.6b00195
Chem. Rev. XXXX, XXX, XXX−XXX

However, in such cases the NA must be relatively low (~0.6) because the optics are far away from the sample.[146,147] Recently, a novel setup, in which the compound objective was placed in the vacuum space in the vicinity of the sample (Figure 10a, iii) has permitted high NA (0.9) observation of single molecules at cryogenic temperature.[120] This setup can also be beneficial for measurements at temperatures higher than the boiling points of liquid helium (4.2 K) and nitrogen (77 K) because the space between the objective and the sample is filled by vacuum instead of with liquid refrigerant, eliminating the effect of vibrations caused by refrigerant boiling. As such, sophisticated objectives with near-maximum NA and no aberration have the potential to extend the application of cryogenic single-molecule spectroscopy to many light-harvesting systems that, while intriguing, have so far not been investigated due to their low fluorescence quantum yield such as photosynthetic reaction centers from different species.

As discussed previously, single molecules can be resolved either spectroscopically or spatially under cryogenic conditions. Spectroscopic methods have primarily been applied to the observation of single molecules doped in a crystalline matrix.[8,131−133,148−150] For such experiments, the microscope does not require a scanning system to obtain fluorescence images and to trace the position of the target molecule in its focal spot.[8,130−133] However, in most single-molecule measurements of light-harvesting system, targets are spatially dispersed and observed individually with a confocal microscope. In cryogenic confocal experiments, the laser scanning system is positioned outside of the cryostat and is therefore easy to control but requires more space and does not allow perfect in-plane scanning due to angular dispersion. Another scanning system involves scanning the sample position directly with a piezoelectric stage located in the cryostat and cooled together with the sample.[135,141,151] The range for precise scanning of piezoelectric stages under cryogenic conditions is limited to approximately a few tens of micrometers, so a fine-movement piezoelectric stage is often stacked on top of another stage with a larger but coarser travel range to permit wide scanning.[151]

Cryogenic spectroscopy has an additional technical benefit that results from the narrowing of the spectral line width, which enhances the absorption cross section. The fluorescent power saturation of single molecules occurs at a much lower excitation power at cryogenic temperatures (~100 mW/cm^2) than at room temperature (~100 kW/cm^2).[129,152] This removes the need for intense excitation light, which decreases the amount of undesirable background emission. Added to this, the photodamage by the excitation light is mitigated at cryogenic temperatures, resulting in a reduced probability for photobleaching of the target molecule.[153,154] As a result, long acquisition times and averaging times become possible, enabling the conformational substates to be characterized and the dynamics between them to be monitored. The long averaging times are especially important for photosynthetic samples because they often exhibit very low fluorescence quantum efficiency, as in LH1 (8.1%), LH2 (9.9%),[58] and LHC II (22%)[155] at room temperature.

The first cryogenic single-molecule spectrum was obtained for a molecule doped in a solid in which the absorption spectrum was measured with double frequency modulation.[5] Subsequently, fluorescence excitation spectra were also obtained at cryogenic temperatures with enhanced signal-to-noise ratio.[8] This approach was used in the first observation of the pigment−protein complex, LH2,[117] and has since been applied to many light-harvesting, photoreceptive systems, including the photosynthetic complexes of LH2[54,156,157] and low-light LH2-analogues,[158−161] LHCII,[162] chlorosomes,[4,14,115,163] the photosynthetic antenna-reaction center complexes of LH1−RC,[164−166] PS I,[127] and PS II.[167,168]

3.2.5. Advanced Microscopy Techniques. In addition to the conventional microscopies above, several other more advanced techniques have been developed. Scanning probe microscopy (SPM) has been widely applied to single-molecule studies.[169] In the near-field scanning optical microscopy (NSOM or SNOM) using an aperture probe,[170] the tapered single mode fiber probe provides a small illumination area through an evanescent wave near the tip end.[171] Scanning the sample or probe position while collecting fluorescence from a single molecule with a far-field objective produces an image at spatial resolution below the diffraction limit.[171,172] While NSOM is not necessary for single-molecule spectroscopy of dilute samples, and thus has not been used for single-molecule spectroscopy of photosynthetic systems, it has been applied to spatially resolve energy transfer through arrays of photosynthetic complexes[173] and to detect the photocurrent induced in photosynthetic reaction centers.[174−177]

NSOM is only one of several approaches that have been developed to resolve objects below the diffraction limit. Other superresolution techniques include those that rely on a sparse subset of emitters (e.g., PALM/STORM) or engineering of the point-spread function (e.g., STED).[178] Because photosynthetic membranes are crowded, techniques that require a sparse subset of emitters at a given time are not straightforward to implement. However, in future experiments, point-spread function engineering may allow heterogeneity in these systems to be studied in situ.

In the experimental apparatuses described in the previous sections, single-molecule fluorescence experiments measure the properties of fluorescence after excitation by a single photon. The fluorescence lifetime is on a nanosecond time scale for photosynthetic complexes, limiting the time resolution. In a technological step forward, van Hulst and co-workers have applied a technique they pioneered, known as smPP (single-molecule pump probe) spectroscopy, to LH2.[179,180] In this technique, there is a two-pulse excitation scheme or a single beam that has a temporal profile with a controllable delay between different frequency components of the beam. Fluorescence intensity is monitored as a function of the time delay between the two beams or the frequency components. The delay time encodes femtosecond time scale information on the fluorescent signal.[181,182] The van Hulst group used this approach to explore excited state coherences.[179] From this data, the authors reported heterogeneity in the frequencies and time scales of the coherences for single LH2 complexes. In addition, van Grondelle and co-workers used this approach to investigate the heterogeneity in energy transfer dynamics.[183] Future experiments will undoubtedly extend this technique to other complexes and questions.

3.3. Detectors and Data Analysis

The primary observables for single-molecule experiments are fluorescence intensity, lifetime, polarization, and spectrum. The first three observables can be detected on single-element detectors, whereas fluorescence intensity, polarization, and spectra can be detected on array detectors. Here, we discuss the benefits of different detectors and detector technology and how

DOI: 10.1021/acs.chemrev.6b00195
Chem. Rev. XXXX, XXX, XXX−XXX

the detected signal can be analyzed to reveal the desired microscopic parameters.

3.3.1. Detectors. The major considerations for detectors are: (1) sensitivity because of the weak fluorescent emission of a single molecule, which is reported as quantum efficiency; (2) noise, including dark noise and readout noise; (3) pixel size; and (4) time resolution, which is particularly important for fluorescence lifetime measurements. Here, we discuss these considerations for different detector technologies.

Detectors used for single-molecule measurements[184−186] can be organized into two main classes: (1) single-element and (2) array. Single-element detectors are primarily used in confocal microscopy. These devices detect photons with high efficiency and time resolution. In single-molecule experiments, time-correlated single-photon counting (TCSPC) is used to measure fluorescence lifetime. In TCSPC, a pulsed laser excites the sample, inducing fluorescence emission. The fluorescent photon is detected with an instrument response time of tens to hundreds of picoseconds, depending on the detector, and the detection time is recorded with a precision determined by the detection electronics (as low as 4 ps). Subsequent analysis is then used to extract the lifetime.

Array detectors (most commonly 2D arrays) access the spatial distribution of the photons, but lifetime data is not detectable. Array detectors record 2D images for epifluorescence (wide-field) and total internal reflection fluorescence (TIRF) techniques or a fluorescence spectrum with confocal microscopy, where the fluorescence is spectrally dispersed on the photosurface of the array. In the following sections, we elaborate on the advantages of different types of detectors. The nature of the sample parameters (signal level, time scale, etc.) drives the choice of detector.

3.3.1.1. Single-Element Detectors. Single-element detectors are the major tools for measurement of fluorescence intensity and lifetime. Thus, the primary considerations are sensitivity and time resolution. Early experiments involving observations of single molecules used photomultiplier tube (PMT) detectors,[8,187] which employ CsTe, GaAsP, and GaAs photocathodes exhibiting quantum efficiencies of ∼30% for UV light, ∼45% for visible light, and ∼15% for near-IR light. Although they have temporal resolutions of a few hundred picoseconds and large detection diameters of approximately 10 mm, PMT are inherently fragile because even brief overexposure to light can induce a high voltage that can damage the detector.

The introduction of single-photon-counting avalanche diodes (SPADs) with high quantum efficiency has facilitated the observation of single-molecule fluorescence.[188] In the visible region, the quantum efficiency of a typical thick reach-through SPAD has been shown to reach >70%.[189] While the temporal resolution is similar to that of the PMT, its detection area (∼150 μm) is much smaller. For measurements of short fluorescence lifetimes, the thin reach-through SPADs provide higher temporal resolution (<100 ps).[190,191] While these detectors traditionally have lower QE, the QE has been improved in the recently developed red-enhanced thin SPADs.[192]

Hybrid photodetectors (HPDs) were also developed with improved signal-to-noise ratio, pulse height resolution, and timing resolution. HPDs are a PMT employing a silicon avalanche diode (AD) instead of traditional multiple dynodes as electron multiplier. HPDs enable photon counting measurements with a temporal resolution of less than 100 ps.[193]

3.3.1.2. Array Detectors. Single-element detectors provide high sensitivity and time resolution for single-molecule experiments. However, single molecules often require long acquisition times to accumulate enough data for statistical analysis. Therefore, to parallelize the observation of single molecules, the two-dimensional array detectors described below have been utilized for wide field observations. Furthermore, these array detectors enable spectrally resolved fluorescence measurements. Recently, one-dimensional array detectors have emerged as an alternative for both spectrally resolved and lifetime measurements.[111]

The charge-coupled device (CCD) camera is the most common 2D array detector and is available in a variety of frame rates, pixel sizes and counts, quantum efficiencies, dynamic ranges, and noise levels, including thermal, shot, and read-out noise. The wide range of instrumental parameters makes the choice of CCD specific for the set of microscopic parameters. For single-molecule measurements, CCD cameras with high sensitivity and low noise are used to maximize the detection of the emitted photons.

CCD cameras can either be front-illuminated or back-illuminated depending on the location of the polysilicon electrode. In a front-illuminated (FI) CCD, the polysilicon electrode that coats the surface of the array absorbs some incident light, leading to a low QE of <40% for visible light and almost 0% for UV light. A back-illuminated (BI) thin CCD lacks the polysilicon substrate. BI-CCD has a QE of >90% in the visible region and >40% even in the UV region.[194] However, the read-out noise increases with high frame rate and the cost is higher than the FI-CCD. A fully depleted BI-CCD increases the QE in the NIR region to ∼90%.[195] Because of the high QE, BI CCDs are used for single-molecule measurements.

High signal-to-noise ratios comes from either cooled CCDs or intensified CCDs, including intensified CCD (I-CCD), electron-bombarded CCD (EB-CCD), and electron multiplication CCD (EM-CCD). For experiments in which a high signal-to-noise ratio is valued over fine time resolution, cooled CCDs become the appropriate choice. Cooling the detector to around −100 °C by liquid nitrogen or Peltier element significantly reduces thermal noise and thus allows the long-time accumulation of photoinduced charges to supersede the read-out noise.

On the other hand, high frame rates (fine time resolution) can be achieved with intensified CCDs. Early single-molecule experiments used I-CCDs or EB-CCDs. Notably, the I- and EB-CCD cameras multiply photoelectrons ejected from a photocathode, and thus their QEs depend on not only a CCD chip but also on the material of the photocathode. The I-CCD is composed of a photocathode input plane, a microchannel plate (MCP), and a phosphor screen in addition to the standard CCD array.[196] The incident photons are converted into photoelectrons on the input plane and accelerated toward the phosphor screen by a high voltage field. When passing through the MCP, many secondary electrons are induced by collision of the photoelectrons with the walls of the MCP and induce photon production at the phosphor screen, which is coupled to the CCD by a lens or fiber. The resultant output then is an intensified image of the sample. Depending on the photocathode material, the QE is as high as ∼40% in the visible and ∼20% in the near-IR region.[184] However, these values are still small compared to the cooled and EM-CCDs (described below) that require no photocathode. Additional drawbacks include the need for high voltage, which makes I-CCD

DOI: 10.1021/acs.chemrev.6b00195
Chem. Rev. XXXX, XXX, XXX−XXX

Table 1. Comparison of the Advantages and Applications of Various Single-Element and Two-Dimensional Array Photodetectors

type	detector	quantum efficiency	advantages	applications
single-element	PMT	30% (200 nm)[a]	high gain	time-sensitive experiments
		45% (600 nm)	wide photosurface	
		15% (800 nm)		
	HPD	35% (350 nm)[b]	wide photosurface	FCS
		45% (600 nm)	high time resolution	short fluorescence lifetime measurements
		15% (800 nm)	low after-pulsing	
	SPAD (thick)	25% (400 nm)[c]	high QE	weak light detection
		75% (600 nm)	low dark count	
		60% (800 nm)		
	SPAD (thin)	20% (400 nm)[d]	low dark count	TCSPC
		55% (600 nm)	high time resolution	Short fluorescence lifetime measurements
		40% (800 nm)		
2D array	CCD (back-illuminated)	60% (400 nm)[e]	High QE	weak/rare photon detection
		80% (600 nm)		
		90% (800 nm)		
	CCD	90% (400−800 nm)[f]	high QE	high SNR without fast frame rate requirement
	(cooled)		low noise	
	CCD (image-intensified)	35% (400 nm)[g]	ultra high frame rate (~GHz)	time resolved imaging
		45% (600 nm)	larger gain than EB- and EM-CCDs	visualization of fast dynamics
			analogue and digital compatible	
	CCD (electron-bombarded)	35% (400 nm)[g]	higher spatial resolution than I-CCD	fluorescence imaging at low light level
		45% (600 nm)	lower multiplication noise than EM- and I-CCDs	
	CCD (electron multiplication)	55% (400 nm)[h]	high QE	weak/rare photon detection
		95% (600 nm)	multiplication with no photocathode	fluorescence spectroscopy of single molecule
		70% (800 nm)	high spatial resolution	localization based super resolution microscopy
			high frame rate (~kHz)	
			resistance to excess exposure	
	CMOS	40% (400 nm)[i]	very high frame rate (~MHz)	time resolved imaging of single particle
		80% (600 nm)	lower cost than CCD	
		50% (800 nm)		

[a]CsTe, GaAsP, and GaAs photocathodes, respectively. [b]Bialkali, GaAsP, and GaAs photocathodes, respectively.[207] [c]τ-SPAD.[189] [d]Red-enhanced SPAD.[208] [e]Fully depleted BI-CCD camera.[195] [f]For example, Andor Technology's BEX2-DD type BI-CCD camera. [g]GaAsP photocathode. [h]For example, Hamamatsu Photonics' ImagEM X2 EM-CCD camera. [i]For example, Hamamatsu Photonics' ORCA-Flash4.0 V2 CMOS camera.

especially vulnerable to excess illumination, and noise due to the fluctuation of the amplification factor. Nevertheless, I-CCDs do have some advantages: (1) the dynamic range can be widened from the analogue region for intense light to the digital region for photon-counting by adjusting the MCP gain, and (2) the I-CCD can achieve nanosecond time resolution for time-resolved imaging by rapidly controlling the voltage applied to the MCP. In the EB-CCD, photoinduced electrons are accelerated with high voltage of a few kilovolts and bombarded onto the CCD surface, where the impact energy generates a flux of secondary electrons.[197] This simplified structure provides higher spatial resolution and lower excess noise than the I-CCD.

EM-CCDs have emerged as the most ubiquitous camera for single-molecule experiments because of their low noise and high sensitivity. The EM-CCD is an intensified camera in which the signal can be enhanced several thousand-fold on each CCD chip before analogue-to-digital conversion in order to overcome the read-out noise.[198−200] This contrasts with other intensified CCDs, where signals are amplified before arrival at the chip. Nevertheless, the EM-CCD has the same basic architecture as other cooled CCDs. The back-illuminated thin CCD provides a high quantum efficiency of >90% in the visible region.

DOI: 10.1021/acs.chemrev.6b00195
Chem. Rev. XXXX, XXX, XXX−XXX

Furthermore, by prolonging the accumulation time with low amplifier gain and cooling down to reduce noises, the EM-CCD can also operate as a highly sensitive standard CCD camera. By binning pixels, the frame rate of <100 Hz with full frame resolution can be increased to 1000 Hz.

The complementary metal-oxide semiconductor (CMOS) camera is an alternative technology that has become increasingly popular for single-molecule experiments. CMOS performance has improved to be competitive with that of CCDs. CMOS employs system-on-chip design where each pixel chip executes independent analogue-to-digital conversions. This has allowed the rapid read-out of data in real time and high-speed imaging with ∼10 μs time resolution.[201] As in intensified CCDs, CMOS has been combined with EB tubes (EB-CMOS)[202] and MCP (I-CMOS).[203,204] The quantum efficiency of the CMOS has traditionally been significantly lower than that of the EM-CCD. However, recent products have improved this to ∼80% in the visible region. Additionally, CMOS cameras are generally offered at a lower cost than EM-CCDs. Thus, these new developments in 2D array detector as well as in some multipixel detectors such as HPD[205] and SPAD arrays[206] will expand the available instrumentation for single-molecule experiments (Table 1).

3.3.2. Data Analysis. Analysis of the detected fluorescence is an important and challenging part of a single-molecule experiment. While in practice this process must be optimized for each experiment, we describe several common approaches. From single-molecule measurements, we can obtain fluctuations in fluorescence intensity or photon counts, temporal characteristics (photon arrival time, the interval time between photon detections, and the delay time relative to laser excitation), and optical properties (wavelength and polarization). To extract information about the excited states, energy transfer dynamics, and protein conformation from the limited number of detected photons, several analytical methodologies have been developed. Here, we overview these methodologies and their applications to photosynthetic systems. In combination with instrumental and technical improvements discussed above, advances in single-molecule analysis will provide even more fruitful information about molecular characteristics and dynamics.

3.3.2.1. Fluorescence Intensity. The most widely and straightforwardly detected parameter is the fluorescence intensity or photon counts. In many single-molecule experiments of light-harvesting systems, analysis of time-averaged fluorescence intensity has been used to investigate the molecular inhomogeneity and quenching properties.[9,209,210] In this analysis, the detected photons are integrated over a given time window (e.g., 1−100 ms) to determine an intensity level. Here, the time resolution is determined by the bin time required. One major drawback to this approach is that time-averaging of the detected photons has been shown to lead to artifacts in further analysis.[211−213] Essentially, increasing the time window for a sufficient signal-to-noise ratio to determine the intensity level also averages over the dynamics of the system. In studies of phenomena such as blinking, this problem has also been shown to produce artifacts, which may also be present in studies of photosynthetic systems.[194]

As an alternative approach, methodology from information theory provides a way to estimate a physical parameter as precisely as possible from the photon stream.[214] Watkins and Yang developed a method that uses a generalized likelihood ratio test to determine the location of changes in intensity.[215] Importantly, the change point analysis is applied to the entire record of detected photons, each with a recorded arrival time, without any temporal binning. After determining the location of changes in intensity, the intensity level between each change is found by averaging the detected photons for that interval. Using photon streams recorded with single-photon counting methods, change point analysis has revealed fluctuations in fluorescence intensities in photosynthetic systems, including allophycocyanin (APC),[12] LH2,[11,216] and LHCII.[18] Change point analysis has been shown to access dynamics down to the microsecond time scale.[216]

Once the intensity levels have been defined, they are categorized as distinct states via a clustering algorithm (e.g., *k*-means, Gaussian mixture model) or a user-defined cutoff value, often to separate emitting (on) and nonemitting (off) levels. The dwell times (length of time before a transition) of the states are often analyzed, in particular for the on and off states. In many different systems studied at the single-molecule level, the probability distribution of dwell times of the materials exhibited inverse power law behavior, with exponents between 1 and 2.[217] Photosynthetic systems exhibited similar behavior, and a detailed analysis of the dwell time has been performed for several systems, including LH2[216] and LHCII.[209]

While these analysis focus on millisecond to second dynamics, correlation function approaches have the potential to access faster dynamics. Fluorescence correlation spectroscopy (FCS) is a microscopy technique in which molecular properties are determined from the temporal dynamics of the fluorescence data.[218−221] The photon-by-photon (time-tagged) measurement enables analysis of temporal correlations of not only fluorescence intensity but also photon arrival time, interval time between photon detections, and delay time relative to the laser excitation.[222,223] From FCS, we can investigate fluctuation amplitude and its time scale, reflecting diffusion properties and intermolecular dynamics[224,225] as well as triplet state kinetics.[226,227] With this approach, the time resolution is limited by the interval time between consecutive photons and not by the bin time, allowing the observation of fast dynamics that are averaged out by binning in photon counting distribution analysis. With two photon counting detectors to eliminate afterpulsing and dead time effects,[228] FCS has submicrosecond time resolution.[123] Similar analyses can be performed on single-molecule fluorescence, either from freely diffusing or immobilized particles to gain the same submicrosecond resolution. While microsecond dynamics have been resolved for LHCII using pulse modulation, correlation function approaches offer another alternative to analyze the recorded data stream and access faster dynamics.[59]

3.3.2.2. Lifetime Analysis. Simultaneous determination of fluorescence intensity and lifetime has been a useful tool to explore nanosecond dynamics in photosynthetic systems at the single-molecule level.[11,12,15,18,59] By correlating these two variables, distinct conformational states have been identified. To determine the fluorescence lifetime, the delay times relative to laser excitation for a detected photon stream are used to construct a histogram. By fitting the recorded histogram, the fluorescence lifetimes are extracted. While ensemble measurements use nonlinear least-squares methods to fit the histogram, single-molecule data is often in the low count limit and thus is most accurately fitted with a maximum-likelihood estimation approach.[229,230] In this method, the parameters of a statistical model are estimated given the detected histogram. In general, the model used is an excited state decay convolved with the

DOI: 10.1021/acs.chemrev.6b00195
Chem. Rev. XXXX, XXX, XXX−XXX

instrument response function plus the background profile, which is measured separately.[12] Here, the temporal resolution of the lifetime is determined by the instrument response function, which ranges from ~50 ps to 1 ns, depending on the detector and electronics used. The time required for acquisition of sufficient photons to extract a lifetime (i.e., 100 ms to 1 s) depends on the fluorescence quantum yield, the laser intensity, and the detection efficiency of the microscope.

3.3.2.3. Spectral Analysis. The analyses based on the fluctuations in fluorescence intensity and lifetime, as described above, are useful to reveal protein dynamics. Spectral analysis of single molecules is particularly valuable for reporting on pigment−protein and pigment−pigment dynamics. Spectral analysis has been applied to a variety of light-harvesting systems to investigate these photophysical properties and their dynamics.[127,148,156,163] The measurement time required for acquisition of emission spectrum or scanning on the whole region of excitation spectrum is usually hundreds of milliseconds to a few seconds to obtain a sufficiently high signal-to-noise ratio. The time required depends on the fluorescence quantum yield and the detection efficiency of the microscope. Observation of a pure homogeneous spectrum and the protein dynamics for low energy barriers often requires cryogenic temperatures.

At cryogenic temperatures, the spectrum is homogeneously broadened with the zero-phonon-line (ZPL) and broad phonon side band (PSB) clearly distinguished.[231] Analysis of the intensity distribution between the ZPL and PSB peaks provides the Huang−Rhys or Debye−Waller factor. The Huang−Rhys factor serves as a quantitative measure of the electron−phonon coupling strength, which reports on the interaction between the pigment and protein environment.[232,233] Analysis of the Huang−Rhys factor, along with peak width and peak position, revealed both electron−phonon coupling and the existence of exciton self-trapping in LH2.[125,234] The fine structure of a single-molecule spectrum also allowed the excited-state energy level and the exciton structure to be estimated with a Frenkel exciton model.[235,236]

Spectral time series provide information about fluctuations in peak position, shape, and polarization. While large peak shifts are often observed at room temperature,[209,237,238] cryogenic temperatures slows the dynamics to permit obervation of temporal changes in spectral properties.[46] These dynamics are often assumed to be related to spatially localized structural changes, commonly described as the transitions within a two-level system (TLS). To reveal how pigments couple within the TLSs in the protein complex, the distributions of spectral first and second moments or cumulants, corresponding to spectral center of mass and line width, respectively, are calculated from spectral time series of each single particle.[239,240] The first cumulant distribution is fit by a Gaussian profile,[239,240] indicating that pigments interact with densely packed TLSs.[241] The TLSs are divided into two classes, corresponding to the interior and exterior of the protein, by a multi-Gaussian fit.[240] The distribution of ZPL position also gives information about dynamics. Because the probability of ZPLs increases if the dynamics are slower than spectral scanning, the ZPL distribution emphasizes the difference in time scale of the dynamics of individual pigments. The rate of peak shift is obtained by tracking the peak position.[46] The Arrhenius plot of the rate constant enables a quantitative estimate of the potential barrier between conformational substates in energy landscape.[242]

Photosynthetic systems contain multiple pigments and thus often exhibit complicated spectra with many peaks. Analysis of these peaks also enables insight into the underlying dynamics. 2D correlation analysis identifies peak pairs with and without correlation in synchronous and asynchronous spectra, respectively.[243] This was applied to investigate the dynamics of excitation energy flow network in PS I.[244] On the other hand, a multivariate statistical analysis (MSA) pattern recognition approach[245,246] can be applied to classify specific signals from the spectral series. In the analysis, diagonalization of the covariance or correlation matrix of a spectral series produces eigenvectors, each corresponding to a discrete spectrum. Similar eigenspectra are then grouped and averaged to improve signal-to-noise.[247] Thus, spectral properties of pigments linked via dynamics can be retrieved from the time series of single-molecule spectra.

4. STRUCTURAL HETEROGENEITY: ASYNCHRONOUS CONFORMATIONAL DYNAMICS

In sections 4−6, we present examples of how single-molecule spectroscopy provides insight into photosynthetic solar energy conversion. In this section, we focus on how single-molecule spectroscopy has revealed the structural heterogeneity within photosynthetic systems. This structural heterogeneity emerges from conformational dynamics that consist of structural fluctuations due to thermal motion and switching between distinct states. These dynamics occur on many different time scales and thus produce both static and dynamic heterogeneity. Static heterogeneity is the differences between individual protein conformations, which may exchange on a time scale slower than the seconds to minutes of data collection. Dynamic heterogeneity is the conformational changes that occur on a time scale accessible to single-molecule techniques. Importantly, static and dynamic heterogeneity are indistinguishable in ensemble measurements, motivating the need for single-molecule approaches.

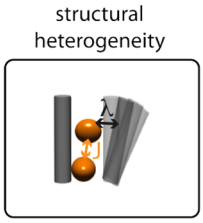

System	Results
LH2	structural fluctuations photo- & pH activated conformational switches photoactivated conformational heterogeneity
LHCII & Lhca	photoprotective conformations
PCP	photoactivated conformational heterogeneity

Single-molecule techniques uniquely access two types of heterogeneous dynamics: (1) asynchronous dynamics, where different members of the ensemble are at different states, and so the dynamics average out; and (2) multistep dynamics, where only the first step can be synchronized in the ensemble. In photosynthetic systems, many of the conformational dynamics are asynchronous, driving the need for single-molecule approaches to study these systems. Essentially, here we observe

DOI: 10.1021/acs.chemrev.6b00195
Chem. Rev. XXXX, XXX, XXX−XXX

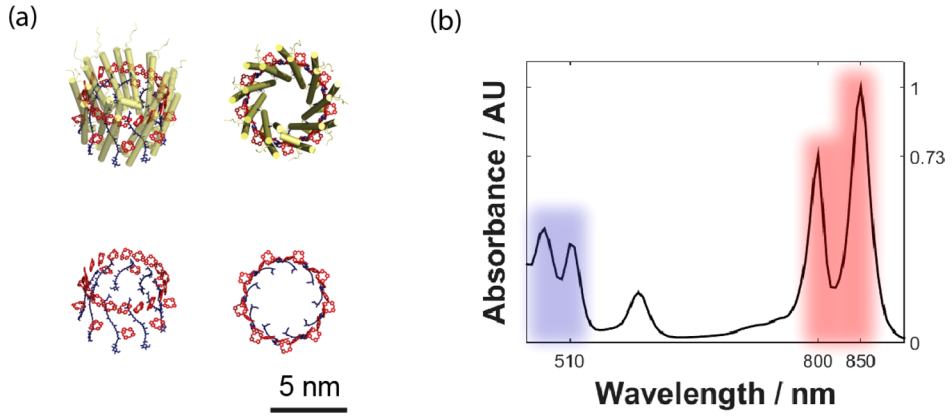

Figure 11. (a) LH2 from 45° (left) and top (right) with pigments and protein (top) and only pigments (bottom); (b) linear absorption spectrum of LH2 with BChl (red) and carotenoid regions (blue) indicated.

structural heterogeneity via its impact on the energetic heterogeneity of photosynthetic systems.

4.1. Protein Dynamics

Thermal fluctuations of the protein structure are stochastic and thus are one important class of asynchronous dynamics. The local protein environment impacts the absorption and emission properties. Here, we explore these dynamics for LH2. LH2 has been one of the most intriguing light-harvesting systems for single-molecule spectroscopy for almost two decades because of both its inhomogeneity and its exceptional photostability.[2,156,163,248] In the structural model from X-ray crystallography, LH2 complexes exhibit circular symmetry, as shown in Figure 11. This well-defined molecular structure has been the foundation for interpreting studies of LH2 function and for models of its electronic structure. However, the structural fluctuations of LH2 destroy the equivalency of the subunits. The resultant inhomogeneity in excited state energies is an order of magnitude larger than other photosynthetic light-harvesting complexes, driving many of the scientific questions about LH2 (Figure 12).[75]

Monitoring the single-molecule spectrum of the B800 band of the LH2 complex serves as a useful probe to directly observe changes in the local protein environment and thus dynamics of the energetic landscape. The temporal shift of the peak position, meaning the dependence of the shift amplitude per unit time, i.e., shift rate, implies a rugged surface surrounding the potential minimum in the energetic landscape.[239,240] The single-molecule spectrum of B800 displayed three sizes of spectral fluctuations: (1) large jumps (~several 100 cm^{-1}) of peak position, which appeared as anticorrelated lines; (2) spectral changes (~5 cm^{-1}) between two successive measurements, which, after hundreds of such measurements, led to an averaged line width of ~50 cm^{-1}; and (3) rapid fluctuations in individual spectra, which led to a broadening (~several cm^{-1}) of each peak.[46] The rates for these spectral changes at 1.4 K were estimated to be 0.001−0.01, 0.03−1, and more than 1 s^{-1}, respectively. These fluctuations were interpreted as protein dynamics between three tiers in the potential energy landscape, where the higher-energy tier corresponds to the specific arrangements of the atoms such as those in the protein scaffold, and the lower-energy tier reflects the vibrational degrees of freedom.[46] The Arrhenius plot of the rate for the spectral shift at the temperature range of 5−18 K revealed several activation energies of <10 cm^{-1} for the protein dynamics,[242] suggesting that single-molecule spectroscopy is

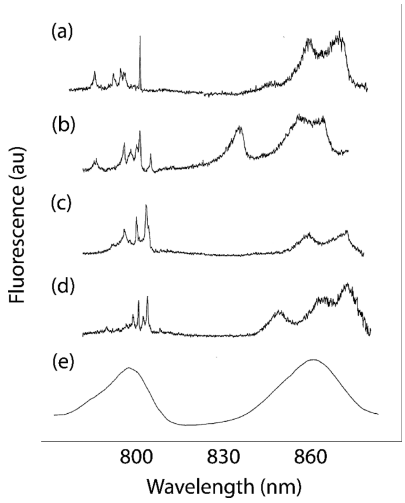

Figure 12. Fluorescence excitation spectra of LH2 complexes at 1.2 K. (a−d) Fluorescence excitation spectra display fluorescence intensity as a function of excitation wavelength. Excitation spectra of single LH2 complexes reveal narrow peaks in the B800 band and broad peaks in the B850 band. The linewidths, positions, and heterogeneity of these features report on the excited state manifold of LH2. (e) The ensemble excitation spectrum, which can also be reproduced by summing the single-molecule excitation spectra. From ref 148. Reprinted with permission from AAAS.

useful for observing the local potential surface and dynamics that are obscured in the ensemble system. On the basis of the observed magnitude of the dynamics, the site energies of the neighboring BChl *a*'s can occasionally become very close to each other. As discussed in section 2, the excited state is characterized not only by the intermolecular interaction of adjacent molecules (J) but also the difference between their site energies (ΔE), i.e., the ratio ($J/\Delta E$). Fluctuations of the site energy cause a change in the ratio, which produced temporal changes in the delocalization of the excited state on the BChl *a*'s in B800. The existence of this dynamic delocalization was demonstrated by the changing angle between the molecular transition dipole moment of the BChl *a*'s.[126]

4.2. Non-Photochemical Quenching

Photosynthetic complexes exhibit not only thermal fluctuations of their structure but also conformational changes between functional states. In particular, conformational changes are thought to underlie the mechanisms by which oxygenic

DOI: 10.1021/acs.chemrev.6b00195
Chem. Rev. XXXX, XXX, XXX−XXX

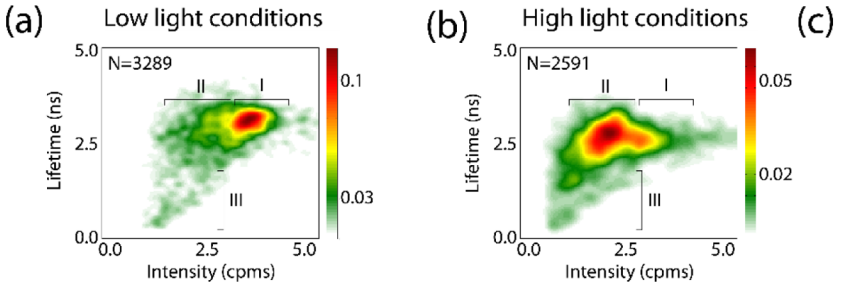

Figure 13. Conformational landscape of LHCII. (a) The probability distribution in intensity-lifetime space of LHCII complexes. Population is observed in three regions, labeled as I, II, and III. (b) The relative populations in these three regions changes under conditions that mimic high light, where the relative population of states II and III increase. (c) Grouping of pigments within LHCII that, according to the working model, reorganize upon switching between states. If the carotenoid (pink) moves left, the carotenoid can quench the Chl *a* (green), in which the emissive states are localized. Quenching of Chl *a* would result in state III. If the carotenoid moves to the right, the carotenoid can quench the Chl *b* (blue), preventing energy from reaching the emissive state, which produces state II. Reproduced from ref 18. Copyright 2015 American Chemical Society.

photosynthetic systems protect themselves from photodamage. Oxygenic photosynthesis produces oxygen, yet oxygen also generates deleterious photoproducts by reacting with the triplet state formed on excited chlorophyll. To prevent these photoproducts, light harvesting is regulated via a series of mechanisms that prevent the buildup of excess energy under high light conditions. Collectively, these mechanisms are known as nonphotochemical quenching (NPQ). The rapid component of NPQ, qE or energy-dependent quenching, dissipates excess energy as heat.[71] In higher plants, qE has been shown to be activated by a drop in pH and a change in carotenoid composition.[68] Furthermore, the antenna complexes have been implicated as the site of quenching. As a result, studies have focused on the primary antenna complex in green plants, LHCII.

The activation of photoprotection involves a functional switch, which produces functional heterogeneity. The mechanism behind this switch is thought to be a conformational change. Here, we describe experiments to explore the structural heterogeneity that may underlie the functional heterogeneity. Using single-molecule spectroscopy, the changing conformations of LHCII and homologous antenna complexes under conditions that mimic high and low light have been extensively studied.[11,18,209,210]

4.2.1. Characterization of Partially-Quenched Conformations. Single-molecule measurements have been used to identify the conformational states of LHCII. One series of experiments used the ABEL trap (discussed in section 3), a technique that enables solution-phase measurements, allowing the intrinsic conformational dynamics to be revealed without the structural perturbations that may be introduced by attachment. By simultaneously measuring fluorescence intensity and lifetime, correlations between these parameters emerge. Importantly, these correlations are information inaccessible with ensemble-averaged techniques. As shown in Figure 13, these correlations reveal three distinct populations. The most likely molecular origin behind these different populations is conformational states based on their long time scale (seconds) and other photophysical analysis, including similar contributions from triplet states, as discussed in more detail in ref 18. In addition to an unquenched conformation, two partially quenched conformations were observed. Because lifetime and intensity changed proportionally, the quenching was attributed to a nonradiative decay process of the emissive state. The emissive state neighbors a carotenoid, and thus the quenched state was assigned to a conformation where the Chl−carotenoid distance decreases, enabling energy transfer to the carotenoid. Notably, one of the partially quenched conformations increases in relative population under conditions that mimic high light, indicating it may be related to photoprotection.[18] Thus, structural heterogeneity revealed through single-molecule measurements may be the cause of functional heterogeneity.

In a recent exciting experiment, these switches into partially quenched states have been unambiguously assigned to conformational changes. A series of experiments on the light-harvesting antenna from cyanobacteria, the phycobilisome, observed these same types of conformational dynamics. Notably, the rate of transitions decreased with the addition of cross-linkers, which stabilize the protein structure.[249] Thus, these experiments provide compelling evidence that these switches into quenched states emerge from structural changes.

4.2.2. Populations of Quenched States. Single-molecule spectroscopy has also identified and explored other functional forms of LHCII that may be important to photoprotection. In addition to partially quenched conformations, LHCII also transiently enters an almost entirely quenched, or dark, state. This type of transient entry into a dark state, known as blinking, has been observed in a host of single particles, including molecular, materials, and biological systems. On the basis of a series of single-molecule fluorescence experiments studying blinking in LHCII, the quenched state was proposed to arise from a conformational change and serve as the state responsible for NPQ.[209,250,251]

To explore these conformational dynamics, the distribution was characterized for a series of conditions that mimic effects of high light (low pH, zeaxanthin enrichment, and low detergent concentration). Low detergent induces aggregation, and LHCII aggregation within the membrane has been proposed to drive the switch into the quenched conformation. In a series of experiments, blinking increased with all conditions that mimic high light. Furthermore, under these conditions, a population of quenched, red-shifted states appears, which the authors assign to a conformation in which the emissive state has mixed excitonic/charge transfer character. Overall, these experiments revealed the population in quenched states increases with a pH drop, zeaxanthin composition, and a decrease in detergent.[251] Thus, the observed structural heterogeneity was controlled by the surrounding environment, which provides a handle to regulate functional heterogeneity.

4.2.3. Role of Lhca. In higher plants, the antenna complexes are divided into two categories, Lhcas and Lhcbs. These complexes are highly homologous, with similar pigment

DOI: 10.1021/acs.chemrev.6b00195
Chem. Rev. XXXX, XXX, XXX−XXX

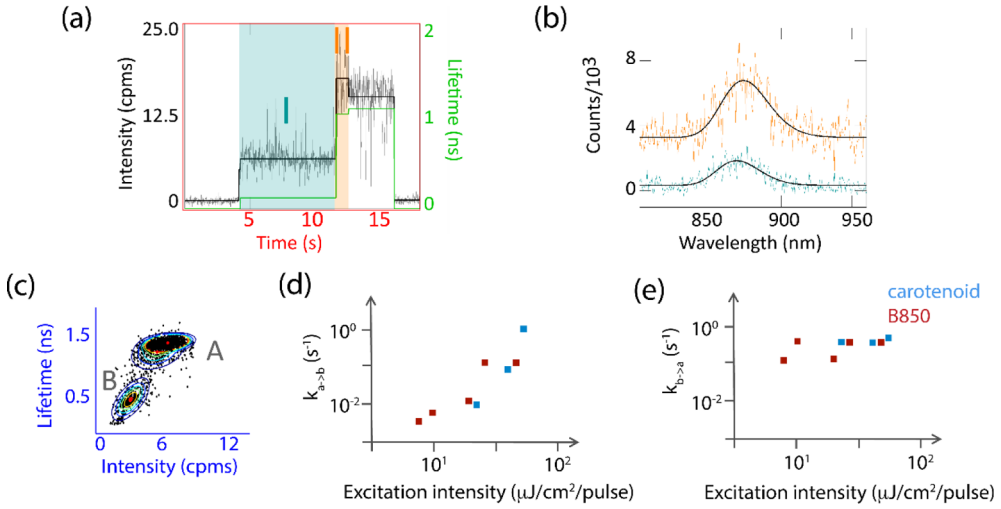

Figure 14. Room-temperature single LH2 measurements of fluorescence intensity, lifetime, and spectra. (a) Intensity-lifetime traces reveal large, concomitant changes in intensity and lifetime. (b) Fluorescence spectra of the intensity levels in (a) reveal occasional spectral shifts (868 nm in level I to 873 nm in level II). (c) Plot of intensity levels with their concomitant lifetime for single LH2 complexes excited for carotenoid (515 nm) excitation with 12 $\mu J/cm^2$/pulse. A Gaussian mixture model (rainbow lines) reveals that two clusters, states A and B, emerge from these levels. (d) The rate of transition from state A to B as a function of excitation intensity for carotenoid and B850 excitation. The rate increases linearly with excitation intensity, indicating a photoactivated process. (e) The rate of transition from state B to state A as a function of excitation intensity. The rate is independent of excitation intensity, indicating a thermal process.

composition and spectroscopic properties. The major difference is thought to arise from the presence of a charge transfer state in the Lhcas that is localized on two of the Chl *a* pigments. LHCII is formed from any combination of three of Lhcb1−3. Thus, in studies of LHCII, the Lhcbs have been extensively studied at the single-molecule level. The Lhcas have been proposed to play a role in photoprotection,[252] and one possible mechanism is conformational switching into a photoprotective state. The role of Lhca in NPQ remains controversial, and so single-molecule studies provide a valuable tool to characterize the conformational dynamics, and to begin to explore whether photoprotective functionality exists.

In a series of single-molecule experiments, the room temperature spectral dynamics of Lhcas in monomeric and dimeric form were characterized. Interestingly, whereas LHCII primarily emits at ∼680 nm and occasionally switches to a red state, Lhca4 primarily emits between 690 and 730 nm and occasionally switches to the state with ∼680 nm emission.[17] Thus, the energetic heterogeneity revealed conformational dynamics that report on both the intrinsic flexibility of the proteins and highlight that these homologous proteins most likely exhibit the same conformational states. However, one conformation is stabilized for the Lhcbs and the other for the Lhcas. Through single-molecule spectroscopy, this relationship between conformational states emerged.

4.3. Conformational Switches in Purple Bacteria

Conformational heterogeneity has also been observed in LH2, the analogous light-harvesting complex from purple bacteria. While the associated functional heterogeneity is not clear, several conformations have been identified and characterized. In this section, we discuss conformational switching of LH2 driven by light intensity (part 1) and by pH (part 2).

4.3.1. Intensity-Dependent Conformational States. Individual conformations were identified through correlated measurements of fluorescence brightness and lifetime. Using the ABEL trap, the intrinsic conformational dynamics of LH2 were revealed. As illustrated in Figure 14a, fluorescence brightness (intensity) and lifetime data identified two previously unknown emissive states. On the basis of the direct proportionality between intensity and lifetime, these states correspond to an unquenched and a quenched conformation.[11]

LH2 exhibits switching between the quenched and unquenched conformations. Rates of transitions were determined by monitoring the switches for many individual complexes. Notably, switching from the unquenched to quenched conformation increases linearly with excitation intensity (Figure 14d), indicating a photoactivated process. In contrast, switching from the quenched to unquenched conformation is independent of excitation intensity (Figure 14e), indicating a thermal process. As a result of this switching functionality, LH2 complexes convert into a quenched conformation under high light intensities. The newly activated quenching has a nanosecond time scale, which is competitive with intersystem crossing, providing an alternative to triplet formation. LH2 switches from the quenched to the ground (unquenched) conformation via thermal fluctuations of the protein. Thus, the protein structure contains an intrinsic feedback loop with photoprotective functionality.[11] Although the anoxygenic bacteria that contain LH2 do not require protection from reactive oxygen species, it is notable that they have an intrinsic feedback loop, as opposed to the cellular feedback loop in oxygenic photosynthesis, as discussed above. Although there is no evidence of a physiological photoprotective role, this photoprotective ability may become important for light levels used to illuminate mixed biological/inorganic artificial solar energy devices that integrate LH2 complexes.[253] These devices are often installed in an oxygenic atmosphere and, through concentrators, under solar intensities orders of magnitude higher than under standard sunlight.[254,255] Furthermore, it has been speculated that this conformational change may be representative of conformational dynamics that were the evolutionary precursor for NPQ in oxygenic photosynthesis.[216]

In a later series of experiments, the dynamics of these conformational changes have been investigated on longer time

DOI: 10.1021/acs.chemrev.6b00195
Chem. Rev. XXXX, XXX, XXX−XXX

scales. Individual LH2 complexes were immobilized and observed for over an hour. The extended observation time allows the dynamics of individual complexes to be monitored over multiple transitions.[216] Notably, these observations revealed that, for some of the conformations, individual LH2 complexes "remember" their previous conformation. For example, if an LH2 complex begins in an initial conformation and then switches to a second one, it is more likely to return to the initial one than would be predicted by the overall rates of switching from the second to the initial one. These results led to the surprising conclusion that the protein structure of an individual LH2 complex retains conformational memory. A changing height of the energy barrier between states may be the underlying cause of the observed conformational memory. The ability of a protein structure to retain a preference for a previous conformation, even through several conformational changes, may serve a role in switchable functionality. Furthermore, these properties of protein dynamics observed in photosynthetic systems may be generalizable. Photosynthetic systems contain spectroscopic reporters (pigments) with properties highly sensitive to the surrounding protein environment. Thus, structural heterogeneity can be read out with high sensitivity via the pigment properties. The conformational memory observed here might be a mechanism for introducing different functionality into individual proteins. Notably, this observation requires time-ordering information, which is hidden in ensemble experiments.

4.3.2. pH-Dependent Switching. Conformational dynamics driven by pH have been explored for LH2 complexes from *Rhodovulum (Rdv.) sulfidophilum*.[238] Perhaps unique to this species, the B850 band undergoes a pH-dependent spectral shift. At pH 7.0, the B850 band shifts from its usual maximum of 850 down to 832 nm as a result of a breakage of the H-bond between the BChl and their neighboring Trp44 and Tyr45 amino acids. The introduction of the spectral shift has been ascribed to species-specific glutamic acid residues that are thought to become protonated at low pH. Therefore, the conformational changes introduce corresponding energetic changes.

Single-molecule experiments monitored the spectral dynamics of these LH2 complexes. The dominant emission spectrum peak is at 858 nm. However, under low pH conditions, the distribution of spectral maxima blue-shifts by a few nanometers and is asymmetric, extending down to 830 nm. The spectral dynamics were assigned to exploration of the conformational space, which, in turn, depends on pH.[238]

4.4. Photo-Induced Heterogeneity

Single-molecule spectroscopy can determine the full distribution of conformations. In single-molecule experiments, laser fluence is generally orders of magnitude above that of sunlight, which leads to rapid cycling through the excited state and relaxation to a distribution of conformations. Thus, a significant population may access conformations that rarely occur under lower light intensities, causing hidden states to become characterizable. In many systems, heterogeneity in fluorescence spectra, intensity, and lifetime increases as a result of high excitation intensity.

Single-molecule experiments on LH2 at room temperature explored the spectral dynamics of the fluorescence emission. While the ensemble fluorescence spectral maximum is ~870 nm, single LH2 complexes were observed to emit with spectral maxima throughout the range of 870 ± 10 nm. Furthermore, individual complexes underwent shifts in the spectral maxima. Notably, the magnitude and frequency of these shifts increased with excitation fluence.[50] Thus, the ability of single-molecule spectroscopy to characterize the full distribution of behaviors allowed the conformational states with red- and blue-shifted emission to be observed.

Single-molecule experiments on peridinin chlorophyll protein (PCP) from dinoflagellates revealed photoinduced heterogeneity in both intensity and lifetime.[95] PCP is trimeric, where each protein contains four peridinin and two chlorophyll. PCP is unusual in that the carotenoids (peridinin) serve a major role in light absorption, and the pigments are arranged to transfer energy with high efficiency from the peridinin to the chlorophyll. In PCP, the population of low intensity states and short lifetime states emerged under high excitation intensity. However, the dominant state remained a higher intensity and longer lifetime state.[95] Thus, these results illustrate conformational states hidden by the dominant population in ensemble experiments.

5. ENERGETIC HETEROGENEITY: CHARACTERIZATION OF THE EXCITED STATE MANIFOLD

In the previous section, we discussed structural heterogeneity of photosynthetic systems, including conformational fluctuations and dynamics. In this section, we focus on the energetic heterogeneity that emerges from the structural heterogeneity. While the contributions from all the conformations are averaged out in an ensemble experiment, single-molecule spectroscopy allows individual conformations to be interrogated, revealing differences in their excited state manifolds. We describe ways in which single-molecule spectroscopy enables characterization of these excited state manifolds.

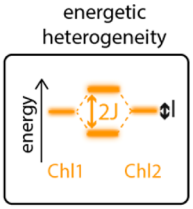

System	Results
LH2	localized & delocalized states energetic shifts uncorrelated & correlated disorder electron-phonon coupling
LH1-RC	circular aggregate-like structure
chlorosome	spectral disorder pigment packing

We primarily focus on the excited state manifold of LH2. While crystallized LH2 complexes exhibit 9-fold symmetry, as discussed in the previous section, the structural fluctuations of LH2 destroy the equivalency of the subunits, leading to localization of the excited state. Understanding the true electronic structure that results from this inequivalency is essential for understanding LH2. Single-molecule spectroscopy has revealed characteristics of the electronic structure that are hidden in ensemble measurements, including structural symmetry, heterogeneity of the excited states, coupling strength between pigments, and coupling strength between pigments and the protein environment.

DOI: 10.1021/acs.chemrev.6b00195
Chem. Rev. XXXX, XXX, XXX−XXX

5.1. Localized vs Delocalized States

In photosynthetic pigment−protein complexes, the close spacing between pigments leads to delocalized excited states. Characterizing this delocalization is difficult, however, because it depends on several parameters (pigment−pigment coupling, pigment−protein coupling, and site energies). The fluorescence excitation spectrum shows fluorescence intensity as a function of excitation energy, which reveals spectral properties that report on the delocalization. The excitation spectra of single LH2 complexes at cryogenic temperatures were used to explore the excited states in both the B800 and B850 bands.

From analysis of the spectral width, the delocalization of the excited states within the two rings of LH2 can be identified. As shown in Figure 11b, the ensemble B800 and B850 peaks exhibit similar spectral widths. In contrast, as shown in Figure 12, the single-molecule excitation peaks exhibit a clear difference in spectral width.[148] In particular, the B800 band consists of several narrow peaks dispersed at different wavelengths, whereas the B850 band exhibits two broad peaks, sometimes together with a third peak at shorter wavelengths.[148]

The difference in spectral widths emerges from the difference in delocalization of the states in the B800 and B850 bands. As discussed in section 2 above, the excited states are delocalized over multiple individual pigments. The extent of delocalization is characterized by the ratio between the pigment−pigment coupling of adjacent pigments (J) and the difference between their site energies (ΔE), i.e., $J/\Delta E$. In the B800 band, the pigment−pigment coupling is estimated to be about 24 cm^{-1}[256] as opposed to the variation in site energy of 125 cm^{-1}.[148] Within this band, the excited states are primarily localized on the individual pigments, and the spectral width emerges primarily from the homogeneous line width, which ranges from 2 to 10 cm^{-1} at 1.5 K.[153] These linewidths are close to lifetime limited (based on the time scale of B800 to B850 energy transfer) but also include additional broadening from vibronic relaxation, delocalization, or B800 to B800 energy transfer.

In the B850 band, the pigment−pigment coupling is estimated to be 200−400 cm^{-1}.[66] As discussed, the strong coupling within the B850 band produces highly delocalized excited states, driving rapid reorganization around the B850 ring. The linewidths of the peaks in the B850 band range from 50 to 250 cm^{-1}, with an average value of 120 cm^{-1}. This corresponds to total dephasing times from 20 to 100 fs, in agreement with ensemble results for energy reorganization around the B850 ring.

5.2. Identification of Inhomogeneous Linewidth

The fluorescence excitation spectra of individual LH2 complexes also report on the inhomogeneity, or static disorder, in both the B800 and B850 rings. Disorder emerges from multiple types of structural fluctuations, and identifying the molecular origin of the static disorder in LH2 has been a long-standing question. Understanding static disorder requires identifying both the magnitude and type of disorder, and single-molecule experiments have investigated both questions. In this section, we focus on the magnitude of disorder and, in section 5.3 below, we focus on the type of disorder.

As shown in Figure 12, fluorescence excitation spectra of the B850 band exhibit two broad, separated peaks. According to the working model, the splitting of the two broad peaks in the B850 band is caused by the energetic disorder of the BChl a's. Within this working model, analysis of the single-molecule spectrum provides an estimate of the magnitudes of different types of disorder that emerge from deformation of the B850 ring,[235,236] which were found to be 250 cm^{-1}.

In addition to the broad B850 band, statistics of the position of the well-separated peaks in the B800 band enabled an estimation of the site energy disorder within the B800 band, which was found to be 130 cm^{-1}.[153] This inhomogeneity reflects the slight difference in the local protein environment, that is, the local minima in the energy landscape of a protein. Thus, here structural heterogeneity leads to energetic heterogeneity. The fluctuations of the site energies caused changes in the electronic coupling and temporal delocalization of the excited state on the BChl a's in B800. These changes were analyzed based on the temporal change of the angle between the molecular transition dipole moments of the BChl a's.[126] Intracomplex heterogeneity of excitonic delocalization has been proposed to explain why the number of peaks at the B800 band is fewer than the number of BChl a's in the B800 ring. Furthermore, the fluorescence excitation spectrum observed with individual LH2 at 1.2 K showed narrow peaks at the absorption region of B800, and spectral properties such as the peak position, amplitude, and line shape were significantly different between individual LH2s.[117] Thus, both intra- and intercomplex energetic heterogeneity have been identified and characterized.

5.3. Structural Origin of Energetic Heterogeneity

As described above in section 5.1, thermal fluctuations of the protein structure destroy degeneracy between subunits, which localizes the excited states as discussed in section 2.3.[257] However, the structural motions that arise from these fluctuations have not been identified and, as a result, identifying the type of disorder has been a long-standing challenge. In terms of the type of disorder, there are two major questions: (1) diagonal (ΔE) or off-diagonal (J) disorder, which is whether the disorder emerges from heterogeneity in the site energies of the individual pigments (ΔE) or in the distances and orientations between the pigments (J); and (2) correlated or uncorrelated disorder, which is whether the disorder emerges from elliptical deformations of the cylindrical structure or from local deformations. In a series of cryogenic and room temperature single-molecule experiments, the details of the emissive properties of LH2 were explored to address the nature of the disorder.

At 1.4 K, the type of energetic disorder in the B850 ring (diagonal/off-diagonal and random/correlated) was analyzed based on the distribution of the splitting width, the intensity ratio, and the relative orientation of the transition dipole moment.[258] Within the framework of the model, the disorder was found to predominantly arise from fluctuations of the site energies (diagonal disorder) with both an uncorrelated component and a correlated component, where the correlated component emerges from elliptical deformations of the B850 ring.[235,236,258] Thus, structural asymmetry of the B850 ring[58] was verified at the single-molecule level. Temporal fluctuations of the structural asymmetry were also reported at room temperature.[9]

At room temperature, polarization-dependent single-molecule experiments on LH2 revealed anisotropic emission, which the authors ascribed to elliptical deformations of the cylindrical structure,[9] in agreement with the low temperature results.[236] In

DOI: 10.1021/acs.chemrev.6b00195
Chem. Rev. XXXX, XXX, XXX−XXX

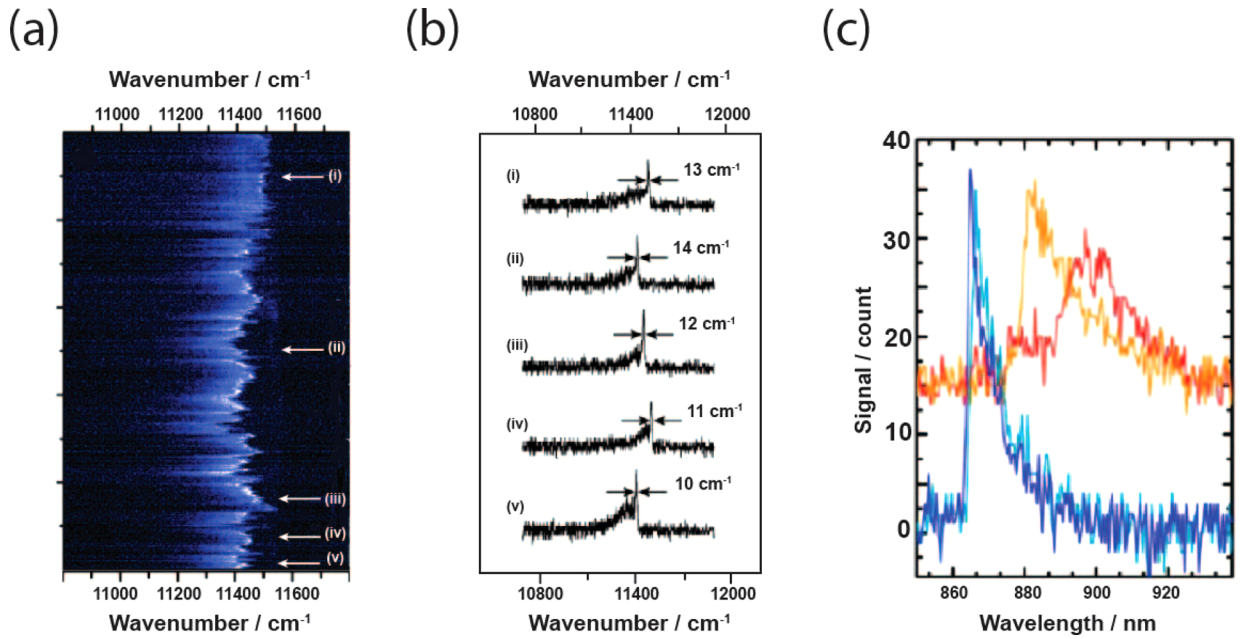

Figure 15. Cryogenic fluorescence emission spectra of LH2. (a) Fluorescence emission spectra of a single LH2 complex, measured 1000 times in a row with exposure time of 5 s at 1.2 K. (b) Five representative spectra of emission profile exhibiting a sharp ZPL at the high-energy end of the spectrum together with a PSB. Adapted with permission from ref 234. Copyright 2016 American Chemical Society. (c) Emission spectra showing a signature of ZPL (blue/light-blue) and broad featureless band (red/orange). The vertical axis is valid for the ZPL trace, because the PSB trace has been offset by +15 for clarity. Adapted with permission from ref 125. Copyright 2016 American Chemical Society.

this way, information about the structural heterogeneity that underlies the energetic heterogeneity was determined.

The possible role of the attachment strategy was investigated through a series of experiments. In early experiments, LH2 complexes were adsorbed to a mica surface. In later experiments, both anchored and unanchored LH2 complexes were held in place with a spin-cast layer of PVA.[259] Here, the anchored complexes exhibited anisotropic emission. The increased anisotropy was ascribed to tilt induced by being anchored during the spin-casting process. This follow-up experiment illustrates the sensitivity of the photophysics of photosynthetic proteins to perturbations.

In a separate series of experiments, fluorescence intensity and spectra were measured for LH2 complexes immobilized via electrostatic interactions with a poly-L-lysine coated surface. From these experiments, a distribution of spectral maxima was extracted. The majority of complexes were centered at 865−870 nm, corresponding to the peak of the ensemble spectrum.[50,260] However, 1−5% of the complexes exhibited spectral maxima ±10 nm from the ensemble peak. The authors reproduced the observed heterogeneity using a disordered exciton model.[6] In this model, heterogeneity is introduced by uncorrelated nonequivalency of the BChl binding sites in the B850 ring, as opposed to the correlated nonequivalency that would arise from an elliptical structure.[10] In contrast to previous studies,[9] the authors ascribe the structural motion to be localized on individual subunits due to agreement between their experimental results and theoretical model. Once again, here energetic heterogeneity informed on the underlying structural heterogeneity.

More recently, single-molecule experiments have been performed on LH2 using a technique known as the ABEL trap, which is described in section 3.1.3 above.[11] The ABEL trap removes the uncertainty produced by these different immobilization strategies because it allows single photosynthetic complexes to be interrogated in a solution-phase environment. In these experiments, heterogeneity in the spectral position of the fluorescence maxima was observed, as illustrated in Figure 14. However, in this case, the complexes only exhibited spectra maxima ±5 nm from the ensemble maximum and only ∼5% of the intensity changes were accompanied by a spectral change.[11] The rarity of the spectral changes suggests that the energetic barrier between the spectrally distinct conformations is high. Thus, while the exact nature of the conformational dynamics that underlie the spectral heterogeneity was not resolved, it was found to involve a high-energy structural motion.

Overall, an important factor in characterizing energetic heterogeneity is the identification of perturbations due to nonphysiological local environments. These perturbations have been shown to alter other emissive properties. For example, the photobleaching quantum yield of LH2 increases in detergent micelles relative to a phosopholipid bilayer environment composed of dimyristoylphosphatidylcholine (DMPC).[261] Conversely, LH2 complexes in a bilayer of dioleoylphosphatidylcholine (DOPC) showed almost the same spectral properties for the B850 band as that in a micelle.[13] This discrepancy was thought to originate from the difference between the phase-transition temperatures of the two phospholipid bilayers.[261] Additionally, the use of different detergents, *n*-octyl-*β*-D-glucopyranoside (OG)[261] and lauryldimethylamine *N*-oxide (LDAO),[13] may create different micelles that also contribute to the conflicting results. The influence of detergent on the deformation of photosynthetic complexes has also been observed in the LH1−RC complex.[166] Thus, energetic heterogeneity can emerge both from the properties of the protein matrix and from that of the surrounding environment.

5.4. Observation of Electron−Phonon Coupling

In the LH2 low temperature excitation spectrum, the narrow peaks within the B800 band also provide information on the

DOI: 10.1021/acs.chemrev.6b00195
Chem. Rev. XXXX, XXX, XXX−XXX

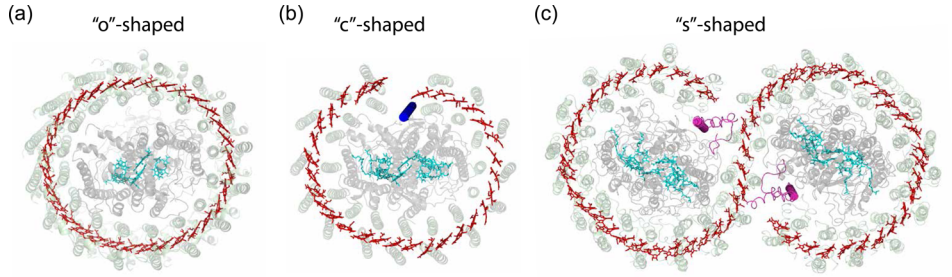

Figure 16. Observed molecular organizations of the LH1 ring. (a) O-shaped closed ring composed of 32 BChl *a*'s from *Thermochromatium tepidum* (PDB: 3WMM),[264] (b) C-shaped incomplete ring composed of 30 BChl *a*'s from *Rhodopseudomonas palustris* (PDB: 1PYH),[265] and (c) S-shaped dimeric complex composed of 56 BChl *a*'s from *Rhodobacter sphaeroides* (PDB: 4V9G).[266] BChl *a* molecules in LH1 are shown in red. The light-blue molecules indicate electron transfer cofactors in the RC. Blue and pink cylinders represent a transmembrane helix (protein M) and PufX polypeptide, respectively.

electron−phonon coupling of the BChl *a* in the binding pocket.[233,247] The electron−phonon coupling can be considered the interaction between the excited state and the collective vibrational mode of the binding pocket/protein environment, here referred to as the phonon. The spectrum of a single molecule at low temperatures is essentially made of a sharp ZPL and a broad PSB, where the former corresponds to the electronic transition with no change in the number of the vibrational modes of the binding host while the latter corresponds to the electronic transition coupled with the excitation of a vibrational mode (Figure 15).[125] On the basis of the area under these two peaks, the electron−phonon coupling strength can be found using the Huang−Rhys or Debye−Waller factor.[231−233] The coupling differed between species of photosynthetic bacteria based on the binding motif for BChl *a* in B800.[233] In addition, species with weak coupling showed a larger spectral shift than those with strong coupling. Thus, spectral analyses serve as a sensitive probe for investigating the interaction of the pigment with the binding site.

The electron−phonon coupling for the B850 band was also obtained from the fluorescence emission spectrum of LH2.[125,234] The emission peak could be mainly classified into two types: (1) type I, displaying a superposition of the ZPL and PSB, thus indicating the weak coupling strength at the shorter-wavelength (blue) region, and (2) type II, displaying a featureless broad peak at the longer-wavelength (red) region.[125] The temporal fluctuations between these two states, i.e., alternative observations of the type I and II emission peaks with time, was demonstrated.[234] Interestingly, a spectral feature in the emission was not reflected in the fluorescence−excitation spectrum, even for the same LH2. Hence, it was assigned to the formation of the self-trapped exciton state.[125] Thus, fluorescence excitation and emission spectroscopy at the single-molecule level give us distinct information on the excited state, i.e., the former monitors the initial state when it is "born" and the latter monitors the final state when it "dies."

5.5. LH1 and LH1−RC Heterogeneity

Single-molecule spectroscopy has also been used to explore the energetic heterogeneity of another protein from purple bacteria, LH1. The light-harvesting protein LH1 is an elliptical assembly of 30−56 strongly coupled BChl *a* molecules that form a ring surrounding the RC. The ring produces an electronic structure described by a circular aggregate model, similar to LH2. Three different molecular organizations of the LH1 ring structure have been reported: (1) O-shaped closed ring structure containing 32 BChl *a*'s,[262−264] (2) C-shaped incomplete ring structure containing 30 BChl *a*'s,[265] and (3) an S-shaped dimeric complex containing 56 BChl *a*'s[266,267](Figure 16). Atomic force microscopy (AFM)[268] revealed that the LH1−RC complex from *Blastochloris (B.) viridis* and *Rhodospirillum (R.) rubrum* formed the O-shaped ring.[262,263] Recently, the clear crystal structure of the LH1−RC complex from *Thermochromatium (T.) tepidum* was determined at 3.0 Å resolution, unveiling a circular arrangement with an ellipticity of ∼0.9.[264] The C-shaped ring structure was determined at 4.8 Å resolution with the LH1−RC complex from *Rhodopseudomonas (Rps.) palustris*, where a single transmembrane helix (protein M) cracked the ring and broke the O-shaped structure.[265] The S-shaped arrangement, which was determined at 8 Å resolution with the LH1−RC complex from *Rhodobacter (Rb.) sphaeroides*, was a dimer made of two C-shaped rings where the PufX polypeptide was located on the binding surface between the two rings.[266] Thus, the type of deviation from the original O-shaped configuration is species-specific. Each arrangement gives rise to a distinct electronic structure, allowing the electronic structure to report on the molecular organization.

The fluorescence excitation spectrum of the main LH1 absorption band of an individual LH1−RC complex at cryogenic temperature is used as the signature of this molecular organization. This is a broad band that can be decomposed into two peaks, with transition dipole moments orthogonal to each other, analogous to the two peaks within the B850 peak for LH2 shown in Figure 12.[164] These two peaks correspond to the lowest allowed states. As described in section 2, these states are degenerate in a circular aggregate and thus the spectral splitting between the two peaks arises from elliptical protein deformation. The splitting amplitude was used to distinguish between molecular organizations of the LH1 ring for different species and conditions. For example, the splitting amplitude was estimated for the O-shaped LH1 of *Rhodospirillum (R.) rubrum*.[165] The amplitude was smaller than that in other species, indicating a more ring-like structure in this organism.

The changing electronic structure at the single-molecule level also helped to elucidate the role of another polypeptide found in the photosynthetic membrane in some species of purple bacteria, known as PufX. LH1−RC complexes from *Rhodobacter (Rb.) sphaeroides* contain PufX, which sits on the binding surface between two neighboring LH1 rings (Figure 16c).[266] PufX is essential for the formation of the S-shaped architecture and its depletion caused the formation of monomeric and completely circular rings, as in the O-shaped type.[267,269] The fluorescence excitation spectrum of the LH1−RC from *Rhodopseudomonas (Rps.) palustris* was compared with that

DOI: 10.1021/acs.chemrev.6b00195
Chem. Rev. XXXX, XXX, XXX−XXX

from the PufX-deleted strain of *Rb. sphaeroides*.[270] The individual LH1−RCs from the PufX-deleted strain showed two broad peaks, whereas those from *Rps. palustris* exhibited narrow lines at the long wavelength side of the broad peak.[270] These narrow lines could be explained with the excitonic structure for a ring arrangement with a physical gap, i.e., the C-shaped structure.[270] These results suggested that *Rps. palustris* forms the C-shaped structure.[270] The splitting amplitude of *Rhodopseudomonas (Rps.) acidophila*[164] was similar to the C-shaped *Rps. palustris*,[166] suggesting it also forms a C-shaped structure.

The energetic separation between the two peaks was also used to estimate the influence of the environment on ring structure deformation. The splitting amplitude for LH1 embedded in DOPC bilayer was smaller than that for a detergent-solubilized LH1.[271] In addition, the distribution of the splitting amplitude was narrower for LH1 in DOPC.[271] Thus, membrane conditions enhanced the conformational stability of LH1, as was also the case with LH2.[261] LH1−RC solubilized with dodecyl-β-D-maltoside (DDM), a mild detergent, and spin-coated with PVA exhibited the same spectral signatures as complexes in the membrane.[166,272] Finally, comparison of the splitting profiles of the isolated LH1 and the LH1−RC complex demonstrated that interactions with the RC stabilizes the ring structure of LH1.[165]

5.6. Electronic Structure of Supramolecular Aggregates

As discussed in section 5.1 for the delocalized states within LH2, single-molecule spectroscopy provides a tool for characterizing the nature of the excited states within a molecular aggregate. The chlorosome is a molecular aggregate (~10^5 BChl) that serves as the antenna complex for green sulfur photosynthetic bacteria[273] as well as acidobacteria.[274] Because of the large number of BChl, which produce a single broad absorption band, studies of the chlorosome are notoriously challenging. However, single-molecule spectroscopy has revealed structural and dynamical heterogeneity within these aggregates. Here, we address how structural heterogeneity generates heterogeneity within the excited state manifold. In section 6, we go on to discuss how structural heterogeneity impacts the energy transfer efficiency for this system.

Chlorosomes are known as the largest antenna employing BChls *c*, *d*, and *e* and their homologues as main pigments. It has an ellipsoidal structure with a size of ca. 100−200 nm × 20−60 nm × 10−20 nm,[275] containing the BChl molecules together with carotenoids and quinones, depending on the species.[276−278] Intriguingly, the supramolecular structure is organized by self-assembly without interaction with a protein scaffold and stabilized by a hydrogen bonding network between pigments inside a lipid monolayer. The huge antenna allows the phototroph to survive under the extremely low light in the deep sea, where the light flux is less than 0.002 μmol photons m^{-2} s^{-1} or only geothermal radiation is available.[279,280] Because of its supramolecular structure, the chlorosome has been an ideal model for artificial light-harvesting devices.[281] However, the pigment composition and organization in the chlorosome vary, partially based on growth conditions.[282−285] The resulting structural heterogeneity and size variation make it difficult to experimentally determine the molecular structure by crystallography. Other techniques including cryoelectron microscopy, X-ray diffraction, and solid-state nuclear magnetic resonance have been used to propose various mesoscopic structural models for the BChl such as rod elements, concentric multicylinders, scrolls, or curved lamellae (Figure 17a).[286−292] To differentiate between these structures, and the heterogeneity within them, single-molecule spectroscopy has been applied at both room and cryogenic temperatures.

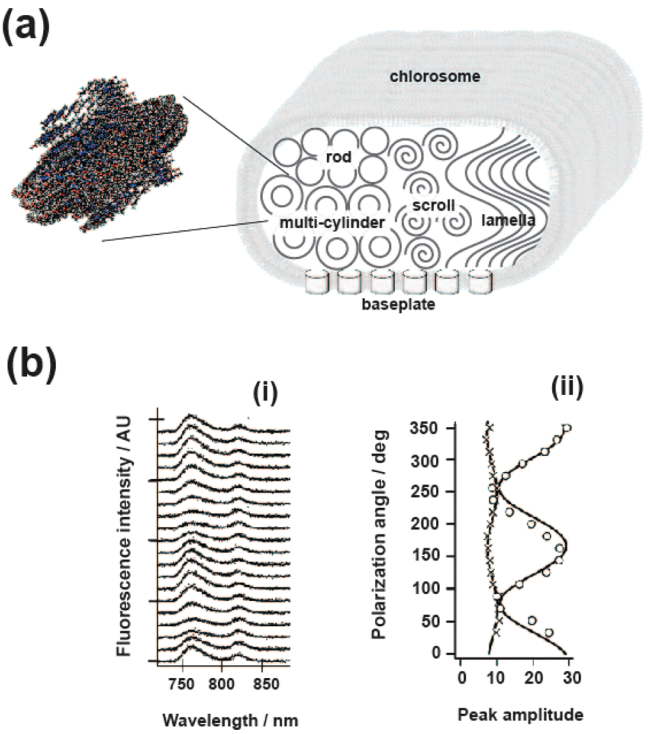

Figure 17. (a) Schematic structure of the chlorosome. BChl aggregates densely packed in a lipid monolayer have been proposed to form rods, multicylinders, scrolls, or lamellae. The light energy absorbed by the BChls is transferred to BChl *a* in baseplates and then to the reaction center. (b) (i) Angular dependence of fluorescence spectra at 13 K of single chlorosomes from *Cfl. aurantiacus*, arranged from bottom to top according to the polarizing angle of detection, each rotated by 20°. The fluorescence peaks around 760 and 820 nm are ascribed to BChl *c* aggregates and BChl *a* in baseplates, respectively. The smooth lines indicate fitting curves calculated by skewed Gaussian functions. (ii) Angular dependences of the fluorescence peak of BChl *c* in BChl aggregates (circle) and BChl *a* in baseplates (cross). The solid lines represent fitting curves. Adapted from ref 293, Copyright 2016 American Chemical Society.

The excited state manifold was found to vary with species, growth conditions, and sample preparation. In the first observation of a single chlorosome, the fluorescence spectrum was measured at room temperature with chlorosomes isolated from a green filamentous photosynthetic bacterium *Chloroflexus (Cfl.) aurantiacus*.[113] The spectral properties (peak position, width, and shape) were similar among individual chlorosomes. A more heterogeneous distribution was found in the chlorosomes from *Chlorobaculum (Chl.) tepidum*, reflecting various compositions of BChl *c* homologues.[14,294] The cooling to 13 K red-shifted and narrowed the fluorescence spectrum of the single chlorosome of *Chl. tempidum*, while the effect was much smaller for *Cfl. aurantiacus*.[146] The large temperature dependence of the *Chl. tempidum* chlorosome was explained by the dense exciton states of the BChl *c* self-aggregates. Additionally, the disorder in the cryogenic fluorescence spectrum of single chlorosome from *Chl. tepidum*, composed of at least two Gaussian components, seemed also to be

DOI: 10.1021/acs.chemrev.6b00195
Chem. Rev. XXXX, XXX, XXX−XXX

generated from the BChl *c* homologues.[146] Conversely, the highly homogeneous chlorosomes, which were carefully isolated from *Chl. tepidum* grown on better controlled conditions (light intensity, cell density, and growth time), showed less spectral disorder.[295] It was also demonstrated that the fluorescence spectrum depended on the ambient environment by comparing single chlorosomes adsorbed on a quartz plate to those floated in a liquid solution.[146] These experiments demonstrated that the single-molecule spectrum of the chlorosome is a highly sensitive reporter of the structure and that structural heterogeneity emerges based on species, growth conditions, and the local environment.

Polarization experiments were used to identify the excited states. The orientation of the principal transition dipole of BChl *c* self-aggregates in single chlorosomes was estimated from the dependence of the fluorescence emission on excitation polarization (Figure 17b).[293,296] The three transition dipoles along the *x*, *y*, and *z* axes, which correspond to the membrane normal, parallel to the membrane surface, and the chlorosomal long axis, respectively, in the internal coordinates of the chlorosome, were determined. The dipole intensity ratio $\mu_x/\mu_y/\mu_z$ was evaluated to be 0.43/0.43/1 and 1/0.76/0.76 for the BChl *c* and BChl *a* in chlorosome from *Cfl. aurantiacus*,[293] and 0.3/0.5/1 and 1/0.6/0.1 for those from *Chl. tepidum*.[296] The mutual arrangement between the BChl *c* and the BChl *a* was consistent with the structural model of chlorosome, where the normal of the ring plane of BChl *a* in baseplate was situated in parallel to the *z*-axis.[297,298] The chlorosome from *Cfl. aurantiacus* showed high cylindrical symmetry, while that from *Chl. tepidum* was slightly distorted.[296] The cylindrical symmetry of the *Chl. tepidum* chlorosome was also estimated by two-dimensional polarization fluorescence microscopy, where the polarization dependence for both excitation and emission lights were simultaneously measured.[295,299] By analyzing the modulation depth, a symmetrical cylinder model was proposed.[295] The high symmetry, which was not found in the *Chl. tepidum* chlorosome frozen in solution,[296] may come from the homogeneous chlorosome preparation.[295] The polarization dependence of the fluorescence excitation spectroscopy at 1.5 K separated two absorption peaks within the absorption spectrum of a single chlorosome.[4,115] The distributions of the peak position and the energetic gap and phase difference between these two peaks were compared to those calculated based on the structural models of the BChl *c* self-aggregates, including the closed cylinder, concentric double cylinders, and scrolls.[4] The polarization dependence at the single-molecule level in combination with modeling revealed the underlying structure of the supramolecular antenna system. Furthermore, unique among the antenna, the extremely high density of pigments allows other spectroscopic and structural techniques to be used at the single copy level. This includes linear dichroism via absorption detection[294] as well as circular dichroism via fluorescence detection.[300] These methodologies applied to single chlorosomes provide additional experimental benchmarks for structural models of the aggregated BChl that form the complex.

Finally, while the chlorosome is known to contain a large number of BChl, not only their structure but also their concentration have remained open questions.[276,277] To remove any uncertainty caused by the large chlorosome aggregate, single-molecule measurements were used to precisely count and study chlorosomes in solution.[278] The spatial distribution and number of single chlorosomes were measured by 3D scanning confocal microscopy and then compared to the concentration of the BChl molecule extracted by acetone into solution. This approach enabled an accurate estimation of the concentration of BChl molecule within the chlorosome, 1.4×10^5 and 9.6×10^4 per chlorosome from *Chl. tepidum* and *Cfl. aurantiacus*, respectively.[278] The concentration is a key parameter in generating structural and energetic models of the chlorosome.

6. FUNCTIONAL HETEROGENEITY: EXPLORATION OF PHOTOPHYSICAL PATHWAYS

We have described how single-molecule experiments reveal conformational dynamics (section 4) and the impact of conformational heterogeneity on the excited state energies (section 5). Here, we describe single-molecule measurements that uncover functional heterogeneity, including hidden aspects of the photophysics and energy transfer pathways. Photosynthetic energy transfer occurs on a femto- to picosecond time scale. While single-molecule experiments have been primarily limited to the nanosecond process of fluorescence, fluorescence parameters report on the photophysical processes and can be used to extract information about the excited state dynamics. We discuss heterogeneity in energy transfer pathways (section 6.1), observation of trap (red) states (section 6.2), and quenched states that emerge in the photodegradation process (section 6.3).

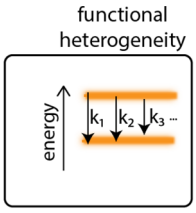

System	Results
LH1-RC	energy transfer efficiency
chlorosome	energy transfer efficiency
LHCII	energy transfer pathways
PSI	trap states
APC	photodamaged & quenching sites

6.1. Energy Transfer Pathways

One application of fluorescence is to characterize the efficiency and the route of energy transfer within the light-harvesting apparatus. Here, we describe a few examples of this application.

6.1.1. Energy Transfer in Purple Bacteria. In purple bacteria, upon absorption of a photon, energy transfers from LH2 to LH1 to the RC, where charge separation occurs.[301,302] To investigate the energy transfer processes between these complexes, photosynthetic units composed of an LH1−RC complex and LH2 antenna were analyzed using cryogenic single-molecule spectroscopy.[303,304] This unit emitted fluorescence from LH1 with excitation of the LH1−RC and LH2.[304] In addition, these fluorescence intensities exhibited the same response to polarizing rotation of the excitation light.[304] These results suggest that excitation energy is efficiently transferred from LH2 to LH1−RC.

Fluorescence excitation and emission spectra were also observed from LH2 and the LH1−RC self-assembled in a lipid

DOI: 10.1021/acs.chemrev.6b00195
Chem. Rev. XXXX, XXX, XXX−XXX

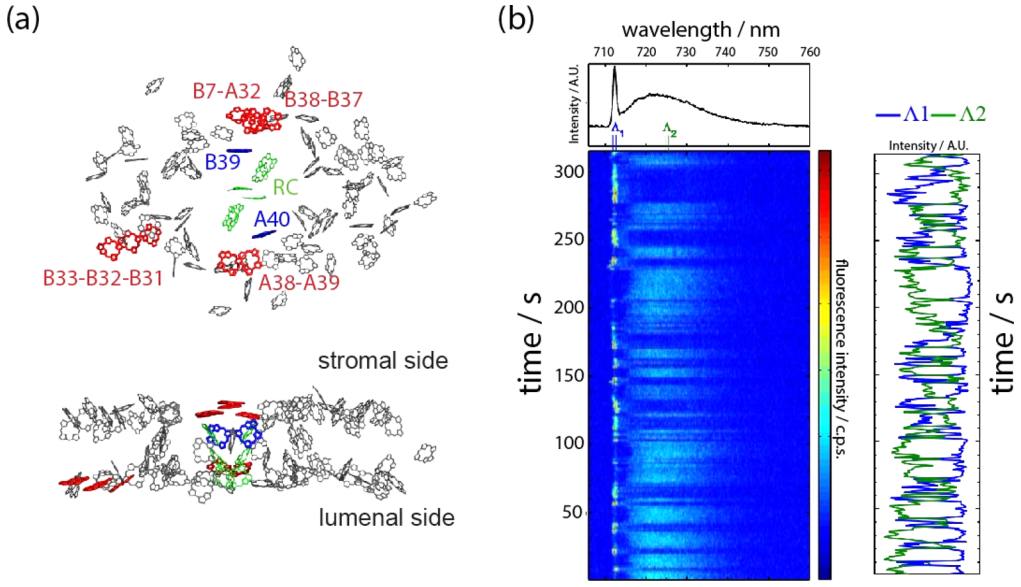

Figure 18. (a) Molecular arrangement of pigments in cyanobacterial PS I (PDB: 1JB0).[29] Top view from stromal side onto the membrane plane (top) and side view (bottom). Candidates for red-Chl *a* aggregates are shown in red. The green molecules belong to the RC core. The linker Chl *a*'s in the spatial gap between the antenna assembly and the RC core are shown in blue. (b) Time dependent fluorescence spectra of a single PS I complex from *T. elongatus* at 1.4 K. The averaged spectrum is shown on top. The side panel shows time traces of the fluorescence intensities integrated on the wavelength ranges Λ_1 (blue) and Λ_2 (green), where the former corresponds to the zero phonon line and the latter to a part of the broad peak. Adapted from ref 244. Reprinted with permission from the National Academy of Sciences.

bilayer.[303] LH2 and an S-shaped LH1−RC dimer from *Rb. sphaeroides* exhibited efficient energy transfer from LH2 to LH1−RC. On the other hand, in the photosynthetic unit made up of LH2 from *Rb. sphaeroides* and a C-shaped LH1−RC monomer from *Rps. palustris*, the B850 peak in the excitation spectrum was reduced while a B850 fluorescence emission peak appeared, indicating a decrease in efficiency. The progress in the reconstitution of the photosynthetic unit enables investigations into the energy transfer processes between light-harvesting complexes, which are an important, yet poorly explored, piece of light harvesting.

6.1.2. Energy Transfer in Green Sulfur Bacteria. Heterogeneity in energy transfer efficiency has also been explored in green sulfur bacteria. The chlorosome, the antenna from green sulfur bacteria, absorbs energy and rapidly transports the absorbed energy to a neighboring pigment−protein complex, the baseplate, shown in Figure 17a.[305] The baseplate is embedded in the membrane envelope of the chlorosome and mediates energy transfer from the chlorosome to the reaction center.[298] At cryogenic temperatures, the spectral peak from the baseplate-containing chlorosome narrows to clearly distinguish two fluorescence peaks (Figure 17b). These peaks originate from BChl *c* self-aggregates (chlorosome) and BChl *a* (baseplate).[146,306] The intensity ratio of the BChl *a* peak to the BChl *c* peak in the fluorescence spectrum of the single chlorosome reflects the energy transfer efficiency from BChl *c* self-aggregates to BChl *a* in baseplate. This ratio was found to be distributed widely from 0.1 to 0.8.[146] The red-shifted BChl *c* aggregate trasfers energy more efficiently, most likely because the shift toward BChl *a* peak increases the spectral overlap and thus the Förster rate of energy transfer. The heterogeneity in the energy transfer efficiency, stemming from the energetic heterogeneity, may increase at physiological temperatures, enabling the chlorosome to adapt to various growth conditions.

6.1.3. Energy Transfer in Higher Plants. The primary antenna in green plants, LHCII, is trimeric. Single-molecule experiments on LHCII were used to explore the energy transfer pathways between monomers. LHCII monomers exhibited a highly polarized fluorescence emission at room temperature.[20] In contrast, LHCII trimers exhibited a much less polarized emission at temperatures ranging from 1.2 K to room temperature. These results suggest that each monomer within the trimer contains an emissive state, as opposed to one monomer serving as the trap, or terminal, state in the energy transport chain.[20] Furthermore, the lack of temperature dependence in the polarization of the trimeric emission indicates that each monomer functions relatively independently. That is, at temperatures where the emissive states of the monomer are separated by an energy gap greater than k_BT, one would expect excitations to transfer to the monomer containing the lowest energy emissive state. However, these results indicate most excitation energy does not transfer between monomers.

In higher plants, energy transfers through a relatively flat energetic landscape of light-harvesting complexes yet reaches the reaction center with high efficiency. Remarkably, these results suggest that energy transfers through the light-harvesting complexes in a constrained pathway that is not entirely dictated by energetics, perhaps offering insight into the design of the pathway of energy flow.

6.2. Red States

The energy transfer dynamics within photosynthetic complexes maintain their efficiency under physiological conditions, which can introduce structural fluctuations. Within the protein matrix of each complex, pigments are densely packed such that interpigment and pigment−protein electrodynamic couplings are strong and therefore highly sensitive to intermolecular distances. These two characteristics suggest the presence of shallow irregularities on the free energy surface of photo-

DOI: 10.1021/acs.chemrev.6b00195
Chem. Rev. XXXX, XXX, XXX−XXX

synthetic proteins. At room temperature, thermal energy is sufficient to overcome these potential barriers to transfer through the photosynthetic apparatus. In contrast, at low temperatures, proteins become trapped within wells. Therefore, cryogenic temperatures remove thermal motion, enabling studies of energetic heterogeneity and resultant functional heterogeneity that are obscured at room temperature.

Cryogenic single-molecule spectroscopy has been applied to PS I, a large pigment−protein containing ∼100 Chl *a* molecules (Figure 18a),[29,127,307] most of which primarily absorb sunlight and rapidly transport the excitation energy to the RC. This energy transfer and the subsequent charge separation are highly efficient and restrict fluorescence emission. As such, PS I exhibits a low fluorescence quantum yield that is currently undetectable at the single-molecule level at room temperature.[308] There is also a special class of Chl *a* molecules called red-Chl *a*, which has been hypothesized to not only mediate energy transfer from the antenna complex to the RC but also to quench deleterious excess excitation energy. The absorption peak of the red Chl *as* is 30 nm more red-shifted than that of the Chl *a* in the RC core (700 nm). This spectral shift requires an unfavorable, uphill transport of energy to the RC core, and so excitation become temporarily trapped by the red-Chl *a* aggregate. Under physiological conditions, the environment provides enough thermal energy to dislodge the trapped energy. As a result, the energy transfer and the subsequent charge separation are highly efficient, limiting the intensity of fluorescence emission so that PS I is currently undetectable at the single-molecule level at room temperature.[308] However, at low temperatures, the thermal energy is too low to dislodge the trapped energy, and therefore the fluorescence quantum yields are enhanced 10−20-fold compared to those at room temperature.[309,310] This temperature-dependent enhancement in fluorescence emission was also observed in individual PS I's, where the average activation energy of single PS I's was estimated to be 500 cm^{-1}, thus allowing for fluorescence analysis of PS I at the single-molecule level.[311]

Cryogenic experiments on the fluorescence emission spectrum of single PS I's have been used to characterize the red-Chl *a* aggregates. The spectroscopic data as well as the high resolution crystal structure was used to assign the individual red states to specific Chl *a* within the molecular structure.[311,29,307] The nomenclature is based on the absorption maxima, and so the Chl *a* have been known as C708, C715, and C719 in *Thermosynechococcus elongates*,[312,313] C706 and C714 in *Synechocystis* PCC 6803,[314] and C708 in *Synechoccocus* PCC 7002.[315] Thus, energetic heterogeneity was observed via the ability of the red states to function as traps at cryogenic temperatures.

The fluorescence emission spectra were used to explore spectral diffusion in single PS I's from *T. elongates*, *Synechocystis*[316] PCC 6803,[49] and *Synechoccocus* PCC 7002.[315,127] It was found that all spectra at 1.4 K exhibited zero-phonon lines (ZPLs) that shifted between frequencies and in distribution ranges during sequential measurements and a broad peak caused by these fast and wide spectral shifts.[49] At a higher temperature (∼10 K), smaller and fewer ZPLs were observed and a larger broad peak was observed due to thermal acceleration of spectral shifts.[317] Hidden ZPLs were revealed after selectively bleaching some red-Chl *a* pools[318] or by reducing the acquisition time. With the shortest acquisition time possible (1 s), the spectral diffusion ranges of each ZPL in the three species were analyzed and assigned to well-known red-Chl *a* pools.[49,127,315,316] An additional red-Chl *a* pool, not observed in ensemble measurements, was also revealed by analyzing the ZPL spectral diffusion.[315] Other hidden red-Chl *a* pools, whose ZPLs were broadened by fast spectral diffusion and embedded in the broad peak, could be identified by analyzing the polarization properties of the emission spectrum[49,127,315,316]

In all, cryogenic single-molecule spectroscopy of the PS I has revealed the spectral characteristics of ZPLs corresponding to two to four red-Chl *a* pools, depending on species. These pools exhibit similar, species-independent, spectral diffusion, which have allowed for the identification of specific red-Chl *a* aggregates based on spectral characteristics.[127] These pools of Chl *a* cannot be observed in ensemble measurements. However, the ability of a single-molecule experiment to isolate and explore individual copies allowed these hidden states to be characterized.

The mechanism behind the spectral diffusion of the ZPL was explored in PS I of *Synechocystis* PCC 6803 by comparing H_2O and D_2O buffers.[232] It was found that D_2O exchange caused the line width to narrow and the spectral diffusion rates to decrease. The hydrogens responsible for these spectral dynamics most likely come from amino residues and internal water molecules close to the pigment. Notably, the fluctuation of the hydrogens involved in bonding with Chl *a*'s induced spectral dynamics even at cryogenic temperatures.[232]

The above measurements focused mainly on analyzing distinct contributions from red-Chl *a* pools and identifying the spectral dynamics of each pool. However, these pools are in fact connected to each other in the energy transfer network of the PS I light-harvesting antenna complex and their spectral dynamics are intricately linked. Correlation analysis between the red pools showed anticorrelations in fluorescence intensities (Figure 18b), suggesting switching between two excitation energy transfer pathway, which cannot be observed in ensemble measurements.[244] Through these experiments, functional heterogeneity is uniquely accessible and so dynamic changes in the energy transfer network in large, complex light-harvesting systems were identified. These approaches have been recently applied to PS II as well.[167,168]

6.3. Photodegradation Pathways and Isolation of Subunits

Single-molecule experiments are usually performed at fluences orders of magnitude higher than sunlight. As a result, photosynthetic proteins photodegrade during these experiments. By monitoring the photodegradation pathway, two types of information emerges: (1) characterization of photodamage, and the intermediates in this process; and (2) isolation of individual subunits.

As described in section 2, above, the excited state energies and dynamics emerge from the coupled pigments within photosynthetic proteins. As a result, identifying the properties of individual pigments within the proteins is often challenging. However, during the photodegradation pathway, individual pigments photobleach and no longer contribute to the spectroscopic properties. Photobleaching is stochastic and so is not synchronized among the pigments. After one pigment photobleaches, the others can be interrogated. Thus, the intermediates in the photodegradation process offer an opportunity to observe the spectroscopic properties of individual pigments without the complication of multiple, coupled pigments.

DOI: 10.1021/acs.chemrev.6b00195
Chem. Rev. XXXX, XXX, XXX−XXX

Analysis of the photodegradation pathway has been used to characterize the spectroscopic properties of the pigments within APC.[15] APC is a component of the light-harvesting antenna in cyanobacteria. In cyanobacteria, initial absorption and energy transport primarily occurs in extra-membrane structures, known as phycobilisomes, that are constructed of a central core and surrounding rods. The cores are cylinders made up of four trimers of another type of protein that loosely organize into hexamers and are held together by linker proteins. APC forms from three monomers that self-associate to form a trimer. Each monomer consists of an α and β protein subunit, both of which contain a single phycobilin pigment.[319,320] The chlorophyll in LH2 and LHCII are held within the surrounding protein by noncovalent ligation within a pigment binding pocket. In contrast, the phycobilin is covalently bound to the protein in the pigment-binding pocket. As a result, the phycobilin photophysics are even more sensitive to the surrounding protein.

In APC, differentiating and characterizing the photophysics of the α and β pigments has been challenging. Analyzing the photodegradation pathway allowed the emissive properties of the two pigments to be individually observed. Figure 19 illustrates the distribution of fluorescence brightness, spectrum, lifetime, and polarization for all intermediates within the photodegradation pathway. Analysis and modeling of these results revealed that the α pigment has a longer lifetime and blue-shifted spectrum as compared to the β pigment.[15] Thus, the differences in the pigment photophysics were visible through the photodegradation pathway. These properties are hidden within an ensemble experiment.

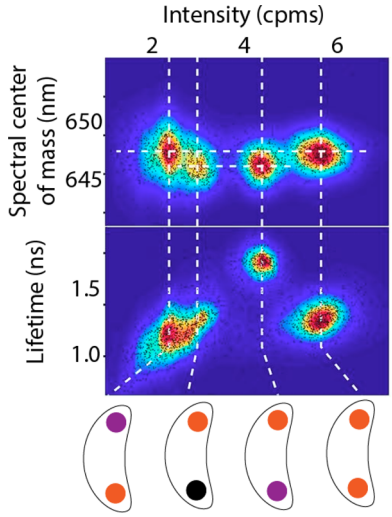

Figure 19. Emissive properties of allophycocyanin (APC) monomers. Single-molecule experiments correlating fluorescence intensity, spectrum, and lifetime identified different photodegradation products and their molecular origin. Monomeric APC contains two pigments. Individual pigments photobleached (purple) or converted into a quencher (black). Figure adapted from ref 15. Reprinted with permission from the National Academy of Sciences.

A second notable aspect of these results is that, upon photobleaching, the pigments often convert into quenchers that lower the fluorescence of their neighbors. The photodegradation process creates a trap, or sink, for excitation energy. APC is just one component of a much larger structure, the phycobilisome. Thus, under conditions that cause photodamage, an APC creates a trap, preventing excitation from damaging the rest of the phycobilisome. This limits the damage (and repair efforts) to one location within the large photosynthetic antenna.

7. CONCLUSION AND OUTLOOK

In this review, we have discussed single-molecule studies of photosynthetic systems, highlighting examples of physical insight into photosynthesis garnered over the past two decades. In particular, these studies explore structural heterogeneity, including conformational dynamics (section 4), energetic heterogeneity, including characterization of different excited state manifolds (section 5), and functional heterogeneity, including distinct photophysical pathways (section 6). As illustrated with these studies, single-molecule spectroscopy of photosynthetic systems has made significant progress, yet challenges remain. These challenges fall into technological, biological, and application areas.

In terms of technological challenges, one emerging area is resolution on the time scale of energy transfer, namely femto- and picoseconds, at the single-molecule level. As discussed in section 3, a new experiment to measure energy transfer dynamics at the single-molecule level has been developed. Scientifically, ultrafast temporal resolution at the single-molecule level will enable a new understanding of the heterogeneity in energy transfer dynamics. It is the heterogeneity in these dynamics that is key to determining how light harvesting is robust to thermal fluctuations of the protein structure.

A second technological challenge is combining the advantages of cryogenic and room temperature experiments. In cryogenic experiments, the narrower linewidths and slower conformational dynamics aid in characterizing the congested spectra of photosynthetic systems. In contrast, in room temperature experiments, the native conformational dynamics are accessible. To connect the behavior at different temperatures, Orrit and co-workers developed a temperature cycle technique, where a focused infrared beam causes highly localized and hence a fast and precisely controllable temperature gradient only near the target molecule.[119,321,322] The short heating and cooling cycles of a single biomolecule allowed the dynamics at each temperature to appear as a series of snapshots, thus identifying conformational substates from each clear spectrum at cryogenic conditions. Applying this technique to photosynthetic complexes would provide new insight into their potential energy landscape.

In terms of biological challenges, one area is moving toward more physiological sample conditions. Single-molecule experiments require high photon fluxes and a low concentration of emitters, which means proteins must be separated from their cellular neighbors. Furthermore, attachment methods often require nonphysiological solutions or interactions. Because of the exquisite sensitivity of photosynthetic proteins to their local environment, performing these experiments under near-physiological conditions would improve the reliability and relevance of the results.

A second biological challenge is increasing the diversity of photosynthetic proteins. LH2 has been extremely well studied, partially due to its high photostability. The advent of more sensitive detectors, better optics, and more effective oxygen removal approaches enables studies of more diverse, and dimmer, organisms, such as cryptophytes, green algae, and higher plants. Furthermore, in the face of our growing energy

DOI: 10.1021/acs.chemrev.6b00195
Chem. Rev. XXXX, XXX, XXX−XXX

needs, a number of bioinspired light-harvesting systems for solar energy applications have been developed.[323,324] Similar to the work on natural systems presented here, there is the opportunity to understand their functionality through single-molecule spectroscopy, which can, in turn, drive the optimization of these devices.

Taken together, these challenges provide an opportunity to advance the technology and science of single-molecule spectroscopy on photosynthetic systems. Despite decades of study, the complexity and diversity of photosynthetic organisms means that much remains to be learned.

AUTHOR INFORMATION

Corresponding Author

*Phone: 617-253-1478. E-mail: gssc@mit.edu.

ORCID

Gabriela S. Schlau-Cohen: 0000-0001-7746-2981

Notes

The authors declare no competing financial interest.

Biographies

Toru Kondo received his Ph.D. in Physics in 2011 for his work on photoreceptor proteins and the photosynthetic reaction center at Nagoya University under the direction of Prof. Shigeru Itoh and Prof. Hiroyuki Mino. In 2010, he participated in the JSPS Excellent Young Researcher Overseas Visit Program in the Prof. Robert Bittl group at the Freie Universität Berlin. In 2012−2015, he worked with Prof. Michio Matsushita at Tokyo Institute of Technology as JSPS postdoctoral fellow, where he studied bacterial reaction centers with cryogenic single-molecule spectroscopy. In 2015, he joined the Prof. Gabriela Schlau-Cohen group at the Massachusetts Institute of Technology. His current interests focus on the development of single-molecule spectroscopy and the elucidation of dynamics-function relationship associated with the photochemical processes in photosynthetic systems.

Wei Jia Crystal Chen received her B.Sc. in chemical physics from the University of Toronto in 2015. She is currently working towards a Ph.D. in the Schlau-Cohen group at the Massachusetts Institute of Technology as an NSERC fellow. Her research focuses on the heterogeneity in energy transfer properties in bioinspired light-harvesting complex analogues.

Gabriela Schlau-Cohen is an Assistant Professor in the Department of Chemistry at the Massachusetts Institute of Technology. Before joining the faculty at MIT, Gabriela was a Postdoctoral Fellow of the Center for Molecular Analysis and Design at Stanford University, where she worked with Prof. W. E. Moerner from 2011 to 2014. Dr. Schlau-Cohen received her Ph.D. in Physical Chemistry in 2011 from the University of California, Berkeley, where she worked under the direction of Prof. Graham Fleming as an AAUW American Fellow. She received her B.S. in Chemical Physics in 2003 from Brown University. She is the recipient of a Beckman Young Investigator Award and the Smith Family Award for Excellence in Biomedical Research, and she was selected as a CIFAR Azrieli Global Scholar. Her research group uses single-molecule spectroscopy and ultrafast spectroscopy to explore the energetic and structural dynamics of biological systems with a focus on photosynthetic light harvesting.

ACKNOWLEDGMENTS

We thank Dr. Michal Gwizdala, Dr. Justin Caram, Dr. Steven Quinn, and Prof. Akihito Ishizaki for critical readings of the manuscript. We thank the Smith Family Foundation Excellence in Biomedical Research Award and the Center for Excitonics, an Energy Frontier Research Center funded by the U.S. Department of Energy, Office of Science, Office of Basic Energy Sciences, under Award no. DE-SC0001088 for support.

REFERENCES

(1) Blankenship, R. E. The Basic Principles of Photosynthetic Energy Storage. In *Molecular Mechanisms of Photosynthesis*; Wiley Blackwell: Hoboken, NJ, 2014; pp 6−7.
(2) Cogdell, R. J.; Gall, A.; Köhler, J. The Architecture and Function of the Light-Harvesting Apparatus of Purple Bacteria: From Single Molecules to in Vivo Membranes. *Q. Rev. Biophys.* **2006**, *39*, 227−324.
(3) Schlau-Cohen, G. S.; Bockenhauer, S.; Wang, Q.; Moerner, W. E. Single-Molecule Spectroscopy of Photosynthetic Proteins in Solution: Exploration of Structure−function Relationships. *Chem. Sci.* **2014**, *5*, 2933−2939.
(4) Jendrny, M.; Aartsma, T. J.; Köhler, J. Insights into the Excitonic States of Individual Chlorosomes from Chlorobaculum Tepidum. *Biophys. J.* **2014**, *106*, 1921−1927.
(5) Moerner, W. E.; Kador, L. Optical Detection and Spectroscopy of Single Molecules in a Solid. *Phys. Rev. Lett.* **1989**, *62*, 2535−2538.
(6) van Amerongen, H.; Valkunas, L.; van Grondelle, R. *Photosynthetic Excitons*; World Scientific: Singapore, 2000.
(7) Güttler, F.; Irngartinger, T.; Plakhotnik, T.; Renn, A.; Wild, U. P. Fluorescence Microscopy of Single Molecules. *Chem. Phys. Lett.* **1994**, *217*, 393−397.
(8) Orrit, M.; Bernard, J. Single Pentacene Molecules Detected by Fluorescence Excitation in a P -Terphenyl Crystal. *Phys. Rev. Lett.* **1990**, *65*, 2716−2719.
(9) Bopp, M. A.; Sytnik, A.; Howard, T. D.; Cogdell, R. J.; Hochstrasser, R. M. The Dynamics of Structural Deformations of Immobilized Single Light-Harvesting Complexes. *Proc. Natl. Acad. Sci. U. S. A.* **1999**, *96*, 11271−11276.
(10) Novoderezhkin, V.; Rutkauskas, D.; van Grondelle, R. Dynamics of the Emission Spectrum of a Single LH2 Complex: Interplay of Slow and Fast Nuclear Motions. *Biophys. J.* **2006**, *90*, 2890−2902.
(11) Schlau-Cohen, G. S.; Wang, Q.; Southall, J.; Cogdell, R. J.; Moerner, W. E. Single-Molecule Spectroscopy Reveals Photosynthetic LH2 Complexes Switch between Emissive States. *Proc. Natl. Acad. Sci. U. S. A.* **2013**, *110*, 10899−10903.
(12) Goldsmith, R. H.; Moerner, W. E. Watching Conformational- and Photo-Dynamics of Single Fluorescent Proteins in Solution. *Nat. Chem.* **2010**, *2*, 179−186.
(13) Richter, M. F.; Baier, J.; Cogdell, R. J.; Köhler, J.; Oellerich, S. Single-Molecule Spectroscopic Characterization of Light-Harvesting 2 Complexes Reconstituted into Model Membranes. *Biophys. J.* **2007**, *93*, 183−191.
(14) Saga, Y.; Wazawa, T.; Mizoguchi, T.; Ishii, Y.; Yanagida, T.; Tamiaki, H. Spectral Heterogeneity in Single Light-Harvesting Chlorosomes from Green Sulfur Photosynthetic Bacterium Chlorobium Tepidum. *Photochem. Photobiol.* **2002**, *75*, 433−436.
(15) Wang, Q.; Moerner, W. E. Dissecting Pigment Architecture of Individual Photosynthetic Antenna Complexes in Solution. *Proc. Natl. Acad. Sci. U. S. A.* **2015**, *112*, 13880−13885.
(16) Ying, L.; Xie, X. S. Fluorescence Spectroscopy, Exciton Dynamics, and Photochemistry of Single Allophycocyanin Trimers. *J. Phys. Chem. B* **1998**, *102*, 10399−10409.
(17) Krüger, T. P. J.; Wientjes, E.; Croce, R.; van Grondelle, R. Conformational Switching Explains the Intrinsic Multifunctionality of Plant Light-Harvesting Complexes. *Proc. Natl. Acad. Sci. U. S. A.* **2011**, *108*, 13516−13521.
(18) Schlau-Cohen, G. S.; Yang, H.-Y.; Krüger, T. P. J.; Xu, P.; Gwizdala, M.; van Grondelle, R.; Croce, R.; Moerner, W. E. Single-Molecule Identification of Quenched and Unquenched States of LHCII. *J. Phys. Chem. Lett.* **2015**, *6*, 860−867.

DOI: 10.1021/acs.chemrev.6b00195
Chem. Rev. XXXX, XXX, XXX−XXX

(19) Bopp, M. A.; Jia, Y.; Li, L.-Q.; Cogdell, R. J.; Hochstrasser, R. M. Fluorescence and Photobleaching Dynamics of Single Light-Harvesting Complexes. *Proc. Natl. Acad. Sci. U. S. A.* **1997**, *94*, 10630−10635.
(20) Tietz, C.; Jelezko, F.; Gerken, U.; Schuler, S.; Schubert, A.; Rogl, H.; Wrachtrup, J. Single Molecule Spectroscopy on the Light-Harvesting Complex II of Higher Plants. *Biophys. J.* **2001**, *81*, 556−562.
(21) Moerner, W. E.; Fromm, D. P. Methods of Single-Molecule Fluorescence Spectroscopy and Microscopy. *Rev. Sci. Instrum.* **2003**, *74*, 3597.
(22) Kulzer, F.; Orrit, M. Single-Molecule Optics. *Annu. Rev. Phys. Chem.* **2004**, *55*, 585−611.
(23) Huang, F.; Hartwich, T. M. P.; Rivera-Molina, F. E.; Lin, Y.; Duim, W. C.; Long, J. J.; Uchil, P. D.; Myers, J. R.; Baird, M. A.; Mothes, W.; et al. Video-Rate Nanoscopy Using sCMOS Camera-Specific Single-Molecule Localization Algorithms. *Nat. Methods* **2013**, *10*, 653−658.
(24) Becker, K.; Lupton, J. M. Efficient Light Harvesting in Dye-Endcapped Conjugated Polymers Probed by Single Molecule Spectroscopy. *J. Am. Chem. Soc.* **2006**, *128*, 6468−6479.
(25) Aratani, N.; Kim, D.; Osuka, A. Discrete Cyclic Porphyrin Arrays as Artificial Light-Harvesting Antenna. *Acc. Chem. Res.* **2009**, *42*, 1922−1934.
(26) Liu, Z.; Yan, H.; Wang, K.; Kuang, T.; Zhang, J.; Gui, L.; An, X.; Chang, W. Crystal Structure of Spinach Major Light-Harvesting Complex at 2.72 Å Resolution. *Nature* **2004**, *428* (6980), 287−292.
(27) Linnanto, J.; Korppi-Tommola, J. Quantum Chemical Simulation of Excited States of Chlorophylls, Bacteriochlorophylls and Their Complexes. *Phys. Chem. Chem. Phys.* **2006**, *8*, 663−687.
(28) Papiz, M. Z.; Prince, S. M.; Howard, T. D.; Cogdell, R. J.; Isaacs, N. W. The Structure and Thermal Motion of the B800−850 LH2 Complex from Rps.acidophila at 2.0A Resolution and 100K: New Structural Features and Functionally Relevant Motions. *J. Mol. Biol.* **2003**, *326*, 1523−1538.
(29) Jordan, P.; Fromme, P.; Witt, H. T.; Klukas, O.; Saenger, W.; Krauss, N. Three-Dimensional Structure of Cyanobacterial Photosystem I at 2.5 A Resolution. *Nature* **2001**, *411* (6840), 909−917.
(30) Loll, B.; Kern, J.; Saenger, W.; Zouni, A.; Biesiadka, J. Towards Complete Cofactor Arrangement in the 3.0 A Resolution Structure of Photosystem II. *Nature* **2005**, *438* (7070), 1040−1044.
(31) Katona, G.; Snijder, A.; Gourdon, P.; Andréasson, U.; Hansson, O.; Andréasson, L.-E.; Neutze, R. Conformational Regulation of Charge Recombination Reactions in a Photosynthetic Bacterial Reaction Center. *Nat. Struct. Mol. Biol.* **2005**, *12*, 630−631.
(32) Beddard, G. S.; Porter, G. Concentration Quenching in Chlorophyll. *Nature* **1976**, *260* (5549), 366−367.
(33) Ishizaki, A.; Calhoun, T. R.; Schlau-Cohen, G. S.; Fleming, G. R. Quantum Coherence and Its Interplay with Protein Environments in Photosynthetic Electronic Energy Transfer. *Phys. Chem. Chem. Phys.* **2010**, *12*, 7319−7337.
(34) Beljonne, D.; Curutchet, C.; Scholes, G. D.; Silbey, R. J. Beyond Förster Resonance Energy Transfer in Biological and Nanoscale Systems. *J. Phys. Chem. B* **2009**, *113*, 6583−6599.
(35) Andrews, D. L.; Curutchet, C.; Scholes, G. D. Resonance Energy Transfer: Beyond the Limits. *Laser Photon. Rev.* **2011**, *5*, 114−123.
(36) Fujihashi, Y.; Fleming, G. R.; Ishizaki, A. Impact of Environmentally Induced Fluctuations on Quantum Mechanically Mixed Electronic and Vibrational Pigment States in Photosynthetic Energy Transfer and 2D Electronic Spectra. *J. Chem. Phys.* **2015**, *142*, 212403.
(37) Fidder, H.; Knoester, J.; Wiersma, D. a. Optical Properties of Disordered Molecular Aggregates: A Numerical Study. *J. Chem. Phys.* **1991**, *95*, 7880.
(38) Adolphs, J.; Renger, T. How Proteins Trigger Excitation Energy Transfer in the FMO Complex of Green Sulfur Bacteria. *Biophys. J.* **2006**, *91*, 2778−2797.
(39) Ishizaki, A.; Fleming, G. R. On the Adequacy of the Redfield Equation and Related Approaches to the Study of Quantum Dynamics in Electronic Energy Transfer. *J. Chem. Phys.* **2009**, *130*, 234110.
(40) Szabó, I.; Bergantino, E.; Giacometti, G. M. Light and Oxygenic Photosynthesis: Energy Dissipation as a Protection Mechanism against Photo-Oxidation. *EMBO Rep.* **2005**, *6*, 629−634.
(41) Frauenfelder, H.; Petsko, G. A.; Tsernoglou, D. Temperature-Dependent X-Ray Diffraction as a Probe of Protein Structural Dynamics. *Nature* **1979**, *280* (5723), 558−563.
(42) Ansari, A.; Berendzen, J.; Bowne, S. F.; Frauenfelder, H.; Iben, I. E.; Sauke, T. B.; Shyamsunder, E.; Young, R. D. Protein States and Proteinquakes. *Proc. Natl. Acad. Sci. U. S. A.* **1985**, *82*, 5000−5004.
(43) Gafert, J.; Pschierer, H.; Friedrich, J. Proteins and Glasses: A Relaxation Study in the Millikelvin Range. *Phys. Rev. Lett.* **1995**, *74*, 3704−3707.
(44) Fritsch, K.; Friedrich, J.; Parak, F.; Skinner, J. L. Spectral Diffusion and the Energy Landscape of a Protein. *Proc. Natl. Acad. Sci. U. S. A.* **1996**, *93*, 15141−15145.
(45) Leeson, D. T.; Wiersma, D. A. Looking into the Energy Landscape of Myoglobin. *Nat. Struct. Biol.* **1995**, *2*, 848−851.
(46) Hofmann, C.; Aartsma, T. J.; Michel, H.; Köhler, J. Direct Observation of Tiers in the Energy Landscape of a Chromoprotein: A Single-Molecule Study. *Proc. Natl. Acad. Sci. U. S. A.* **2003**, *100*, 15534−15538.
(47) Friedrich, J.; Gafert, J.; Zollfrank, J.; Vanderkooi, J.; Fidy, J. Spectral Hole-Burning and Selection of Conformational Substates in Chromoproteins. *Proc. Natl. Acad. Sci. U. S. A.* **1994**, *91*, 1029−1033.
(48) Gafert, J.; Friedrich, J.; Vanderkooi, J. M.; Fidy, J. Structural Changes and Internal Fields in Proteins: A Hole-Burning Stark Effect Study of Horseradish Peroxidase. *J. Phys. Chem.* **1995**, *99*, 5223−5227.
(49) Brecht, M.; Radics, V.; Nieder, J. B.; Studier, H.; Bittl, R. Red Antenna States of Photosystem I from Synechocystis PCC 6803. *Biochemistry* **2008**, *47*, 5536−5543.
(50) Rutkauskas, D.; Novoderezkhin, V.; Cogdell, R. J.; van Grondelle, R. Fluorescence Spectral Fluctuations of Single LH2 Complexes from Rhodopseudomonas Acidophila Strain 10050. *Biochemistry* **2004**, *43*, 4431−4438.
(51) Rutkauskas, D.; Olsen, J. D.; Gall, A.; Cogdell, R. J.; Hunter, C. N.; van Grondelle, R. Comparative Study of Spectral Flexibilities of Bacterial Light-Harvesting Complexes: Structural Implications. *Biophys. J.* **2006**, *90*, 2463−2474.
(52) Shibata, Y.; Kurita, A.; Kushida, T. Real-Time Observation of Conformational Fluctuations in Zn-Substituted Myoglobin by Time-Resolved Transient Hole-Burning Spectroscopy. *Biophys. J.* **1998**, *75*, 521−527.
(53) Störkel, U.; Creemers, T. M. H.; den Hartog, F. T. H.; Völker, S. Glass versus Protein Dynamics at Low Temperature Studied by Time-Resolved Spectral Hole Burning. *J. Lumin.* **1998**, *76*−*77*, 327−330.
(54) Tietz, C.; Chekhlov, O.; Dräbenstedt, A.; Schuster, J.; Wrachtrup, J. Spectroscopy on Single Light-Harvesting Complexes at Low Temperature. *J. Phys. Chem. B* **1999**, *103*, 6328−6333.
(55) Scheuring, S.; Sturgis, J. N. Chromatic Adaptation of Photosynthetic Membranes. *Science* **2005**, *309* (5733), 484−487.
(56) Scheuring, S.; Rigaud, J.-L.; Sturgis, J. N. Variable LH2 Stoichiometry and Core Clustering in Native Membranes of Rhodospirillum Photometricum. *EMBO J.* **2004**, *23*, 4127−4133.
(57) Scheuring, S.; Gonçalves, R. P.; Prima, V.; Sturgis, J. N. The Photosynthetic Apparatus of Rhodopseudomonas Palustris: Structures and Organization. *J. Mol. Biol.* **2006**, *358*, 83−96.
(58) Monshouwer, R.; Abrahamsson, M.; van Mourik, F.; van Grondelle, R. Superradiance and Exciton Delocalization in Bacterial Photosynthetic Light-Harvesting Systems. *J. Phys. Chem. B* **1997**, *101*, 7241−7248.
(59) Gruber, J. M.; Chmeliov, J.; Krüger, T. P. J.; Valkunas, L.; van Grondelle, R. Singlet-Triplet Annihilation in Single LHCII Complexes. *Phys. Chem. Chem. Phys.* **2015**, *17*, 19844−19853.
(60) Qin, X.; Suga, M.; Kuang, T.; Shen, J.-R. Structural Basis for Energy Transfer Pathways in the Plant PSI-LHCI Supercomplex. *Science* **2015**, *348* (6238), 989−995.
(61) Mazor, Y.; Borovikova, A.; Nelson, N. The Structure of Plant Photosystem I Super-Complex at 2.8 Å Resolution. *eLife* **2015**, *4*, e07433.

DOI: 10.1021/acs.chemrev.6b00195
Chem. Rev. XXXX, XXX, XXX−XXX

(62) Schlau-Cohen, G. S.; Calhoun, T. R.; Ginsberg, N. S.; Read, E. L.; Ballottari, M.; Bassi, R.; van Grondelle, R.; Fleming, G. R. Pathways of Energy Flow in LHCII from Two-Dimensional Electronic Spectroscopy. *J. Phys. Chem. B* **2009**, *113*, 15352−15363.
(63) Andersson, B.; Anderson, J. M. Lateral Heterogeneity in the Distribution of Chlorophyll-Protein Complexes of the Thylakoid Membranes of Spinach Chloroplasts. *Biochim. Biophys. Acta, Bioenerg.* **1980**, *593*, 427−440.
(64) Croce, R.; van Amerongen, H. Light-Harvesting and Structural Organization of Photosystem II: From Individual Complexes to Thylakoid Membrane. *J. Photochem. Photobiol., B* **2011**, *104*, 142−153.
(65) Schlau-Cohen, G. S.; Calhoun, T. R.; Ginsberg, N. S.; Ballottari, M.; Bassi, R.; Fleming, G. R. Spectroscopic Elucidation of Uncoupled Transition Energies in the Major Photosynthetic Light-Harvesting Complex, LHCII. *Proc. Natl. Acad. Sci. U. S. A.* **2010**, *107*, 13276−13281.
(66) Erickson, E.; Wakao, S.; Niyogi, K. K. Light Stress and Photoprotection in Chlamydomonas Reinhardtii. *Plant J.* **2015**, *82*, 449−465.
(67) Croce, R.; van Amerongen, H. Natural Strategies for Photosynthetic Light Harvesting. *Nat. Chem. Biol.* **2014**, *10*, 492−501.
(68) Niyogi, K. K.; Truong, T. B. Evolution of Flexible Non-Photochemical Quenching Mechanisms That Regulate Light Harvesting in Oxygenic Photosynthesis. *Curr. Opin. Plant Biol.* **2013**, *16*, 307−314.
(69) Morosinotto, T.; Bassi, R. Non-Photochemical Quenching and Energy Dissipation in Plants, Algae and Cyanobacteria. *Advances in Photosynthesis and Respiration*; Demmig-Adams, B., Garab, G., Adams, III, W., Eds.; Springer: Dordrecht, Netherlands, 2014; Vol. *40*.
(70) Ruban, A. V.; Johnson, M. P.; Duffy, C. D. P. The Photoprotective Molecular Switch in the Photosystem II Antenna. *Biochim. Biophys. Acta, Bioenerg.* **2012**, *1817*, 167−181.
(71) Zaks, J.; Amarnath, K.; Sylak-Glassman, E. J.; Fleming, G. R. Models and Measurements of Energy-Dependent Quenching. *Photosynth. Res.* **2013**, *116*, 389−409.
(72) Moerner, W. E.; Basché, T. Optical Spectroscopy of Single Impurity Molecules in Solids. *Angew. Chem., Int. Ed. Engl.* **1993**, *32*, 457−628.
(73) Lang, E.; Baier, J.; Köhler, J. Epifluorescence, Confocal and Total Internal Reflection Microscopy for Single-Molecule Experiments: A Quantitative Comparison. *J. Microsc.* **2006**, *222*, 118−123.
(74) Lakowicz, J. R.*Principles of Fluorescence Spectroscopy*; Springer: Boston, MA, 1983; DOI: 10.1007/978-1-4615-7658-7.
(75) Löhner, A.; Ashraf, K.; Cogdell, R. J.; Köhler, J. Fluorescence-Excitation and Emission Spectroscopy on Single FMO Complexes. *Sci. Rep.* **2016**, *6* (April), 31875.
(76) *Alexa Fluor Dyes Spanning the Visible and Infrared Spectrum*; ThermoFisher Scientific.
(77) Porra, R. J.; Thompson, W. A.; Kriedemann, P. E. Determination of Accurate Extinction Coefficients and Simultaneous Equations for Assaying Chlorophylls a and B Extracted with Four Different Solvents: Verification of the Concentration of Chlorophyll Standards by Atomic Absorption Spectroscopy. *Biochim. Biophys. Acta, Bioenerg.* **1989**, *975*, 384−394.
(78) Grabowski, J.; Gantt, E. Photophysical Properties of Phycobiliproteins from Phycobilisomes: Fluorescence Lifetimes, Quantum Yields, and Polarization Spectra. *Photochem. Photobiol.* **1978**, *28*, 39−45.
(79) Ha, T.; Tinnefeld, P. Photophysics of Fluorescent Probes for Single-Molecule Biophysics and Super-Resolution Imaging. *Annu. Rev. Phys. Chem.* **2012**, *63*, 595−617.
(80) Dittrich, P. S.; Schwille, P. Photobleaching and Stabilization Of. Fluorophores Used for Single-Molecule Analysis. with One- and Two-Photon Excitation. *Appl. Phys. B: Lasers Opt.* **2001**, *73*, 829−837.
(81) Song, L.; Hennink, E. J.; Young, I. T.; Tanke, H. J. Photobleaching Kinetics of Fluorescein in Quantitative Fluorescence Microscopy. *Biophys. J.* **1995**, *68*, 2588−2600.
(82) Aitken, C. E.; Marshall, R. A.; Puglisi, J. D. An Oxygen Scavenging System for Improvement of Dye Stability in Single-Molecule Fluorescence Experiments. *Biophys. J.* **2008**, *94*, 1826−1835.
(83) Swoboda, M.; Henig, J.; Cheng, H.-M.; Brugger, D.; Haltrich, D.; Plumeré, N.; Schlierf, M. Enzymatic Oxygen Scavenging for Photostability without pH Drop in Single-Molecule Experiments. *ACS Nano* **2012**, *6*, 6364−6369.
(84) Frank, H. A.; Cogdell, R. J. Carotenoids in Photosynthesis. *Photochem. Photobiol.* **1996**, *63*, 257−264.
(85) Walter, N. G. Single Molecule Detection, Analysis, and Manipulation. *Encyclopedia of Analytical Chemistry*; John Wiley & Sons Ltd: Chichester, UK, 2008.
(86) Manley, S.; Gillette, J. M.; Lippincott-Schwartz, J. Single-Particle Tracking Photoactivated Localization Microscopy for Mapping Single-Molecule Dynamics. *Methods Enzymol.* **2010**, *475*, 109−120.
(87) Hurbain, I.; Sachse, M. The Future Is Cold: Cryo-Preparation Methods for Transmission Electron Microscopy of Cells. *Biol. Cell* **2011**, *103*, 405−420.
(88) Rigort, A.; Bäuerlein, F. J. B.; Leis, A.; Gruska, M.; Hoffmann, C.; Laugks, T.; Böhm, U.; Eibauer, M.; Gnaegi, H.; Baumeister, W.; et al. Micromachining Tools and Correlative Approaches for Cellular Cryo-Electron Tomography. *J. Struct. Biol.* **2010**, *172*, 169−179.
(89) van Driel, L. F.; Valentijn, J. A.; Valentijn, K. M.; Koning, R. I.; Koster, A. J. Tools for Correlative Cryo-Fluorescence Microscopy and Cryo-Electron Tomography Applied to Whole Mitochondria in Human Endothelial Cells. *Eur. J. Cell Biol.* **2009**, *88*, 669−684.
(90) Friedel, M.; Baumketner, A.; Shea, J.-E. Effects of Surface Tethering on Protein Folding Mechanisms. *Proc. Natl. Acad. Sci. U. S. A.* **2006**, *103*, 8396−8401.
(91) Bai, H.; Kath, J. E.; Zörgiebel, F. M.; Sun, M.; Ghosh, P.; Hatfull, G. F.; Grindley, N. D. F.; Marko, J. F. Remote Control of DNA-Acting Enzymes by Varying the Brownian Dynamics of a Distant DNA End. *Proc. Natl. Acad. Sci. U. S. A.* **2012**, *109*, 16546−16551.
(92) Cohen, A. E.; Moerner, W. E. Controlling Brownian Motion of Single Protein Molecules and Single Fluorophores in Aqueous Buffer. *Opt. Express* **2008**, *16*, 6941−6956.
(93) Wang, Q.; Moerner, W. E. An Adaptive Anti-Brownian ELectrokinetic Trap with Real-Time Information on Single-Molecule Diffusivity and Mobility. *ACS Nano* **2011**, *5*, 5792−5799.
(94) Wang, Q.; Moerner, W. E. Single-Molecule Motions Enable Direct Visualization of Biomolecular Interactions in Solution. *Nat. Methods* **2014**, *11*, 555−558.
(95) Bockenhauer, S.; Moerner, W. E. Photo-Induced Conformational Flexibility in Single Solution-Phase Peridinin-Chlorophyll-Proteins. *J. Phys. Chem. A* **2013**, *117*, 8399−8406.
(96) Cohen, A. E.; Moerner, W. E. Method for Trapping and Manipulating Nanoscale Objects in Solution. *Appl. Phys. Lett.* **2005**, *86*, 093109.
(97) Seddon, A. M.; Curnow, P.; Booth, P. J. Membrane Proteins, Lipids and Detergents: Not Just a Soap Opera. *Biochim. Biophys. Acta, Biomembr.* **2004**, *1666*, 105−117.
(98) Hussels, M.; Brecht, M. Evidence for Direct Binding of Glycerol to Photosystem I. *FEBS Lett.* **2011**, *585*, 2445−2449.
(99) Hussels, M.; Brecht, M. Effect of Glycerol and PVA on the Conformation of Photosystem I. *Biochemistry* **2011**, *50*, 3628−3637.
(100) Freiberg, A.; Lin, S.; Timpmann, K.; Blankenship, R. E. Exciton Dynamics in FMO Bacteriochlorophyll Protein at Low Temperatures. *J. Phys. Chem. B* **1997**, *101*, 7211−7220.
(101) Sase, I.; Miyata, H.; Corrie, J.; Craik, J. S.; Kinosita, K., Jr. Real-Time Imaging of Single Fluorophores on Moving Actin with an Epifluorescence Microscope. *Biophys. J.* **1995**, *69*, 323−328.
(102) Arimoto, R.; Murray, J. M. A Common Aberration with Water-Immersion Objective Lenses. *J. Microsc.* **2004**, *216*, 49−51.
(103) Wan, D.-S.; Rajadhyaksha, M.; Webb, R. H. Analysis of Spherical Aberration of a Water Immersion Objective: Application to Specimens with Refractive Indices 1.33−1.40. *J. Microsc.* **2000**, *197*, 274−284.
(104) Lien, I.; Nagelhus, T. A.; Knutsen, S. M.; Sande, L. M.; Lindmo, T. Correction Methods for Fluorescence Quantitation in

DOI: 10.1021/acs.chemrev.6b00195
Chem. Rev. XXXX, XXX, XXX−XXX

Thick Specimens by Confocal Microscopy. *Proc. SPIE* **1996**, *2678*, 176−183.
(105) Toomre, D.; Manstein, D. J. Lighting up the Cell Surface with Evanescent Wave Microscopy. *Trends Cell Biol.* **2001**, *11*, 298−303.
(106) Roy, R.; Hohng, S.; Ha, T. A Practical Guide to Single-Molecule FRET. *Nat. Methods* **2008**, *5*, 507−516.
(107) Axelrod, D.; Burghardt, T. P.; Thompson, N. L. Total Internal Reflection Fluorescence. *Annu. Rev. Biophys. Bioeng.* **1984**, *13*, 247−268.
(108) Axelrod, D. Cell-Substrate Contacts Illuminated by Total Internal-Reflection Fluorescence. *J. Cell Biol.* **1981**, *89*, 141−145.
(109) Fish, K. N. Total Internal Reflection Fluorescence (TIRF) Microscopy. In *Current Protocols in Cytometry*; John Wiley & Sons, Inc.: Hoboken, NJ, 2009; pp 12.18.1−12.18.13.
(110) Funatsu, T.; Harada, Y.; Tokunaga, M.; Saito, K.; Yanagida, T. Imaging of Fluorescent Molecules and Individual ATP Turnovers by Single Myosin Molecules in Aqueous-Solution. *Nature* **1995**, *374* (6522), 555−559.
(111) Coskun, A. F.; Su, T.-W.; Ozcan, A. Wide Field-of-View Lens-Free Fluorescent Imaging on a Chip. *Lab Chip* **2010**, *10*, 824.
(112) Tokunaga, M.; Kitamura, K.; Saito, K.; Iwane, A. H.; Yanagida, T. Single Molecule Imaging of Fluorophores and Enzymatic Reactions Achieved by Objective-Type Total Internal Reflection Fluorescence Microscopy. *Biochem. Biophys. Res. Commun.* **1997**, *235*, 47−53.
(113) Saga, Y.; Wazawa, T.; Nakada, T.; Ishii, Y.; Yanagida, T.; Tamiaki, H. Fluorescence Emission Spectroscopy of Single Light-Harvesting Complex from Green Filamentous Photosynthetic Bacteria. *J. Phys. Chem. B* **2002**, *106*, 1430−1433.
(114) Nishizaka, T.; Oiwa, K.; Noji, H.; Kimura, S.; Muneyuki, E.; Yoshida, M.; Kinosita, K. Chemomechanical Coupling in F1-ATPase Revealed by Simultaneous Observation of Nucleotide Kinetics and Rotation. *Nat. Struct. Mol. Biol.* **2004**, *11*, 142−148.
(115) Jendrny, M.; Aartsma, T. J.; Köhler, J. Fluorescence Excitation Spectra from Individual Chlorosomes of the Green Sulfur Bacterium Chlorobaculum Tepidum. *J. Phys. Chem. Lett.* **2012**, *3*, 3745−3750.
(116) Lee, S.; Oh, J.; Kim, D.; Kim, S.; Lee, J.-B.; Nam, H. G. Polarization-Controlled Photoswitching Resolves Dipole Directions with Subwavelength Resolution. *Phys. Rev. Lett.* **2012**, *109*, 248101.
(117) van Oijen, A. M.; Ketelaars, M.; Köhler, J.; Aartsma, T. J.; Schmidt, J. Spectroscopy of Single Light-Harvesting Complexes from Purple Photosynthetic Bacteria at 1.2 K. *J. Phys. Chem. B* **1998**, *102*, 9363−9366.
(118) Vácha, M.; Yokoyama, H.; Tokizaki, T.; Furuki, M.; Tani, T. Laser Scanning Microscope for Low Temperature Single Molecule and Microscale Spectroscopy Based on Gradient Index Optics. *Rev. Sci. Instrum.* **1999**, *70*, 2041.
(119) Zondervan, R.; Kulzer, F.; van der Meer, H.; Disselhorst, J. A. J. M.; Orrit, M. Laser-Driven Microsecond Temperature Cycles Analyzed by Fluorescence Polarization Microscopy. *Biophys. J.* **2006**, *90*, 2958−2969.
(120) Shibata, Y.; Katoh, W.; Chiba, T.; Namie, K.; Ohnishi, N.; Minagawa, J.; Nakanishi, H.; Noguchi, T.; Fukumura, H. Development of a Novel Cryogenic Microscope with Numerical Aperture of 0.9 and Its Application to Photosynthesis Research. *Biochim. Biophys. Acta, Bioenerg.* **2014**, *1837*, 880−887.
(121) Fujiyoshi, S.; Hirano, M.; Matsushita, M.; Iseki, M.; Watanabe, M. Structural Change of a Cofactor Binding Site of Flavoprotein Detected by Single-Protein Fluorescence Spectroscopy at 1.5 K. *Phys. Rev. Lett.* **2011**, *106*, 078101.
(122) Maruo, M.; Inagawa, H.; Toratani, Y.; Kondo, T.; Matsushita, M.; Fujiyoshi, S. Three-Dimensional Laser-Scanning Confocal Reflecting Microscope for Multicolor Single-Molecule Imaging at 1.5K. *Chem. Phys. Lett.* **2014**, *591*, 233−236.
(123) Felekyan, S.; Kühnemuth, R.; Kudryavtsev, V.; Sandhagen, C.; Becker, W.; Seidel, C. A. M. Full Correlation from Picoseconds to Seconds by Time-Resolved and Time-Correlated Single Photon Detection. *Rev. Sci. Instrum.* **2005**, *76*, 083104.
(124) Kumazaki, S.; Hasegawa, M.; Ghoneim, M.; Shimizu, Y.; Okamoto, K.; Nishiyama, M.; Oh-Oka, H.; Terazima, M. A Line-Scanning Semi-Confocal Multi-Photon Fluorescence Microscope with a Simultaneous Broadband Spectral Acquisition and Its Application to the Study of the Thylakoid Membrane of a Cyanobacterium Anabaena PCC7120. *J. Microsc.* **2007**, *228* (Pt 2), 240−254.
(125) Kunz, R.; Timpmann, K.; Southall, J.; Cogdell, R. J.; Freiberg, A.; Köhler, J. Exciton Self Trapping in Photosynthetic Pigment-Protein Complexes Studied by Single-Molecule Spectroscopy. *J. Phys. Chem. B* **2012**, *116*, 11017−11023.
(126) Hofmann, C.; Ketelaars, M.; Matsushita, M.; Michel, H.; Aartsma, T. J.; Köhler, J. Single-Molecule Study of the Electronic Couplings in a Circular Array of Molecules: Light-Harvesting-2 Complex from Rhodospirillum Molischianum. *Phys. Rev. Lett.* **2003**, *90*, 013004.
(127) Brecht, M. Spectroscopic Characterization of Photosystem I at the Single-Molecule Level. *Mol. Phys.* **2009**, *107*, 1955−1974.
(128) Tamarat, P.; Maali, A.; Lounis, B.; Orrit, M. Ten Years of Single-Molecule Spectroscopy. *J. Phys. Chem. A* **2000**, *104*, 1−16.
(129) Ambrose, W. P.; Basché, T.; Moerner, W. E. Detection and Spectroscopy of Single Pentacene Molecules in a P-Terphenyl Crystal by Means of Fluorescence Excitation. *J. Chem. Phys.* **1991**, *95*, 7150.
(130) Heinecke, E.; Donovang, K.; Müller, C.; Hese, A. Single Molecule Spectroscopy in He Gas Using a Highly Efficient Mirror Arrangement. *Rev. Sci. Instrum.* **1997**, *68*, 2990.
(131) Brunel, C.; Lounis, B.; Tamarat, P.; Orrit, M. Triggered Source of Single Photons Based on Controlled Single Molecule Fluorescence. *Phys. Rev. Lett.* **1999**, *83*, 2722−2725.
(132) Fleury, L.; Tamarat, P.; Lounis, B.; Bernard, J.; Orrit, M. Fluorescence Spectra of Single Pentacene Molecules in P-Terphenyl at 1.7 K. *Chem. Phys. Lett.* **1995**, *236*, 87−95.
(133) Wild, U. P.; Güttler, F.; Pirotta, M.; Renn, A. Single Molecule Spectroscopy: Stark Effect of Pentacene in P-Terphenyl. *Chem. Phys. Lett.* **1992**, *193*, 451−455.
(134) van Oijen, A. M.; Ketelaars, M.; Köhler, J.; Aartsma, T. J.; Schmidt, J. Spectroscopy of Individual LH2 Complexes of Rhodopseudomonas Acidophila: Localized Excitations in the B800 Band. *Chem. Phys.* **1999**, *247*, 53−60.
(135) Göhde, W.; Tittel, J.; Basché, T.; Bräuchle, C.; Fischer, U. C.; Fuchs, H. A Low-Temperature Scanning Confocal and near-Field Optical Microscope. *Rev. Sci. Instrum.* **1997**, *68*, 2466.
(136) Jasny, J.; Sepiol, J.; Irngartinger, T.; Traber, M.; Renn, A.; Wild, U. P. Fluorescence Microscopy in Superfluid Helium: Single Molecule Imaging. *Rev. Sci. Instrum.* **1996**, *67*, 1425.
(137) Fujiyoshi, S.; Fujiwara, M.; Kim, C.; Matsushita, M.; van Oijen, A. M.; Schmidt, J. Single-Component Reflecting Objective for Low-Temperature Spectroscopy in the Entire Visible Region. *Appl. Phys. Lett.* **2007**, *91*, 051125.
(138) Fujiwara, M.; Fujiyoshi, S.; Matsushita, M. Single-Component Reflecting Objective for Ultraviolet Imaging and Spectroscopy at Cryogenic Temperature. *J. Opt. Soc. Am. B* **2009**, *26*, 1395.
(139) Fujiyoshi, S.; Furuya, Y.; Iseki, M.; Watanabe, M.; Matsushita, M. Vibrational Microspectroscopy of Single Proteins. *J. Phys. Chem. Lett.* **2010**, *1*, 2541−2545.
(140) Fujiyoshi, S.; Fujiwara, M.; Matsushita, M. Visible Fluorescence Spectroscopy of Single Proteins at Liquid-Helium Temperature. *Phys. Rev. Lett.* **2008**, *100*, 168101.
(141) Inagawa, H.; Toratani, Y.; Motohashi, K.; Nakamura, I.; Matsushita, M.; Fujiyoshi, S. Reflecting Microscope System with a 0.99 Numerical Aperture Designed for Three-Dimensional Fluorescence Imaging of Individual Molecules at Cryogenic Temperatures. *Sci. Rep.* **2015**, *5*, 12833.
(142) Nakamura, I.; Yoshihiro, T.; Inagawa, H.; Fujiyoshi, S.; Matsushita, M. Spectroscopy of Single Pr3+ Ion in LaF3 Crystal at 1.5 K. *Sci. Rep.* **2014**, *4*, 7364.
(143) Smith, E. A.; Cinquin, B. P.; Do, M.; McDermott, G.; Le Gros, M. A.; Larabell, C. A. Correlative Cryogenic Tomography of Cells Using Light and Soft X-Rays. *Ultramicroscopy* **2014**, *143*, 33−40.
(144) Le Gros, M. A.; McDermott, G.; Uchida, M.; Knoechel, C. G.; Larabell, C. A. High-Aperture Cryogenic Light Microscopy. *J. Microsc.* **2009**, *235*, 1−8.

DOI: 10.1021/acs.chemrev.6b00195
Chem. Rev. XXXX, XXX, XXX−XXX

(145) Metzger, M.; Konrad, A.; Skandary, S.; Ashraf, I.; Meixner, A. J.; Brecht, M. Resolution Enhancement for Low-Temperature Scanning Microscopy by Cryo-Immersion. *Opt. Express* **2016**, *24*, 13023.
(146) Shibata, Y.; Saga, Y.; Tamiaki, H.; Itoh, S. Low-Temperature Fluorescence from Single Chlorosomes, Photosynthetic Antenna Complexes of Green Filamentous and Sulfur Bacteria. *Biophys. J.* **2006**, *91*, 3787−3796.
(147) Shibata, Y.; Katoh, W.; Tahara, Y. Study of Cell-Differentiation and Assembly of Photosynthetic Proteins during Greening of Etiolated Zea Mays Leaves Using Confocal Fluorescence Microspectroscopy at Liquid-Nitrogen Temperature. *Biochim. Biophys. Acta, Bioenerg.* **2013**, *1827*, 520−528.
(148) van Oijen, A. M.; Ketelaars, M.; Köhler, J.; Aartsma, T. J.; Schmidt, J. Unraveling the Electronic Structure of Individual Photosynthetic Pigment−Protein Complexes. *Science* **1999**, *285* (5426), 400−402.
(149) Köhler, J.; Disselhorst, J. A. J. M.; Donckers, M. C. J. M.; Groenen, E. J. J.; Schmidt, J.; Moerner, W. E. Magnetic Resonance of a Single Molecular Spin. *Nature* **1993**, *363*, 242−244.
(150) Wrachtrup, J.; Vonborczyskowski, C.; Bernard, J.; Orritt, M.; Brown, R. Optical-Detection of Magnetic-Resonance in a Single Molecule. *Nature* **1993**, *363* (6426), 244−245.
(151) Hussels, M.; Konrad, A.; Brecht, M. Confocal Sample-Scanning Microscope for Single-Molecule Spectroscopy and Microscopy with Fast Sample Exchange at Cryogenic Temperatures. *Rev. Sci. Instrum.* **2012**, *83*, 123706.
(152) Nie, S.; Chiu, D.; Zare, R. Probing Individual Molecules with Confocal Fluorescence Microscopy. *Science (Washington, DC, U. S.)* **1994**, *266* (5187), 1018−1021.
(153) van Oijen, A. M.; Ketelaars, M.; Köhler, J.; Aartsma, T. J.; Schmidt, J. Spectroscopy of Individual Light-Harvesting 2 Complexes of Rhodopseudomonas Acidophila: Diagonal Disorder, Intercomplex Heterogeneity, Spectral Diffusion, and Energy Transfer in the B800 Band. *Biophys. J.* **2000**, *78*, 1570−1577.
(154) Zondervan, R.; Kulzer, F.; Kol'chenk, M. A.; Orrit, M. Photobleaching of Rhodamine 6G in Poly(vinyl Alcohol) at the Ensemble and Single-Molecule Levels. *J. Phys. Chem. A* **2004**, *108*, 1657−1665.
(155) Palacios, M. A.; de Weerd, F. L.; Ihalainen, J. A.; van Grondelle, R.; van Amerongen, H. Superradiance and Exciton (De)localization in Light-Harvesting Complex II from Green Plants? †. *J. Phys. Chem. B* **2002**, *106*, 5782−5787.
(156) Oellerich, S.; Köhler, J. Low-Temperature Single-Molecule Spectroscopy on Photosynthetic Pigment-Protein Complexes from Purple Bacteria. *Photosynth. Res.* **2009**, *101*, 171−179.
(157) Kunz, R.; Timpmann, K.; Southall, J.; Cogdell, R. J.; Freiberg, A.; Köhler, J. Single-Molecule Spectroscopy Unmasks the Lowest Exciton State of the B850 Assembly in LH2 from Rps. Acidophila. *Biophys. J.* **2014**, *106*, 2008−2016.
(158) Ketelaars, M.; Segura, J.-M.; Oellerich, S.; de Ruijter, W. P. F.; Magis, G.; Aartsma, T. J.; Matsushita, M.; Schmidt, J.; Cogdell, R. J.; Köhler, J. Probing the Electronic Structure and Conformational Flexibility of Individual Light-Harvesting 3 Complexes by Optical Single-Molecule Spectroscopy. *J. Phys. Chem. B* **2006**, *110*, 18710−18717.
(159) de Ruijter, W. P. F.; Segura, J.-M.; Cogdell, R. J.; Gardiner, A. T.; Oellerich, S.; Aartsma, T. J. Fluorescence-Emission Spectroscopy of Individual LH2 and LH3 Complexes. *Chem. Phys.* **2007**, *341*, 320−325.
(160) de Ruijter, W. P. F.; Oellerich, S.; Segura, J.-M.; Lawless, A. M.; Papiz, M. Z.; Aartsma, T. J. Observation of the Energy-Level Structure of the Low-Light Adapted B800 LH4 Complex by Single-Molecule Spectroscopy. *Biophys. J.* **2004**, *87*, 3413−3420.
(161) Brotosudarmo, T. H. P.; Kunz, R.; Böhm, P. S.; Gardiner, A. T.; Moulisová, V.; Cogdell, R. J.; Köhler, J. Single-Molecule Spectroscopy Reveals That Individual Low-Light LH2 Complexes from Rhodopseudomonas Palustris 2.1.6. Have a Heterogeneous Polypeptide Composition. *Biophys. J.* **2009**, *97*, 1491−1500.
(162) Jelezko, F.; Tietz, C.; Gerken, U.; Thews, E.; Schuler, S.; Wechsler, A.; Wrachtrup, J. Single Molecule Spectroscopy on Photosynthetic Pigment-Protein Complexes. *Opt. Spectrosc.* **2001**, *91*, 457−460.
(163) Saga, Y.; Shibata, Y.; Tamiaki, H. Spectral Properties of Single Light-Harvesting Complexes in Bacterial Photosynthesis. *J. Photochem. Photobiol., C* **2010**, *11*, 15−24.
(164) Ketelaars, M.; Hofmann, C.; Köhler, J.; Howard, T. D.; Cogdell, R. J.; Schmidt, J.; Aartsma, T. J. Spectroscopy on Individual Light-Harvesting 1 Complexes of Rhodopseudomonas Acidophila. *Biophys. J.* **2002**, *83*, 1701−1715.
(165) Gerken, U.; Lupo, D.; Tietz, C.; Wrachtrup, J.; Ghosh, R. Circular Symmetry of the Light-Harvesting 1 Complex from Rhodospirillum Rubrum Is Not Perturbed by Interaction with the Reaction Center. *Biochemistry* **2003**, *42*, 10354−10360.
(166) Böhm, P. S.; Southall, J.; Cogdell, R. J.; Köhler, J. Single-Molecule Spectroscopy on RC-LH1 Complexes of Rhodopseudomonas Acidophila Strain 10050. *J. Phys. Chem. B* **2013**, *117*, 3120−3126.
(167) Brecht, M.; Skandary, S.; Hellmich, J.; Glöckner, C.; Konrad, A.; Hussels, M.; Meixner, A. J.; Zouni, A.; Schlodder, E. Spectroscopic Properties of Photosystem II Core Complexes from Thermosynechococcus Elongatus Revealed by Single-Molecule Experiments. *Biochim. Biophys. Acta, Bioenerg.* **2014**, *1837*, 773−781.
(168) Skandary, S.; Hussels, M.; Konrad, A.; Renger, T.; Müh, F.; Bommer, M.; Zouni, A.; Meixner, A. J.; Brecht, M. Variation of Exciton-Vibrational Coupling in Photosystem II Core Complexes from Thermosynechococcus Elongatus as Revealed by Single-Molecule Spectroscopy. *J. Phys. Chem. B* **2015**, *119*, 4203−4210.
(169) Hecht, B.; Sick, B.; Wild, U. P.; Deckert, V.; Zenobi, R.; Martin, O. J. F.; Pohl, D. W. Scanning near-Field Optical Microscopy with Aperture Probes: Fundamentals and Applications. *J. Chem. Phys.* **2000**, *112*, 7761.
(170) Synge, E. H. XXXVIII. *A Suggested Method for Extending Microscopic Resolution into the Ultra-Microscopic Region. London, Edinburgh, Dublin Philos. Mag. J. Sci.* **1928**, *6*, 356−362.
(171) Betzig, E.; Trautman, J. K. Near-Field Optics: Microscopy, Spectroscopy, and Surface Modification Beyond the Diffraction Limit. *Science (Washington, DC, U. S.)* **1992**, *257* (5067), 189−195.
(172) Betzig, E.; Chichester, R. J. Single Molecules Observed by Near-Field Scanning Optical Microscopy. *Science (Washington, DC, U. S.)* **1993**, *262* (5138), 1422−1425.
(173) Eisenberg, I.; Yochelis, S.; Ben-Harosh, R.; David, L.; Faust, A.; Even-Dar, N.; Taha, H.; Haegel, N. M.; Adir, N.; Keren, N.; et al. Room Temperature Biological Quantum Random Walk in Phycocyanin Nanowires. *Phys. Chem. Chem. Phys.* **2014**, *16*, 11196−11201.
(174) Gerster, D.; Reichert, J.; Bi, H.; Barth, J. V.; Kaniber, S. M.; Holleitner, A. W.; Visoly-Fisher, I.; Sergani, S.; Carmeli, I. Photocurrent of a Single Photosynthetic Protein. *Nat. Nanotechnol.* **2012**, *7*, 673−676.
(175) Frolov, L.; Rosenwaks, Y.; Carmeli, C.; Carmeli, I. Fabrication of a Photoelectronic Device by Direct Chemical Binding of the Photosynthetic Reaction Center Protein to Metal Surfaces. *Adv. Mater.* **2005**, *17*, 2434−2437.
(176) Das, R.; Kiley, P. J.; Segal, M.; Norville, J.; Yu, A. A.; Wang, L.; Trammell, S. A.; Reddick, L. E.; Kumar, R.; Stellacci, F.; et al. Integration of Photosynthetic Protein Molecular Complexes in Solid-State Electronic Devices. *Nano Lett.* **2004**, *4*, 1079−1083.
(177) Lee, I.; Lee, J. W.; Greenbaum, E. Biomolecular Electronics: Vectorial Arrays of Photosynthetic Reaction Centers. *Phys. Rev. Lett.* **1997**, *79*, 3294−3297.
(178) Hell, S. W.; Wichmann, J. Breaking the Diffraction Resolution Limit by Stimulated Emission: Stimulated-Emission-Depletion Fluorescence Microscopy. *Opt. Lett.* **1994**, *19*, 780−782.
(179) Brinks, D.; Hildner, R.; van Dijk, E. M. H. P.; Stefani, F. D.; Nieder, J. B.; Hernando, J.; van Hulst, N. F. Ultrafast Dynamics of Single Molecules. *Chem. Soc. Rev.* **2014**, *43*, 2476.
(180) Hildner, R.; Brinks, D.; Nieder, J. B.; Cogdell, R. J.; van Hulst, N. F. Quantum Coherent Energy Transfer over Varying Pathways in

DOI: 10.1021/acs.chemrev.6b00195
Chem. Rev. XXXX, XXX, XXX−XXX

Single Light-Harvesting Complexes. *Science* **2013**, *340* (6139), 1448−1451.
(181) van Dijk, E. M. H. P.; Hernando, J.; García-López, J.-J.; Crego-Calama, M.; Reinhoudt, D. N.; Kuipers, L.; García-Parajó, M. F.; van Hulst, N. F. Single-Molecule Pump-Probe Detection Resolves Ultrafast Pathways in Individual and Coupled Quantum Systems. *Phys. Rev. Lett.* **2005**, *94*, 078302.
(182) van Dijk, E. M. H. P.; Hernando, J.; García-Parajó, M. F.; van Hulst, N. F. Single-Molecule Pump-Probe Experiments Reveal Variations in Ultrafast Energy Redistribution. *J. Chem. Phys.* **2005**, *123*, 064703.
(183) Malý, P.; Gruber, J. M.; Cogdell, R. J.; Mančal, T.; van Grondelle, R. Ultrafast Energy Relaxation in Single Light-Harvesting Complexes. *Proc. Natl. Acad. Sci. U. S. A.* **2016**, *113*, 2934−2939.
(184) Michalet, X.; Colyer, R. A.; Scalia, G.; Ingargiola, A.; Lin, R.; Millaud, J. E.; Weiss, S.; Siegmund, O. H. W.; Tremsin, A. S.; Vallerga, J. V.; et al. Development of New Photon-Counting Detectors for Single-Molecule Fluorescence Microscopy. *Philos. Trans. R. Soc., B* **2013**, *368* (1611), 20120035.
(185) Eisaman, M. D.; Fan, J.; Migdall, A.; Polyakov, S. V. Single-Photon Sources and Detectors. *Rev. Sci. Instrum.* **2011**, *82*, 071101.
(186) Michalet, X.; Siegmund, O. H. W.; Vallerga, J. V.; Jelinsky, P.; Millaud, J. E.; Weiss, S. Detectors for Single-Molecule Fluorescence Imaging and Spectroscopy. *J. Mod. Opt.* **2007**, *54*, 239.
(187) Brooks Shera, E.; Seitzinger, N. K.; Davis, L. M.; Keller, R. A.; Soper, S. A. Detection of Single Fluorescent Molecules. *Chem. Phys. Lett.* **1990**, *174*, 553−557.
(188) Li, L.-Q.; Davis, L. M. Single Photon Avalanche Diode for Single Molecule Detection. *Rev. Sci. Instrum.* **1993**, *64* (1993), 1524.
(189) Kell, G.; Bülter, A.; Wahl, M.; Erdmann, R. τ-SPAD: A New Red Sensitive Single Photon Counting Module. *Proc. SPIE* **2011**, *8033*, 803303.
(190) Cova, S.; Ghioni, M.; Lotito, A.; Rech, I; Zappa, F. Evolution and Prospects for Single-Photon Avalanche Diodes and Quenching Circuits. *J. Mod. Opt.* **2004**, *51*, 1267−1288.
(191) Rech, I.; Luo, G.; Ghioni, M.; Yang, H.; Xie, X. S.; Cova, S. Photon-Timing Detector Module for Single-Molecule Spectroscopy with 60-Ps Resolution. *IEEE J. Sel. Top. Quantum Electron.* **2004**, *10*, 788−795.
(192) Gulinatti, A.; Rech, I.; Maccagnani, P.; Ghioni, M.; Cova, S. Improving the Performance of Silicon Single Photon Avalanche Diodes. *Proc. SPIE* **2011**, *8033*, 803302.
(193) Michalet, X.; Cheng, A.; Antelman, J.; Suyama, M.; Arisaka, K.; Weiss, S. Hybrid Photodetector for Single-Molecule Spectroscopy and Microscopy. *Proc. SPIE* **2008**, *6862*, 68620F.
(194) Andel, F.; Hasson, K. C.; Gai, F.; Anfinrud, P. A.; Mathies, R. A. Femtosecond Time-Resolved Spectroscopy of the Primary Photochemistry of Phytochrome. *Biospectroscopy* **1997**, *3*, 421−433.
(195) Bebek, C. J.; Bercovitz, J. H.; Groom, D. E.; Holland, S. E.; Kadel, R. W.; Karcher, A.; Kolbe, W. F.; Oluseyi, H. M.; Palaio, N. P.; Prasad, V.; et al. *Fully Depleted Back-Illuminated P-Channel CCD Development*: Lawrence Berkeley National Laboratory: Berkeley, CA, 2003.
(196) Frenkel, A.; Sartor, M. A.; Wlodawski, M. S. Photon-Noise-Limited Operation of Intensified CCD Cameras. *Appl. Opt.* **1997**, *36*, 5288−5297.
(197) Buontempo, S.; Chiodi, G.; Dalinenko, I. N.; Ereditato, A.; Ekimov, A. V.; Fabre, J. P.; Fedorov, V. Y.; Frenkel, A.; Galeazzi, F.; Garufi, F.; et al. The Megapixel EBCCD: A High-Resolution Imaging Tube Sensitive to Single Photons. *Nucl. Instrum. Methods Phys. Res., Sect. A* **1998**, *413*, 255−262.
(198) Jerram, P.; Pool, P. J.; Bell, R.; Burt, D. J.; Bowring, S.; Spencer, S.; Hazelwood, M.; Moody, I.; Catlett, N.; Heyes, P. S. The LLLCCD: Low Light Imaging without the Need for an Intensifier. In *Photonics West 2001—Electronic Imaging*; Blouke, M. M., Canosa, J., Sampat, N., Eds.; International Society for Optics and Photonics: Bellingham, WA, 2001; pp 178−186.
(199) Robbins, M. S.; Hadwen, B. J. The Noise Performance of Electron Multiplying Charge-Coupled Devices. *IEEE Trans. Electron Devices* **2003**, *50*, 1227−1232.
(200) Denvir, D. J.; Coates, C. G. Electron-Multiplying CCD Technology: Application to Ultrasensitive Detection of Biomolecules. In *International Symposium on Biomedical Optics*; Bornhop, D. J., Dunn, D. A., Mariella, Jr., R. P., Murphy, C. J., Nicolau, D. V., Nie, S., Palmer, M., Raghavachari, R., Eds.; International Society for Optics and Photonics: Bellingham, WA, 2002; pp 502−512.
(201) Ueno, H.; Nishikawa, S.; Iino, R.; Tabata, K. V.; Sakakihara, S.; Yanagida, T.; Noji, H. Simple Dark-Field Microscopy with Nanometer Spatial Precision and Microsecond Temporal Resolution. *Biophys. J.* **2010**, *98*, 2014−2023.
(202) Barbier, R.; Cajgfinger, T.; Calabria, P.; Chabanat, E.; Chaize, D.; Depasse, P.; Doan, Q. T.; Dominjon, A.; Guérin, C.; Houles, J.; et al. A Single-Photon Sensitive ebCMOS Camera: The LUSIPHER Prototype. *Nucl. Instrum. Methods Phys. Res., Sect. A* **2011**, *648*, 266−274.
(203) Vallerga, J. V.; McPhate, J.; Tremsin, A.; Siegmund, O. H. W. Optically Sensitive MCP Image Tube with a Medipix2 ASIC Readout. In *SPIE Astronomical Telescopes + Instrumentation*; Dorn, D. A., Holland, A. D., Eds.; International Society for Optics and Photonics: Bellingham, WA, 2008; pp 702115.
(204) Ohnuki, T.; Michalet, X.; Tripathi, A.; Weiss, S.; Arisaka, K. Development of an Ultrafast Single Photon Counting Imager for Single Molecule Imaging. In *Biomedical Optics 2006*; Enderlein, J., Gryczynski, Z. K., Eds.; International Society for Optics and Photonics: Bellingham, WA, 2006; p 60920P.
(205) Kawai, Y.; Haba, J.; Suyama, M. R&D Status of 64-Channel Photon-Counting Imaging Module. *Nucl. Instrum. Methods Phys. Res., Sect. A* **2010**, *623*, 282−284.
(206) Rech, I.; Marangoni, S.; Resnati, D.; Ghioni, M.; Cova, S. Multipixel Single-Photon Avalanche Diode Array for Parallel Photon Counting Applications. *J. Mod. Opt.* **2009**, *56*, 326−333.
(207) Fukasawa, A.; Kamiya, A.; Muramatsu, S.; Negi, Y.; Suyama, M. High-Performance HPD for Photon Counting. *Proc. SPIE* **2011**, *8033*, 80330S.
(208) Gulinatti, A.; Rech, I.; Maccagnani, P.; Ghioni, M.; Cova, S. Improving the Performance of Silicon Single-Photon Avalanche Diodes. In *SPIE Defense, Security, and Sensing*; Itzler, M. A., Campbell, J. C., Eds.; International Society for Optics and Photonics: Bellingham, WA, 2011; pp 803302 .
(209) Krüger, T. P. J.; Ilioaia, C.; Johnson, M. P.; Ruban, A. V.; Papagiannakis, E.; Horton, P.; van Grondelle, R. Controlled Disorder in Plant Light-Harvesting Complex II Explains Its Photoprotective Role. *Biophys. J.* **2012**, *102*, 2669−2676.
(210) Krüger, T. P. J.; Ilioaia, C.; Johnson, M. P.; Belgio, E.; Horton, P.; Ruban, A. V.; van Grondelle, R. The Specificity of Controlled Protein Disorder in the Photoprotection of Plants. *Biophys. J.* **2013**, *105*, 1018−1026.
(211) Lippitz, M.; Kulzer, F.; Orrit, M. Statistical Evaluation of Single Nano-Object Fluorescence. *ChemPhysChem* **2005**, *6*, 770−789.
(212) Terentyeva, T. G.; Engelkamp, H.; Rowan, A. E.; Komatsuzaki, T.; Hofkens, J.; Li, C.-B.; Blank, K. Dynamic Disorder in Single-Enzyme Experiments: Facts and Artifacts. *ACS Nano* **2012**, *6*, 346−354.
(213) Amecke, N.; Heber, A.; Cichos, F. Distortion of Power Law Blinking with Binning and Thresholding. *J. Chem. Phys.* **2014**, *140*, 114306.
(214) Watkins, L. P.; Yang, H. Information Bounds and Optimal Analysis of Dynamic Single Molecule Measurements. *Biophys. J.* **2004**, *86*, 4015−4029.
(215) Watkins, L. P.; Yang, H. Detection of Intensity Change Points in Time-Resolved Single-Molecule Measurements. *J. Phys. Chem. B* **2005**, *109*, 617−628.
(216) Schörner, M.; Beyer, S. R.; Southall, J.; Cogdell, R. J.; Köhler, J. Multi-Level, Multi Time-Scale Fluorescence Intermittency of Photosynthetic LH2 Complexes: A Precursor of Non-Photochemical Quenching? *J. Phys. Chem. B* **2015**, *119*, 13958−13963.

DOI: 10.1021/acs.chemrev.6b00195
Chem. Rev. XXXX, XXX, XXX−XXX

(217) Cichos, F.; von Borczyskowski, C.; Orrit, M. Power-Law Intermittency of Single Emitters. *Curr. Opin. Colloid Interface Sci.* **2007**, *12*, 272−284.
(218) Koppel, D. E. Statistical Accuracy in Fluorescence Correlation Spectroscopy. *Phys. Rev. A: At., Mol., Opt. Phys.* **1974**, *10*, 1938−1945.
(219) Elson, E.; Magde, D. Fluorescence Correlation Spectroscopy. I. Conceptual Basis and Theory. *Biopolymers* **1974**, *13*, 1−27.
(220) Ehrenberg, M.; Rigler, R. Rotational Brownian Motion and Fluorescence Intensify Fluctuations. *Chem. Phys.* **1974**, *4*, 390−401.
(221) Magde, D.; Elson, E.; Webb, W. W. Thermodynamic Fluctuations in a Reacting System—Measurement by Fluorescence Correlation Spectroscopy. *Phys. Rev. Lett.* **1972**, *29*, 705−708.
(222) Yang, H.; Xie, X. S. Probing Single-Molecule Dynamics Photon by Photon. *J. Chem. Phys.* **2002**, *117*, 10965.
(223) Barsegov, V.; Mukamel, S. Probing Single Molecule Kinetics by Photon Arrival Trajectories. *J. Chem. Phys.* **2002**, *116*, 9802−9810.
(224) Wenger, J.; Rigneault, H. Photonic Methods to Enhance Fluorescence Correlation Spectroscopy and Single Molecule Fluorescence Detection. *Int. J. Mol. Sci.* **2010**, *11*, 206−221.
(225) Digman, M. A.; Gratton, E. Lessons in Fluctuation Correlation Spectroscopy. *Annu. Rev. Phys. Chem.* **2011**, *62*, 645−668.
(226) Blom, H.; Chmyrov, A.; Hassler, K.; Davis, L. M.; Widengren, J. Triplet-State Investigations of Fluorescent Dyes at Dielectric Interfaces Using Total Internal Reflection Fluorescence Correlation Spectroscopy. *J. Phys. Chem. A* **2009**, *113*, 5554−5566.
(227) Schönle, A.; Von Middendorff, C.; Ringemann, C.; Hell, S. W.; Eggeling, C. Monitoring Triplet State Dynamics with Fluorescence Correlation Spectroscopy: Bias and Correction. *Microsc. Res. Tech.* **2014**, *77*, 528−536.
(228) Hanbury Brown, R.; Twiss, R. Q. A Test of a New Type of Stellar Interferometer on Sirius. *Nature* **1956**, *178* (4541), 1046−1048.
(229) Maus, M.; Cotlet, M.; Hofkens, J.; Gensch, T.; de Schryver, F. C.; Schaffer, J.; Seidel, C. A. M. An Experimental Comparison of the Maximum Likelihood Estimation and Nonlinear Least-Squares Fluorescence Lifetime Analysis of Single Molecules. *Anal. Chem.* **2001**, *73*, 2078−2086.
(230) Enderlein, J.; Goodwin, P. M.; Van Orden, A.; Patrick Ambrose, W.; Erdmann, R.; Keller, R. A. A Maximum Likelihood Estimator to Distinguish Single Molecules by Their Fluorescence Decays. *Chem. Phys. Lett.* **1997**, *270*, 464−470.
(231) Jankowiak, R.; Hayes, J. M.; Small, G. J. Spectral Hole-Burning Spectroscopy in Amorphous Molecular Solids and Proteins. *Chem. Rev.* **1993**, *93*, 1471−1502.
(232) Brecht, M.; Studier, H.; Radics, V.; Nieder, J. B.; Bittl, R. Spectral Diffusion Induced by Proton Dynamics in Pigment-Protein Complexes. *J. Am. Chem. Soc.* **2008**, *130*, 17487−17493.
(233) Baier, J.; Gabrielsen, M.; Oellerich, S.; Michel, H.; van Heel, M.; Cogdell, R. J.; Köhler, J. Spectral Diffusion and Electron-Phonon Coupling of the B800 BChl a Molecules in LH2 Complexes from Three Different Species of Purple Bacteria. *Biophys. J.* **2009**, *97*, 2604−2612.
(234) Kunz, R.; Timpmann, K.; Southall, J.; Cogdell, R. J.; Freiberg, A.; Köhler, J. Fluctuations in the Electron-Phonon Coupling of a Single Chromoprotein. *Angew. Chem.* **2013**, *125*, 8888−8892.
(235) Ketelaars, M.; van Oijen, A. M.; Matsushita, M.; Köhler, J.; Schmidt, J.; Aartsma, T. J. Spectroscopy on the B850 Band of Individual Light-Harvesting 2 Complexes of Rhodopseudomonas Acidophila. I. Experiments and Monte Carlo Simulations. *Biophys. J.* **2001**, *80*, 1591−1603.
(236) Matsushita, M.; Ketelaars, M.; van Oijen, A. M.; Köhler, J.; Aartsma, T. J.; Schmidt, J. Spectroscopy on the B850 Band of Individual Light-Harvesting 2 Complexes of Rhodopseudomonas Acidophila. II. Exciton States of an Elliptically Deformed Ring Aggregate. *Biophys. J.* **2001**, *80*, 1604−1614.
(237) Krüger, T. P. J.; Novoderezhkin, V. I.; Ilioaia, C.; van Grondelle, R. Fluorescence Spectral Dynamics of Single LHCII Trimers. *Biophys. J.* **2010**, *98*, 3093−3101.
(238) Gall, A.; Ilioaia, C.; Krüger, T. P. J.; Novoderezhkin, V.; Robert, B.; van Grondelle, R. Conformational Switching in a Light-Harvesting Protein as Followed by Single-Molecule Spectroscopy. *Biophys. J.* **2015**, *108*, 2713−2720.
(239) Baier, J.; Richter, M. F.; Cogdell, R. J.; Oellerich, S.; Köhler, J. Do Proteins at Low Temperature Behave as Glasses? A Single-Molecule Study. *J. Phys. Chem. B* **2007**, *111*, 1135−1138.
(240) Baier, J.; Richter, M. F.; Cogdell, R. J.; Oellerich, S.; Köhler, J. Determination of the Spectral Diffusion Kernel of a Protein by Single-Molecule Spectroscopy. *Phys. Rev. Lett.* **2008**, *100*, 018108.
(241) Kador, L. Stochastic Theory of Inhomogeneous Spectroscopic Line Shapes Reinvestigated. *J. Chem. Phys.* **1991**, *95*, 5574.
(242) Oikawa, H.; Fujiyoshi, S.; Dewa, T.; Nango, M.; Matsushita, M. How Deep Is the Potential Well Confining a Protein in a Specific Conformation? A Single-Molecule Study on Temperature Dependence of Conformational Change between 5 and 18 K. *J. Am. Chem. Soc.* **2008**, *130*, 4580−4581.
(243) Noda, I.; Dowrey, A. E.; Marcoli, C.; Story, G. M.; Ozaki, Y. Generalized Two-Dimensional Correlation Spectroscopy. *Appl. Spectrosc.* **2000**, *54* (7), 236A−248A.
(244) Brecht, M.; Radics, V.; Nieder, J. B.; Bittl, R. Protein Dynamics-Induced Variation of Excitation Energy Transfer Pathways. *Proc. Natl. Acad. Sci. U. S. A.* **2009**, *106*, 11857−11861.
(245) van Heel, M.; Gowen, B.; Matadeen, R.; Orlova, E. V.; Finn, R.; Pape, T.; Cohen, D.; Stark, H.; Schmidt, R.; Schatz, M.; Patwardhan, A.; et al. Single-Particle Electron Cryo-Microscopy: Towards Atomic Resolution. *Q. Rev. Biophys.* **2000**, *33* (4), 307−369.
(246) Borland, L.; van Heel, M. Classification of Image Data in Conjugate Representation Spaces. *J. Opt. Soc. Am. A* **1990**, *7*, 601.
(247) Hofmann, C.; Michel, H.; van Heel, M.; Köhler, J. Multivariate Analysis of Single-Molecule Spectra: Surpassing Spectral Diffusion. *Phys. Rev. Lett.* **2005**, *94*, 195501.
(248) Cogdell, R. J.; Köhler, J. Use of Single-Molecule Spectroscopy to Tackle Fundamental Problems in Biochemistry: Using Studies on Purple Bacterial Antenna Complexes as an Example. *Biochem. J.* **2009**, *422*, 193−205.
(249) Gwizdala, M.; Berera, R.; Kirilovsky, D.; van Grondelle, R.; Krüger, T. P. J. Controlling Light Harvesting with Light. *J. Am. Chem. Soc.* **2016**, *138*, 11616−11622.
(250) Krüger, T. P. J.; Ilioaia, C.; Valkunas, L.; van Grondelle, R. Fluorescence Intermittency from the Main Plant Light-Harvesting Complex: Sensitivity to the Local Environment. *J. Phys. Chem. B* **2011**, *115*, 5083−5095.
(251) Krüger, T. P. J.; Ilioaia, C.; Johnson, M. P.; Ruban, A. V.; van Grondelle, R. Disentangling the Low-Energy States of the Major Light-Harvesting Complex of Plants and Their Role in Photoprotection. *Biochim. Biophys. Acta, Bioenerg.* **2014**, *1837*, 1027−1038.
(252) Alboresi, A.; Ballottari, M.; Hienerwadel, R.; Giacometti, G. M.; Morosinotto, T. Antenna Complexes Protect Photosystem I from Photoinhibition. *BMC Plant Biol.* **2009**, *9*, 71.
(253) Schmitt, F. J.; Maksimov, E. G.; Hätti, P.; Weißenborn, J.; Jeyasangar, V.; Razjivin, A. P.; Paschenko, V. Z.; Friedrich, T.; Renger, G. Coupling of Different Isolated Photosynthetic Light Harvesting Complexes and CdSe/ZnS Nanocrystals via Förster Resonance Energy Transfer. *Biochim. Biophys. Acta, Bioenerg.* **2012**, *1817*, 1461−1470.
(254) Reynolds, N. P.; Janusz, S.; Escalante-Marun, M.; Timney, J.; Ducker, R. E.; Olsen, J. D.; Otto, C.; Subramaniam, V.; Leggett, G. J.; Hunter, C. N. Directed Formation of Micro- and Nanoscale Patterns of Functional Light-Harvesting LH2 Complexes. *J. Am. Chem. Soc.* **2007**, *129*, 14625−14631.
(255) Lopez, A. L.; Hegedus, S. In *Handbook of Photovoltaic Science and Engineering*; John Wiley & Sons: Chichester, UK, 2003
(256) Sauer, P. R.; Lottspeich, F.; Unger, E.; Mentele, R.; Michel, H. Deletion of a B800−850 Light-Harvesting Complex in Rhodospirillum Molischianum DSM119 Leads To "revertants" expressing a B800−820 Complex: Insights into Pigment Binding. *Biochemistry* **1996**, *35*, 6500−6507.
(257) Novoderezhkin, V.; Monshouwer, R.; van Grondelle, R. Exciton (De)Localization in the LH2 Antenna of Rhodobacter Sphaeroides As Revealed by Relative Difference Absorption Measure-

DOI: 10.1021/acs.chemrev.6b00195
Chem. Rev. XXXX, XXX, XXX−XXX

ments of the LH2 Antenna and the B820 Subunit. *J. Phys. Chem. B* **1999**, *103*, 10540−10548.
(258) Hofmann, C.; Aartsma, T. J.; Köhler, J. Energetic Disorder and the B850-Exciton States of Individual Light-Harvesting 2 Complexes from Rhodopseudomonas Acidophila. *Chem. Phys. Lett.* **2004**, *395*, 373−378.
(259) Tubasum, S.; Sakai, S.; Dewa, T.; Sundström, V.; Scheblykin, I. G.; Nango, M.; Pullerits, T. Anchored LH2 Complexes in 2D Polarization Imaging. *J. Phys. Chem. B* **2013**, *117*, 11391−11396.
(260) Rutkauskas, D.; Novoderezhkin, V.; Cogdell, R. J.; van Grondelle, R. Fluorescence Spectroscopy of Conformational Changes of Single LH2 Complexes. *Biophys. J.* **2005**, *88*, 422−435.
(261) Uchiyama, D.; Hoshino, H.; Otomo, K.; Kato, T.; Onda, K.; Watanabe, A.; Oikawa, H.; Fujiyoshi, S.; Matsushita, M.; Nango, M.; et al. Single-Protein Study of Photoresistance of Pigment−protein Complex in Lipid Bilayer. *Chem. Phys. Lett.* **2011**, *511*, 135−137.
(262) Scheuring, S.; Seguin, J.; Marco, S.; Lévy, D.; Robert, B.; Rigaud, J.-L. Nanodissection and High-Resolution Imaging of the Rhodopseudomonas Viridis Photosynthetic Core Complex in Native Membranes by AFM. Atomic Force Microscopy. *Proc. Natl. Acad. Sci. U. S. A.* **2003**, *100*, 1690−1693.
(263) Fotiadis, D.; Qian, P.; Philippsen, A.; Bullough, P. A.; Engel, A.; Hunter, C. N. Structural Analysis of the Reaction Center Light-Harvesting Complex I Photosynthetic Core Complex of Rhodospirillum Rubrum Using Atomic Force Microscopy. *J. Biol. Chem.* **2004**, *279*, 2063−2068.
(264) Niwa, S.; Yu, L.-J.; Takeda, K.; Hirano, Y.; Kawakami, T.; Wang-Otomo, Z.-Y.; Miki, K. Structure of the LH1-RC Complex from Thermochromatium Tepidum at 3.0 Å. *Nature* **2014**, *508* (7495), 228−232.
(265) Roszak, A. W.; Howard, T. D.; Southall, J.; Gardiner, A. T.; Law, C. J.; Isaacs, N. W.; Cogdell, R. J. Crystal Structure of the RC-LH1 Core Complex from Rhodopseudomonas Palustris. *Science* **2003**, *302* (5652), 1969−1972.
(266) Qian, P.; Papiz, M. Z.; Jackson, P. J.; Brindley, A. A.; Ng, I. W.; Olsen, J. D.; Dickman, M. J.; Bullough, P. A.; Hunter, C. N. Three-Dimensional Structure of the Rhodobacter Sphaeroides RC-LH1-PufX Complex: Dimerization and Quinone Channels Promoted by PufX. *Biochemistry* **2013**, *52*, 7575−7585.
(267) Siebert, C. A.; Qian, P.; Fotiadis, D.; Engel, A.; Hunter, C. N.; Bullough, P. A. Molecular Architecture of Photosynthetic Membranes in Rhodobacter Sphaeroides: The Role of PufX. *EMBO J.* **2004**, *23*, 690−700.
(268) Scheuring, S.; Sturgis, J. N. Atomic Force Microscopy of the Bacterial Photosynthetic Apparatus: Plain Pictures of an Elaborate Machinery. *Photosynth. Res.* **2009**, *102*, 197−211.
(269) Francia, F.; Wang, J.; Venturoli, G.; Melandri, B. A.; Barz, W. P.; Oesterhelt, D. The Reaction Center-LH1 Antenna Complex of Rhodobacter Sphaeroides Contains One PufX Molecule Which Is Involved in Dimerization of This Complex. *Biochemistry* **1999**, *38*, 6834−6845.
(270) Richter, M. F.; Baier, J.; Prem, T.; Oellerich, S.; Francia, F.; Venturoli, G.; Oesterhelt, D.; Southall, J.; Cogdell, R. J.; Köhler, J. Symmetry Matters for the Electronic Structure of Core Complexes from Rhodopseudomonas Palustris and Rhodobacter Sphaeroides PufX-. *Proc. Natl. Acad. Sci. U. S. A.* **2007**, *104*, 6661−6665.
(271) Gerken, U.; Jelezko, F.; Götze, B.; Branschädel, M.; Tietz, C.; Ghosh, R.; Wrachtrup, J. Membrane Environment Reduces the Accessible Conformational Space Available to an Integral Membrane Protein. *J. Phys. Chem. B* **2003**, *107*, 338−343.
(272) Böhm, P. S.; Kunz, R.; Southall, J.; Cogdell, R. J.; Köhler, J. Does the Reconstitution of RC-LH1 Complexes from Rhodopseudomonas Acidophila Strain 10050 into a Phospholipid Bilayer Yield the Optimum Environment for Optical Spectroscopy? *J. Phys. Chem. B* **2013**, *117*, 15004−15013.
(273) Cohen-Bazire, G. The Fine Structure of Green Bacteria. *J. Cell Biol.* **1964**, *22*, 207−225.
(274) Bryant, D. A.; Costas, A. M. G.; Maresca, J. A.; Chew, A. G. M.; Klatt, C. G.; Bateson, M. M.; Tallon, L. J.; Hostetler, J.; Nelson, W. C.; Heidelberg, J. F.; Ward, D. M. Candidatus Chloracidobacterium Thermophilum: An Aerobic Phototrophic Acidobacterium. *Science* **2007**, *317* (5837), 523−526.
(275) Olson, J. M. Chlorophyll Organization and Function in Green Photosynthetic Bacteria. *Photochem. Photobiol.* **1998**, *67*, 61−75.
(276) Martinez-Planells, A.; Arellano, J. B.; Borrego, C. M.; López-Iglesias, C.; Gich, F.; Garcia-Gil, L. J. Determination of the Topography and Biometry of Chlorosomes by Atomic Force Microscopy. *Photosynth. Res.* **2002**, *71*, 83−90.
(277) Montaño, G. A.; Bowen, B. P.; LaBelle, J. T.; Woodbury, N. W.; Pizziconi, V. B.; Blankenship, R. E. Characterization of Chlorobium Tepidum Chlorosomes: A Calculation of Bacteriochlorophyll c per Chlorosome and Oligomer Modeling. *Biophys. J.* **2003**, *85*, 2560−2565.
(278) Saga, Y.; Shibata, Y.; Itoh, S.; Tamiaki, H. Direct Counting of Submicrometer-Sized Photosynthetic Apparatus Dispersed in Medium at Cryogenic Temperature by Confocal Laser Fluorescence Microscopy: Estimation of the Number of Bacteriochlorophyll c in Single Light-Harvesting Antenna Complexes Chloroso. *J. Phys. Chem. B* **2007**, *111*, 12605−12609.
(279) Manske, A. K.; Glaeser, J.; Kuypers, M. M. M.; Overmann, J. Physiology and Phylogeny of Green Sulfur Bacteria Forming a Monospecific Phototrophic Assemblage at a Depth of 100 Meters in the Black Sea. *Appl. Environ. Microbiol.* **2005**, *71*, 8049−8060.
(280) Beatty, J. T.; Overmann, J.; Lince, M. T.; Manske, A. K.; Lang, A. S.; Blankenship, R. E.; Van Dover, C. L.; Martinson, T. A.; Plumley, F. G. An Obligately Photosynthetic Bacterial Anaerobe from a Deep-Sea Hydrothermal Vent. *Proc. Natl. Acad. Sci. U. S. A.* **2005**, *102*, 9306−9310.
(281) Eisele, D. M.; Arias, D. H.; Fu, X.; Bloemsma, E. A.; Steiner, C. P.; Jensen, R. A.; Rebentrost, P.; Eisele, H.; Tokmakoff, A.; Lloyd, S.; et al. Robust Excitons Inhabit Soft Supramolecular Nanotubes. *Proc. Natl. Acad. Sci. U. S. A.* **2014**, *111*, E3367−E3375.
(282) Ma, Y. Z.; Cox, R. P.; Gillbro, T.; Miller, M. Bacteriochlorophyll Organization and Energy Transfer Kinetics in Chlorosomes from Chloroflexus Aurantiacus Depend on the Light Regime during Growth. *Photosynth. Res.* **1996**, *47*, 157−165.
(283) Borrego, C. M.; Garcia-Gil, L. J. Rearrangement of Light Harvesting Bacteriochlorophyll Homologues as a Response of Green Sulfur Bacteria to Low Light Intensities. *Photosynth. Res.* **1995**, *45*, 21−30.
(284) Saga, Y.; Oh-Oka, H.; Hayashi, T.; Tamiaki, H. Presence of Exclusively Bacteriochlorophyll-c Containing Substrain in the Culture of Green Sulfur Photosynthetic Bacterium Chlorobium Vibrioforme Strain NCIB 8327 Producing Bacteriochlorophyll-D. *Anal. Sci.* **2003**, *19*, 1575−1579.
(285) Saga, Y.; Osumi, S.; Higuchi, H.; Tamiaki, H. Bacteriochlorophyll-c Homolog Composition in Green Sulfur Photosynthetic Bacterium Chlorobium Vibrioforme Dependent on the Concentration of Sodium Sulfide in Liquid Cultures. *Photosynth. Res.* **2005**, *86*, 123−130.
(286) Psencik, J.; Ikonen, T. P.; Laurinmäki, P.; Merckel, M. C.; Butcher, S. J.; Serimaa, R. E.; Tuma, R. Lamellar Organization of Pigments in Chlorosomes, the Light Harvesting Complexes of Green Photosynthetic Bacteria. *Biophys. J.* **2004**, *87*, 1165−1172.
(287) Holzwarth, A. R.; Schaffner, K. On the Structure of Bacteriochlorophyll Molecular Aggregates in the Chlorosomes of Green Bacteria. A Molecular Modelling Study. *Photosynth. Res.* **1994**, *41*, 225−233.
(288) Oostergetel, G. T.; Reus, M.; Gomez Maqueo Chew, A.; Bryant, D. A.; Boekema, E. J.; Holzwarth, A. R. Long-Range Organization of Bacteriochlorophyll in Chlorosomes of Chlorobium Tepidum Investigated by Cryo-Electron Microscopy. *FEBS Lett.* **2007**, *581*, 5435−5439.
(289) Ganapathy, S.; Oostergetel, G. T.; Wawrzyniak, P. K.; Reus, M.; Gomez Maqueo Chew, A.; Buda, F.; Boekema, E. J.; Bryant, D. A.; Holzwarth, A. R.; de Groot, H. J. M. Alternating Syn-Anti Bacteriochlorophylls Form Concentric Helical Nanotubes in Chlorosomes. *Proc. Natl. Acad. Sci. U. S. A.* **2009**, *106*, 8525−8530.

DOI: 10.1021/acs.chemrev.6b00195
Chem. Rev. XXXX, XXX, XXX−XXX

(290) Miyatake, T.; Tamiaki, H. Self-Aggregates of Bacteriochlorophylls-C, D and E in a Light-Harvesting Antenna System of Green Photosynthetic Bacteria: Effect of Stereochemistry at the Chiral 3-(1-Hydroxyethyl) Group on the Supramolecular Arrangement of Chlorophyllous Pigments. *J. Photochem. Photobiol., C* **2005**, *6*, 89−107.
(291) Linnanto, J.; Korppi-Tommola, J. Investigation on Chlorosomal Antenna Geometries: Tube, Lamella and Spiral-Type Self-Aggregates. *Photosynth. Res.* **2008**, *96*, 227−245.
(292) Oostergetel, G. T.; van Amerongen, H.; Boekema, E. J. The Chlorosome: A Prototype for Efficient Light Harvesting in Photosynthesis. *Photosynth. Res.* **2010**, *104*, 245−255.
(293) Shibata, Y.; Saga, Y.; Tamiaki, H.; Itoh, S. Polarized Fluorescence of Aggregated Bacteriochlorophyll c and Baseplate Bacteriochlorophyll a in Single Chlorosomes Isolated from Chloroflexus Aurantiacus. *Biochemistry* **2007**, *46*, 7062−7068.
(294) Furumaki, S.; Vacha, F.; Habuchi, S.; Tsukatani, Y.; Bryant, D. A.; Vacha, M. Absorption Linear Dichroism Measured Directly on a Single Light-Harvesting System: The Role of Disorder in Chlorosomes of Green Photosynthetic Bacteria. *J. Am. Chem. Soc.* **2011**, *133*, 6703−6710.
(295) Tian, Y.; Camacho, R.; Thomsson, D.; Reus, M.; Holzwarth, A. R.; Scheblykin, I. G. Organization of Bacteriochlorophylls in Individual Chlorosomes from Chlorobaculum Tepidum Studied by 2-Dimensional Polarization Fluorescence Microscopy. *J. Am. Chem. Soc.* **2011**, *133*, 17192−17199.
(296) Shibata, Y.; Saga, Y.; Tamiaki, H.; Itoh, S. Anisotropic Distribution of Emitting Transition Dipoles in Chlorosome from Chlorobium Tepidum: Fluorescence Polarization Anisotropy Study of Single Chlorosomes. *Photosynth. Res.* **2009**, *100*, 67−78.
(297) Pedersen, M. Ø.; Pham, L.; Steensgaard, D. B.; Miller, M. A Reconstituted Light-Harvesting Complex from the Green Sulfur Bacterium Chlorobium Tepidum Containing CsmA and Bacteriochlorophyll A. *Biochemistry* **2008**, *47*, 1435−1441.
(298) Pedersen, M. Ø.; Underhaug, J.; Dittmer, J.; Miller, M.; Nielsen, N. C. The Three-Dimensional Structure of CsmA: A Small Antenna Protein from the Green Sulfur Bacterium Chlorobium Tepidum. *FEBS Lett.* **2008**, *582*, 2869−2874.
(299) Mirzov, O.; Bloem, R.; Hania, P. R.; Thomsson, D.; Lin, H.; Scheblykin, I. G. Polarization Portraits of Single Multichromophoric Systems: Visualizing Conformation and Energy Transfer. *Small* **2009**, *5*, 1877−1888.
(300) Furumaki, S.; Yabiku, Y.; Habuchi, S.; Tsukatani, Y.; Bryant, D. A.; Vacha, M. Circular Dichroism Measured on Single Chlorosomal Light-Harvesting Complexes of Green Photosynthetic Bacteria. *J. Phys. Chem. Lett.* **2012**, *3*, 3545−3549.
(301) Hu, X.; Schulten, K. How Nature Harvests Sunlight. *Phys. Today* **1997**, *50*, 28−34.
(302) Kühlbrandt, W. Many Wheels Make Light Work. *Nature* **1995**, *374* (6522), 497−498.
(303) Uchiyama, D.; Oikawa, H.; Otomo, K.; Nango, M.; Dewa, T.; Fujiyoshi, S.; Matsushita, M. Reconstitution of Bacterial Photosynthetic Unit in a Lipid Bilayer Studied by Single-Molecule Spectroscopy at 5 K. *Phys. Chem. Chem. Phys.* **2011**, *13*, 11615−11619.
(304) Hofmann, C.; Francia, F.; Venturoli, G.; Oesterhelt, D.; Köhler, J. Energy Transfer in a Single Self-Aggregated Photosynthetic Unit. *FEBS Lett.* **2003**, *546*, 345−348.
(305) Fujita, T.; Huh, J.; Saikin, S. K.; Brookes, J. C.; Aspuru-Guzik, A. Theoretical Characterization of Excitation Energy Transfer in Chlorosome Light-Harvesting Antennae from Green Sulfur Bacteria. *Photosynth. Res.* **2014**, *120*, 273−289.
(306) Saga, Y.; Tamiaki, H.; Shibata, Y.; Itoh, S. Excitation Energy Transfer in Individual Light-Harvesting Chlorosome from Green Photosynthetic Bacterium Chloroflexus Aurantiacus at Cryogenic Temperature. *Chem. Phys. Lett.* **2005**, *409*, 34−37.
(307) Amunts, A.; Drory, O.; Nelson, N. The Structure of a Plant Photosystem I Supercomplex at 3.4 A Resolution. *Nature* **2007**, *447*, 58−63.
(308) Pedrós, R.; Goulas, Y.; Jacquemoud, S.; Louis, J.; Moya, I. FluorMODleaf: A New Leaf Fluorescence Emission Model Based on the PROSPECT Model. *Remote Sens. Environ.* **2010**, *114*, 155−167.
(309) Byrdin, M.; Rimke, I.; Schlodder, E.; Stehlik, D.; Roelofs, T. A. Decay Kinetics and Quantum Yields of Fluorescence in Photosystem I from Synechococcus Elongatus with P700 in the Reduced and Oxidized State: Are the Kinetics of Excited State Decay Trap-Limited or Transfer-Limited? *Biophys. J.* **2000**, *79*, 992−1007.
(310) Pålsson, L. O.; Flemming, C.; Gobets, B.; van Grondelle, R.; Dekker, J. P.; Schlodder, E. Energy Transfer and Charge Separation in Photosystem I: P700 Oxidation upon Selective Excitation of the Long-Wavelength Antenna Chlorophylls of Synechococcus Elongatus. *Biophys. J.* **1998**, *74*, 2611−2622.
(311) Jelezko, F.; Tietz, C.; Gerken, U.; Wrachtrup, J.; Bittl, R. Single-Molecule Spectroscopy on Photosystem I Pigment−Protein Complexes. *J. Phys. Chem. B* **2000**, *104*, 8093−8096.
(312) Zazubovich, V.; Matsuzaki, S.; Johnson, T. W.; Hayes, J. M.; Chitnis, P. R.; Small, G. J. Red Antenna States of Photosystem I from Cyanobacterium Synechococcus Elongatus: A Spectral Hole Burning Study. *Chem. Phys.* **2002**, *275*, 47−59.
(313) Pålsson, L. O.; Dekker, J. P.; Schlodder, E.; Monshouwer, R.; van Grondelle, R. Polarized Site-Selective Fluorescence Spectroscopy of the Long-Wavelength Emitting Chlorophylls in Isolated Photosystem I Particles of Synechococcus Elongatus. *Photosynth. Res.* **1996**, *48*, 239−246.
(314) Hayes, J. M.; Matsuzaki, S.; Rätsep, M.; Small, G. J. Red Chlorophyll a Antenna States of Photosystem I of the Cyanobacterium Synechocystis Sp. PCC 6803. *J. Phys. Chem. B* **2000**, *104*, 5625−5633.
(315) Brecht, M.; Nieder, J. B.; Studier, H.; Schlodder, E.; Bittl, R. Red Antenna States of Photosystem I from Synechococcus Sp. PCC 7002. *Photosynth. Res.* **2008**, *95*, 155−162.
(316) Brecht, M.; Studier, H.; Elli, A. F.; Jelezko, F.; Bittl, R. Assignment of Red Antenna States in Photosystem I from Thermosynechococcus Elongatus by Single-Molecule Spectroscopy. *Biochemistry* **2007**, *46*, 799−806.
(317) Riley, K. J.; Reinot, T.; Jankowiak, R.; Fromme, P.; Zazubovich, V. Red Antenna States of Photosystem I from Cyanobacteria Synechocystis PCC 6803 and Thermosynechococcus Elongatus: Single-Complex Spectroscopy and Spectral Hole-Burning Study. *J. Phys. Chem. B* **2007**, *111*, 286−292.
(318) Elli, A. F.; Jelezko, F.; Tietz, C.; Studier, H.; Brecht, M.; Bittl, R.; Wrachtrup, J. Red Pool Chlorophylls of Photosystem I of the Cyanobacterium Thermosynechococcus Elongatus: A Single-Molecule Study. *Biochemistry* **2006**, *45*, 1454−1458.
(319) Tian, L.; Gwizdala, M.; van Stokkum, I. H. M.; Koehorst, R. B. M.; Kirilovsky, D.; van Amerongen, H. Picosecond Kinetics of Light Harvesting and Photoprotective Quenching in Wild-Type and Mutant Phycobilisomes Isolated from the Cyanobacterium Synechocystis PCC 6803. *Biophys. J.* **2012**, *102*, 1692−1700.
(320) Marx, A.; Adir, N. Allophycocyanin and Phycocyanin Crystal Structures Reveal Facets of Phycobilisome Assembly. *Biochim. Biophys. Acta, Bioenerg.* **2013**, *1827*, 311−318.
(321) Yuan, H.; Orrit, M. Temperature Cycles Unravel the Dynamics of Single Biomolecules. *Biophys. J.* **2014**, *106*, 3−4.
(322) Yuan, H.; Gaiduk, A.; Siekierzycka, J. R.; Fujiyoshi, S.; Matsushita, M.; Nettels, D.; Schuler, B.; Seidel, C. A. M.; Orrit, M. Temperature-Cycle Microscopy Reveals Single-Molecule Conformational Heterogeneity. *Phys. Chem. Chem. Phys.* **2015**, *17*, 6532−6544.
(323) Odobel, F.; Pellegrin, Y.; Warnan, J. Bio-Inspired Artificial Light-Harvesting Antennas for Enhancement of Solar Energy Capture in Dye-Sensitized Solar Cells. *Energy Environ. Sci.* **2013**, *6*, 2041−2052.
(324) Choi, M.-S.; Yamazaki, T.; Yamazaki, I.; Aida, T. Bioinspired Molecular Design of Light-Harvesting Multiporphyrin Arrays. *Angew. Chem., Int. Ed.* **2003**, *43*, 150−158.

DOI: 10.1021/acs.chemrev.6b00195
Chem. Rev. XXXX, XXX, XXX−XXX